EOARD CONTRACT SPC-94-4015

Title: **CONSTRAINED LAYER DAMPING AND PIEZOCERAMIC ACTIVE CONTROL**

FINAL REPORT: APRIL 1997

AUTHOR: G R Tomlinson, University of Sheffield, UK.

1. Introduction

A special (EOARD) contract was issued by the Department of the Air Force (AFMC) in 1994 to the University of Manchester on the above topic.

The final report was due in January 1995 but due to the researcher leaving to take up another post in December 94 and the fact that Professor Tomlinson left the University of Manchester to take up the Head of Departments post at the University of Sheffield in October 1995 resulted in a significant delay. The author wishes to apologise to the EOARD for this delay.

Due to the delay, the final report has been kept as succinct as possible covering the Technical Brief, Technical Achievements and Conclusions/Recommendations.

Appendices are attached which contain the principal output from the work.

2. **Technical Brief**

The principal objectives were as follows:

- To investigate the use of a hybrid active damping method based on PZT patches actuating a constrained layer damper as shown in Figure 1 and referred to as ACLD. The alternative version is the concept that is being actively researched in the USA by Baz, Inman, Wang, Tsou etc, as shown in Figure 2.

- To derive mathematical models of the ACLD system for the active damping control of structures.

- To apply the principles experimentally to beam and plate type structures.

3. **Technical Achievements**

All of the objectives were achieved and surpassed. In particular the following aspects are worthy of note:

(i) Mathematical models for both longitudinal and flexural hybrid constrained layer/piezoceramic active damping concepts have been developed using analytical (Rayleigh-Ritz) and FE models and validated experimentally. These are described in Technical Papers Numbers 1 and 2 in Appendix 1.

(ii) The methodology was applied to a plate structure representing an aircraft instrument panel and the first three modes of vibration (two flexure, one torsion) were effectively suppressed using the hybrid method. The results are described in the Technical Paper Number 3 Appendix II.

(iii) the technology has been extended to ring structures (i.e. applicable to aero engines) as described in Technical Papers Numbers 4 and 5 in Appendix III.

4. **Conclusions and Recommendations**

1. The concept of hybrid (passive constrained layer and active) damping appears to hold significant potential.

2. Correctly designed passive constrained damping provides authority over the higher frequency modes. However, the addition of actuators, in this case PZT patches, placed at appropriate locations (maximum curvature points) on top of the constraining layer produces clear benefits.

3. The benefits can be described by two aspects:

   (a) increased damping control over a wide frequency range.
   (b) the ability to implement simple control algorithms arising from the inherent stability of the system from the constrained layer damping.

4. All of the objectives defined in the original work programme have been achieved and surpassed; the concepts being extended to ring type structures.

Recommendations

Further work should be carried out to investigate the following in relation to optimisation, namely:-

- the size (coverage) of the constrained layer material which is activated by the PZT patches and its optimal location,
- a detailed comparison between the two approaches to active damping, namely PZT actuators (or equivalent) applied to viscoelastic material directly (the 'USA' method) or, as in our case, PZT actuators applied to the constraining layer which constrains the viscoelastic damping material.

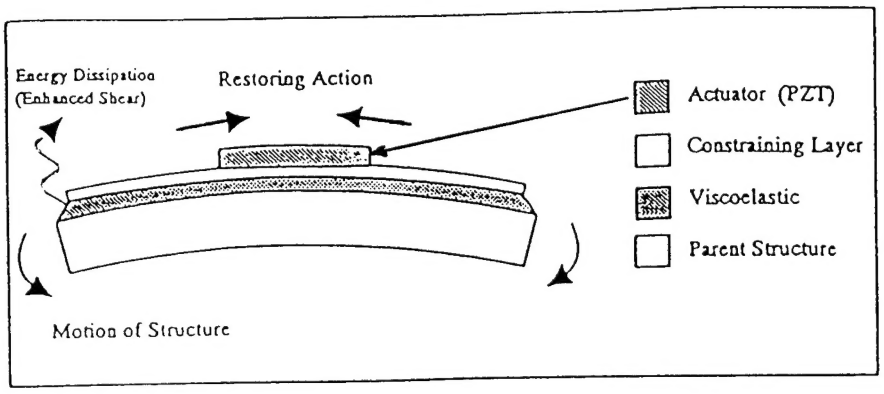

Figure 1 : Active Constrained Layer Damping (ACLD)

G R Tomlinson
Date: 14 April 1997

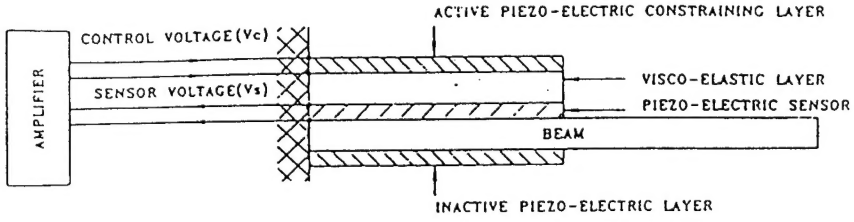

Figure 2 : Alternative version of ACLD

APPENDIX I

Technical Papers 1 and 2:

Modelling of a Hybrid Constrained Layer/Piezoceramic

Approach to Active Damping.

Use of Active Constrained Layer Damping for

Controlling Resonant Vibration.

J. A. Rongong[1]

J. R. Wright

R. J. Wynne[2]

G. R. Tomlinson[3]

Dynamics and Control Research Group,
University of Manchester,
Manchester, U.K.

Modelling of a Hybrid Constrained Layer/Piezoceramic Approach to Active Damping

It has been shown that significant reductions in structural vibration levels can be achieved using a hybrid system involving constrained layer damping and active control with piezoceramics. In this paper, mathematical models based on the Rayleigh Ritz approach, are developed to describe the longitudinal and flexural vibration behaviour of a cantilevered beam when excited using piezoceramic patches bonded to a constrained layer damping treatment. Predictions of static and steady state dynamic behaviour, obtained using the models are validated by comparison with results from finite element analysis and laboratory experiments. The models are then used in open loop and closed loop velocity feedback control simulations to demonstrate the improvements in stability and performance achieved using this method over that achieved using conventional active control.

1 Introduction

The active control of structural vibration using induced strain actuators has been the subject of many studies in the last decade. It has been shown that significant reductions in the vibration levels of beams and plates can be achieved in this way. Theoretical models have been developed to represent the interaction of the actuator and the parent structure. These have been used for optimisation and to develop control strategies.

Piezoelectric ceramic patches, such as lead zirconate titanate (PZT), are often chosen as induced strain actuators as they are compact and have a wide frequency range.

In the active control of lightly damped structures, the stability, robustness and disturbance rejection of the control strategy employed are critical to its success. In control system design for light, flexible structures the spillover, where unmodelled higher order modes are destabilised by the energy from the control system, must be minimised. Spillover effects in the control of vibrating structures were first discussed by Balas [1]. These issues have indicated the need for damping to be introduced in active control systems.

Efforts have been made to reduce structural vibration by actively enhancing the performance of passive constrained layer damping [2, 3, 4, 5]. Passive constraining layer methods reduce vibration by dissipating energy through hysteresis loss in a constrained viscoelastic layer. Effectiveness depends on the amount of shear induced in the viscoelastic material through the relative motion of the parent structure and constraining layer.

One method that has been used successfully is to bond PZT actuator material to a stiff constraining layer which is in turn bonded to the structure by a thin viscoelastic layer [6]. The relative motion of the constraining layer, and hence the shear in the viscoelastic layer, can be increased by activating the PZT material. Strains induced in the constraining layer in this way also develop bending moments, owing to their eccentricity from the neutral axis, which can be used to control vibrations. Thus, two mechanisms occur in this "active damping" approach. Significant reductions in resonant amplitudes have been demonstrated by applying this strategy to beams and plates using simple velocity feedback [7]. The "active damping" concept, as defined in this paper, is shown in Fig. 1.

The experimental work carried out in this field [3, 5, 7] has indicated that effectiveness is dependent on the dimensions, positioning and material properties of the viscoelastic, PZT and constraining layers. The complexity of the problem has highlighted the need for an accurate model which can be used to investigate the effect of parameter variations and to draw comparisons with other methods for optimisation and control strategies.

In addition to the advantages gained from the increase in the inherent damping of the structure, it has been shown that by placing actuators on a constraining layer rather than bonding them directly to the structure, significantly higher feedback voltages can be used before the actuators saturate and the system becomes unstable [7].

Previous work has adapted existing theory for the vibration of sandwich beams to include piezoelectric actuators to act as the constraining layer [8]. This normally results in modifications of the sixth order partial differential equations for vibration systems as developed in the late 1960s [8]. The effort required to solve these problems is considerable.

For application of active damping with structures more complex than simple beams and plates, finite element analysis may prove the most efficient [10, 11]. However when the requirement of the model is for investigation of the characteristics of the active damping concept, to assess its advantages against other possible configurations and to carry out studies involving parameter variations, a finite element model lacks the flexibility to do these operations easily. For example, a study into the effect of viscoelastic layer thickness on overall performance would require a separate finite element mesh to be created for each case.

This paper presents a model which uses the Rayleigh-Ritz assumed series method to analyze the situation where a viscoelastic layer and a stiff constraining layer with an additional PZT patch are used to create an "active damping" mechanism.

The model obtained is verified by comparison between predicted *dynamic* behaviour and that obtained from laboratory tests. A comparison is also made between the *static* and *modal* behaviour predicted by the model and that estimated using a commercial finite element package.

2 Theoretical Modelling

The analysis presented is for a rectangular section cantilevered beam with symmetrically placed constraining layers and PZT actuator patches as shown in Fig. 2.

[1,3] Now at the University of Sheffield, UK.

[2] Now at the Sheffield Hallam University, UK.

Contributed by the Technical Committee on Vibration and Sound for publication in the JOURNAL OF VIBRATION AND ACOUSTICS. Manuscript received Feb. 1995; revised Sept. 1995. Associate Technical Editor: J. Mottershead.

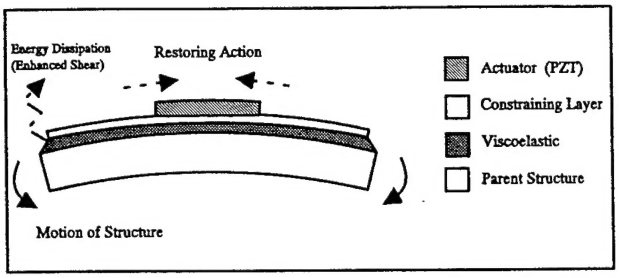

Fig. 1 "Active damping" concept–as defined in this paper

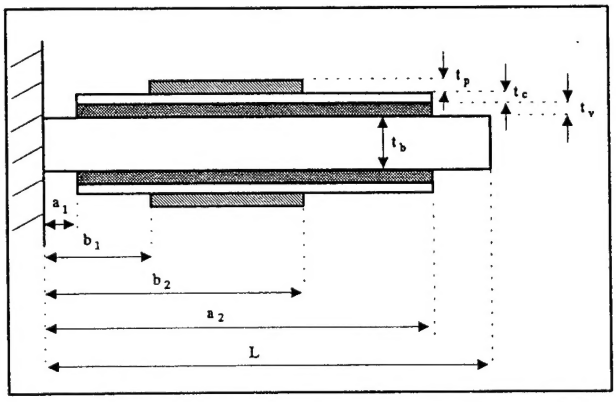

Fig. 2 Cantilevered beam used for analysis

Initially, motion in the longitudinal direction is considered. This is achieved by activating the PZTs on either side of the beam in phase with each other with the same input signal. A model is also derived for flexural motion. In this case, the polarity of the signal to one of the actuators is reversed thus creating a net bending moment around the neutral axis of the beam.

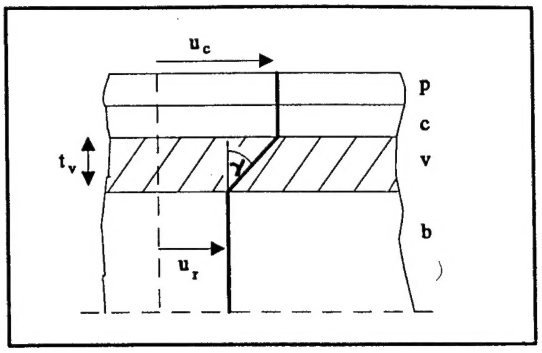

Fig. 3 Deformation of the beam in longitudinal motion

2.1 Longitudinal Motion. The variation in the longitudinal displacement in the beam and constraining layer is assumed to be respectively,

$$u_r(x, t) = \sum_{j=1}^{N_r} r_j(t) \cdot \phi_j(x) = \boldsymbol{\phi}^T \mathbf{r} \quad \text{and}$$

$$u_c(x, t) = \sum_{j=1}^{N_c} c_j(t) \cdot \psi_j(x) = \boldsymbol{\psi}^T \mathbf{c} \tag{1}$$

The vectors $\boldsymbol{\phi}$, $\boldsymbol{\psi}$ are of assumed shape functions and $\mathbf{r}$, $\mathbf{c}$ are vectors of unknown time varying coefficients.

It is assumed that the PZT and constraining layers have compatible deformations as shown in Fig. 3, giving the relationship for strain, ϵ as

$$\epsilon_{p(geom)} = \epsilon_c = \frac{\partial u_c}{\partial x} = u_c' \tag{2}$$

and similarly for the beam,

$$\epsilon_b = \frac{\partial u_r}{\partial x} = u_r' \tag{3}$$

where $'$ denotes $\partial/\partial x$.

Nomenclature

English Letters

A = cross sectional area
C = damping matrix
E = Young's modulus
FE = finite element
G = shear modulus
I = second moment of area around 'x' axis
K = stiffness matrix
L = length of beam
M = mass matrix
$\mathbf{P}$ = voltage-to-force transformation vector
PZT = Lead Zirconate Titanate (piezoelectric actuator)
RR = Rayleigh Ritz
T = kinetic energy
U = potential (strain) energy
V_{33} = voltage across PZT
a_1, a_2 = limits of viscous and constrained layers on the beam
b_1, b_2 = limits of PZT on the beam
b = vector of beam coefficients in flexural motion
$\mathbf{c}$ = vector of constraining layer coefficients in longitudinal motion
d_{31} = piezoelectric charge constant
$\mathbf{q}$ = vector of generalised coordinates
$\mathbf{r}$ = vector of beam coefficients in longitudinal motion
t = time
t_i = thickness (subscript indicates layer in question)
u = longitudinal displacement
w = flexural displacement

Greek letters

γ = shear strain
ϵ = normal strain
η = material loss factor
μ = d_{31}/t_p
σ = normal stress
τ = shear stress
ϕ = vector of shape functions for longitudinal displacement of the beam
φ = vector of shape functions for flexural displacement of the beam
ψ = vector of shape functions for longitudinal displacement of the constraining layer
Ω_{ex} = frequency of harmonic excitation

Subscripts

b = beam
c = constraining layer
p = PZT
r = beam (in longitudinal motion)
v = viscoelastic layer

Superscripts

T = matrix or vector transpose
$'$, $''$ = first and second spatial derivatives ($\partial/\partial x$ and $\partial^2/\partial x^2$)
$\dot{}$, $\ddot{}$ = first and second time derivatives ($\partial/\partial t$ and $\partial^2/\partial t^2$)

The viscoelastic layer is assumed to carry shear stress only which is constant across the layer. Referring to Fig. 3, the shear strain, γ, is

$$\gamma_v = \frac{u_c - u_r}{t_v} \tag{4}$$

The PZT actuators are assumed to be linear over the operating range. In induced strain applications it is common to use d_{31} type actuators i.e. strain output in the "1" direction is perpendicular to the direction of poling "3" and hence the applied field. For one dimensional (simple) extension the piezoelectric equations reduce to;

$$\epsilon_1 = \frac{\sigma_1}{E_1} + \frac{d_{31}}{t_p} V_{33} \quad \text{or} \quad \epsilon_{geom} = \frac{\sigma_{el}}{E} + \mu V \tag{5}$$

where d_{31} is the piezoelectric charge coefficient, V_{33} the applied voltage and $\mu = d_{31}/t_p$. This is analogous to thermally induced strain. This implies that although in this analysis piezoelectric actuators have been used, any linear induced strain actuator could be used.

The equations of motion are derived using Lagrange's equation. As there are no external forces (the force applied by the PZT is included as an applied strain) or gyroscopic terms and there is no added damping (only hysteretic material damping being considered), Lagrange's equation reduces to:

$$\frac{d}{dt}\left(\frac{\partial T}{\partial \dot{q}_i}\right) + \frac{\partial U}{\partial q_i} = 0 \tag{6}$$

where q_i are generalised coordinates, T is kinetic energy and U is potential energy.

The *kinetic energy* of the composite beam is the sum of the kinetic energy in each layer of the composite beam, i.e.

$$T = T_b + 2\{T_v + T_c + T_p\} \tag{7}$$

where,

$$T_b = \frac{1}{2}\int_0^L m_b \dot{u}_r^2 dx \quad T_v = \frac{1}{2}\int_{a_1}^{a_2} m_v \frac{\dot{u}_c^2 + \dot{u}_c\dot{u}_r + \dot{u}_r^2}{3} dx$$

$$T_c = \frac{1}{2}\int_{a_1}^{a_2} m_c \dot{u}_c^2 dx \quad T_p = \frac{1}{2}\int_{b_1}^{b_2} m_p \dot{u}_c^2 dx$$

where m refers to mass per unit length. The velocity of the viscoelastic layer is assumed to vary linearly across its thickness.

The *strain* (potential) energy of each layer can be obtained from,

$$U = \tfrac{1}{2}\int_{\text{volume}} (\text{stress} \times \text{elastic strain})\, d\,\text{vol} \tag{8}$$

Substituting the relationships developed for the strain in each layer in Eqs. (2), (3), (4) and (5) into Eq. (8) the total strain energy is found to be,

$$U = U_b + 2\{U_v + U_c + U_p\} \tag{9}$$

where

$$U_b = \frac{1}{2}\int_0^L E_b A_b u_r'^2 dx$$

$$U_v = \frac{1}{2}\int_{a_1}^{a_2} G_v A_v \gamma_v^2 dx = \frac{1}{2}\int_{a_1}^{a_2} G_v A_v \left(\frac{u_c - u_r}{t_v}\right)^2 dx$$

$$U_c = \frac{1}{2}\int_{a_1}^{a_2} E_c A_c u_c'^2 dx \quad U_p = \frac{1}{2}\int_{b_1}^{b_2} E_p A_p (u_c' - \mu V)^2 dx$$

where E is Young's modulus, G is shear modulus and A refers to the cross-sectional area.

Substituting the kinetic and potential energy terms from Eqs. (7) and (9) into the Lagrange Eq. (6) gives the equation of motion for the beam as

$$[M]\ddot{\mathbf{q}} + [K]\mathbf{q} = \mathbf{P}V \tag{10}$$

where

$$M = \begin{bmatrix} \int_0^L m_b \phi\phi^T dx + \frac{2}{3}\int_{a_1}^{a_2} m_v \phi\phi^T dx & \frac{1}{3}\int_{a_1}^{a_2} m_v \phi\psi^T dx \\ \frac{1}{3}\int_{a_1}^{a_2} m_v \psi\phi^T dx & \frac{2}{3}\int_{a_1}^{a_2} m_v \psi\psi^T dx + 2\int_{a_1}^{a_2} m_c \psi\psi^T dx + 2\int_{b_1}^{b_2} m_p \psi\psi^T dx \end{bmatrix}$$

$$K = \begin{bmatrix} \int_0^L E_b A_b \phi'\phi'^T dx + 2\int_{a_1}^{a_2} \frac{G_v A_v}{t_v^2} \phi\phi^T dx & -2\int_{a_1}^{a_2} \frac{G_v A_v}{t_v^2} \phi\psi^T dx \\ -2\int_{a_1}^{a_2} \frac{G_v A_v}{t_v^2} \psi\phi^T dx & 2\int_{a_1}^{a_2} \left[\frac{G_v A_v}{t_v^2} \psi\psi^T + E_c A_c \psi'\psi'^T\right] dx + 2\int_{b_1}^{b_2} E_p A_p \psi'\psi'^T dx \end{bmatrix}$$

$$\mathbf{P} = \begin{bmatrix} \mathbf{0} \\ 2\int_{b_1}^{b_2} E_p A_p \mu\psi' dx \end{bmatrix} \quad \mathbf{q} = \begin{bmatrix} \mathbf{r} \\ \mathbf{c} \end{bmatrix}$$

The shape functions for the series expansions are assumed as clamped-free longitudinal beam modes, namely

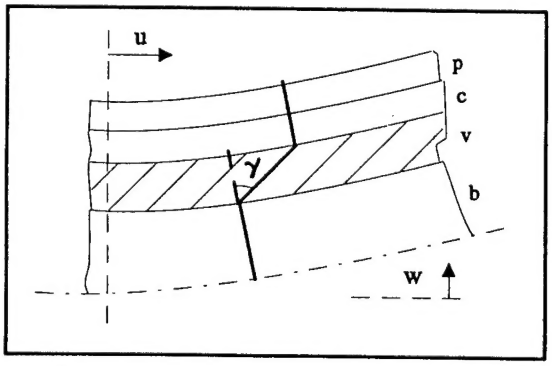

Fig. 4 Deformations of the beam in flexural motion

$$\phi_j(x) = \psi_j(x) = \sin\frac{(2j-1)\pi}{2L}x; \quad j = 1, 2, \ldots \quad (11)$$

Note that the mathematical model will not represent the detailed load diffusion around the ends of the PZT and constraining layers accurately. However, the overall behaviour of the beam to the PZT activation should be adequately represented if sufficient terms are used in the series expansion.

This model can also approximate the case where the actuators are bonded directly to the beam. This can be done by setting the constraining layer thickness to zero and by giving the shear layer the dimensions and properties of a stiff bonding layer such as cyanoacrylate.

Hysteretic damping is assumed in all members of the composite beam and this is included in the model using complex modulus notation, i.e.

$$E = E'(1 + i\eta) \quad (12)$$

where E is the complex modulus of elasticity, E' is the storage modulus and η is the loss factor. Assuming harmonic motion yields,

$$E\mathbf{q} = E'(\mathbf{q} + i\eta\mathbf{q}) = E'\left(\mathbf{q} + \frac{\eta}{\Omega_{ex}}\dot{\mathbf{q}}\right) \quad (13)$$

where Ω_{ex} is the frequency of excitation.

Assuming steady state motion, this assumption can be applied to each layer of the composite beam in the stiffness matrix yielding the effective viscous *damping* matrix.

$$C = \frac{1}{\Omega_{ex}}\begin{bmatrix} \int_0^L E_b A_b \eta_b \phi' \phi'^T dx + 2\int_{a_1}^{a_2} \frac{G_v A_v \eta_v}{t_v^2}\phi\phi^T dx & -2\int_{a_1}^{a_2} \frac{G_v A_v \eta_v}{t_v^2}\psi\psi^T dx \\ -2\int_{a_1}^{a_2} \frac{G_v A_v \eta_v}{t_v^2}\phi\psi^T dx & 2\int_{a_1}^{a_2}\left[\frac{G_v A_v \eta_v}{t_v^2}\psi\psi^T + E_c A_c \eta_c \psi'\psi'^T\right]dx + 2\int_{b_1}^{b_2} E_p A_p \eta_p \psi'\psi'^T dx \end{bmatrix} \quad (14)$$

It should be noted that the stiffness and loss factor of viscoelastic materials vary with frequency. These values are obtainable for most commercial materials from the material reduced frequency master curve [12].

2.2 Flexural Motion. The same approach is now applied to flexural deformations of the beam which result when the signals applied to the PZT on either side of the beam are of opposite polarity. These deformations are shown in Fig. 4.

It is assumed that the flexural stiffness of the viscoelastic, PZT and constraining layers about their mid surfaces is negligible and that the lateral deflection (w) of all layers is equal. Shear deformation and rotary inertia of the beam are not included. From symmetry the nett longitudinal motion of the beam

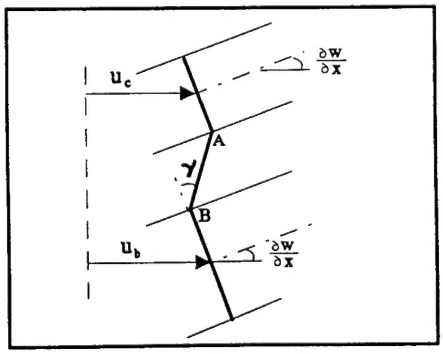

Fig. 5 Shear angle of the viscoelastic layer in flexural motion

Table 1

Component	Coverage over length	Cross Section (mm × mm)	Density (kg/m³)	Young's Modulus (GPa)
Beam - 0.158 m long	0 - 1	38 × 3.175	2700	70
Viscoelastic	0 - 1	38 × 0.202	1600	0.009*
Constraining Layer	0 - 1	38 × 0.254	2700	70
Piezo-actuator**	0.4 - 0.7	38 × 0.400	7800	70

* Young's Modulus of 3 MPa used for dynamic behaviour, Poisson's Ratio set at 0.499
** Piezoelectric charge coefficient assumed to be -180^{-12} C/N

(u_b) is zero. Once again the PZT and constraining layer are assumed to have compatible deformations.

The flexural motion is approximated by,

$$u_c(x, t) = \sum_{j=1}^{N_c} c_j(t)\cdot\psi_j(x) = \boldsymbol{\psi}^T\mathbf{c} \quad \text{and}$$

$$w(x, t) = \sum_{j=1}^{N_w} b_j(t)\cdot\varphi_j(x) = \boldsymbol{\varphi}^T\mathbf{b} \quad (15)$$

where,

$$\psi_j = \sin\frac{(2j-1)\pi}{2L}x; \quad j = 1, 2, 3 \ldots$$

$$\varphi_j(x) = \alpha_1 \sin\left(\frac{\lambda_j}{L}x\right) + \alpha_2 \cos\left(\frac{\lambda_j}{L}x\right) + \alpha_3 \sinh\left(\frac{\lambda_j}{L}x\right) + \alpha_4 \cosh\left(\frac{\lambda_j}{L}x\right)$$

These are normal mode shapes for a cantilevered beam in longitudinal and flexural motion respectively. The constants λ and α are tabulated in books such as Blevins [13].

From Fig. 5 the shear angle of the viscoelastic layer is,

$$\gamma = \frac{\partial w}{\partial x} + \frac{\partial u}{\partial z} = \frac{\partial w}{\partial x} + \frac{u_A - u_B}{t_v}$$

also,

$$u_A = u_c + \frac{t_c + t_p}{2}\cdot\frac{\partial w}{\partial x}; \quad u_B = u_b + \frac{t_b}{2}\cdot\frac{\partial w}{\partial x}$$

hence,

$$\gamma = \frac{u_c + \frac{t_D}{2}\frac{\partial w}{\partial x}}{t_v} = \frac{u_c + w'\frac{t_D}{2}}{t_v}; \quad t_D = t_b + 2t_v + t_c + t_p \quad (16)$$

The *kinetic* energy expression becomes,

$$T = [T_b + 2\{T_v + T_c + T_p\}]_{\text{flexural}} + [2\{T_v + T_c + T_p\}]_{\text{long}}$$

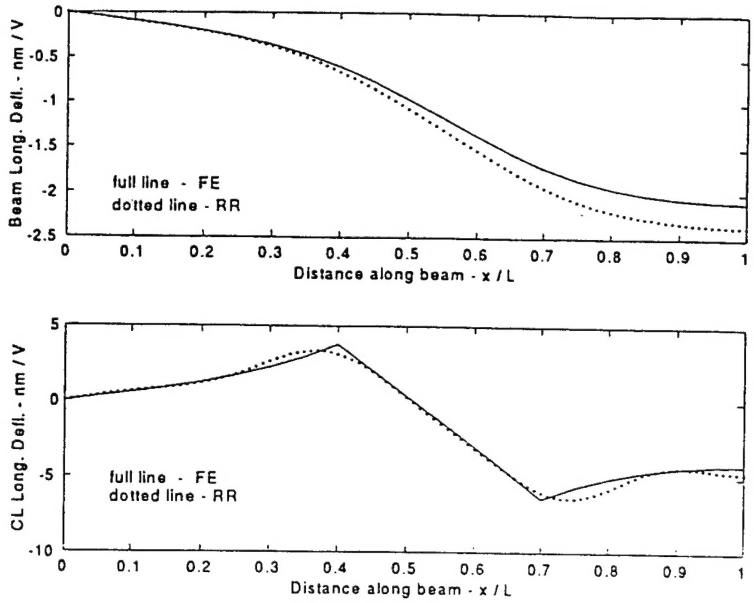

Fig. 6 Static longitudinal deflection of beam and constraining layer

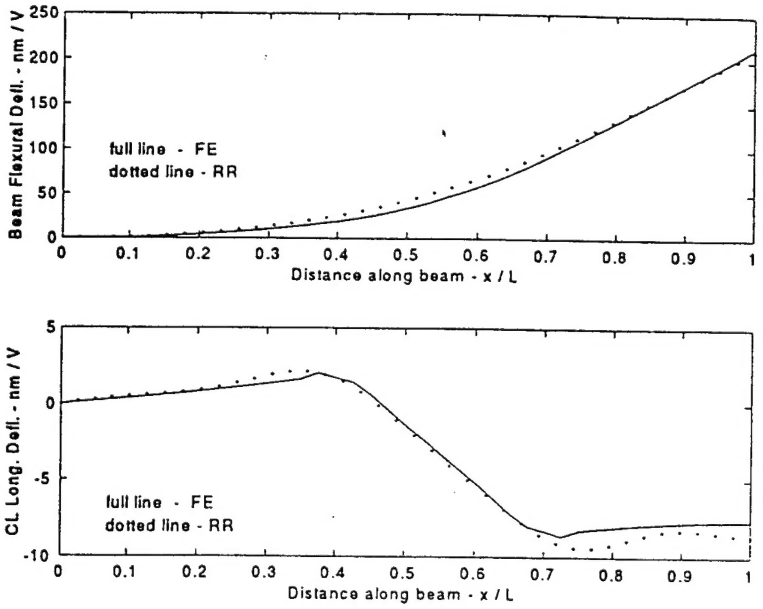

Fig. 7 Static flexural deflection of beam and longitudinal deflection of constraining layer

$$T_{\text{flexural}_{\text{total}}} = \frac{1}{2}\int_0^L m_b \dot{w}^2 dx + 2\left\{\frac{1}{2}\int_{a_1}^{a_2}(m_v + m_c)\dot{w}^2 dx + \frac{1}{2}\int_{b_1}^{b_2} m_p \dot{w}^2 dx\right\}$$

$$T_{\text{long}_{\text{total}}} = 2\left\{\frac{1}{2}\int_{a_1}^{a_2} m_v \frac{4\dot{u}_c^2 + 2\dot{u}_c\dot{w}' + \dot{w}'^2 t_b^2}{12} dx + \frac{1}{2}\int_{a_1}^{a_2} m_c \dot{u}_c^2 dx + \frac{1}{2}\int_{b_1}^{b_2} m_p \dot{u}_p^2 dx\right\} \quad (17)$$

The *strain* energy expression is,

$$U = U_b + 2\{U_v + U_c + U_p\}$$

$$U_b = \frac{1}{2}\int_0^L E_b I_b (w'')^2 dx \quad U_v = \frac{1}{2}\int_{a_1}^{a_2} A_v G_v \left(\frac{u_c + w'\frac{t_D}{2}}{t_v}\right)^2 dx$$

$$U_c = \frac{1}{2}\int_{a_1}^{a_2} A_c E_c (u_c')^2 dx$$

$$U_p = \frac{1}{2}\int_{b_1}^{b_2} A_p E_p (u_c'^2 - 2u_c'\mu V + \mu^2 V^2) dx \quad (18)$$

where I is the second moment of area of the beam cross section.

Once again, substituting into Lagrange's equation and including hysteretic damping gives the steady state equation of motion.

$$[M]\ddot{\mathbf{q}} + [C]\dot{\mathbf{q}} + [K]\mathbf{q} = \mathbf{P}V \quad (19)$$

$$M = \begin{bmatrix} \left[\int_0^L m_b\varphi\varphi^T dx + 2\int_{a_1}^{a_2}(m_v + m_c)\varphi\varphi^T dx + 2\int_{b_1}^{b_2} m_p\varphi\varphi^T dx + \frac{t_b^2}{6}\int_{a_1}^{a_2} m_v\varphi'\varphi'^T dx\right] & \frac{t_b}{6}\int_{a_1}^{a_2} m_v\varphi\psi'^T dx \\ \frac{t_b}{6}\int_{a_1}^{a_2} m_v\psi\varphi'^T dx & \frac{2}{3}\int_{a_1}^{a_2} m_v\psi\psi^T dx + 2\int_{a_1}^{a_2} m_c\psi\psi^T dx + 2\int_{b_1}^{b_2} m_p\psi\psi^T dx \end{bmatrix}$$

$$K = \begin{bmatrix} \int_0^L E_b I_b\varphi''\varphi''^T dx + \int_{a_1}^{a_2}\frac{A_v G_V t_D^2}{2t_v^2}\varphi'\varphi'^T dx & \int_{a_1}^{a_2}\frac{A_v G_v t_D}{t_v^2}\varphi'\psi^T dx \\ \int_{a_1}^{a_2}\frac{A_v G_v t_D}{t_v^2}\psi\varphi'^T dx & 2\int_{a_1}^{a_2}\left[\frac{A_v G_v}{t_v^2}\psi\psi^T + A_c E_c\psi'\psi'^T\right]dx + 2\int_{b_1}^{b_2} A_p E_p\psi'\psi'^T dx \end{bmatrix}$$

$$C = \frac{1}{\Omega_{ex}}\begin{bmatrix} \int_0^L E_b I_b\eta_b\varphi''\varphi''^T dx + \int_{a_1}^{a_2}\frac{A_v G_v\eta_v t_D^2}{2t_v^2}\varphi'\varphi'^T dx & \int_{a_1}^{a_2}\frac{A_v G_v\eta_v t_D}{t_v^2}\varphi'\psi^T dx \\ \int_{a_1}^{a_2}\frac{A_v G_v\eta_v t_D}{t_v^2}\psi\varphi'^T dx & \left[2\int_{a_1}^{a_2}\frac{A_v G_v\eta_v}{t_v^2}\psi\psi^T dx + 2\int_{a_1}^{a_2} A_c E_c\eta_c\psi'\psi'^T dx + 2\int_{b_1}^{b_2} E_p A_p\eta_p\psi'\psi'^T dx\right] \end{bmatrix}$$

$$\mathbf{P} = \begin{bmatrix} \mathbf{0} \\ 2\int_{b_1}^{b_2} A_p E_p\mu\psi' dx \end{bmatrix} \quad \mathbf{q} = \begin{bmatrix} \mathbf{b} \\ \mathbf{c} \end{bmatrix}$$

3 Validation of the Mathematical Model

The model which has been developed includes approximations for the deformations of the beam, both longitudinally and in flexure, and also includes assumptions regarding the nature of the stresses and strains developed. The use of the approach employed must be validated. Thus, the Rayleigh-Ritz (RR) model, developed in the previous section, is now compared with results obtained from both finite element analysis and physical experiments.

3.1 Comparison With Finite Element Analysis. Finite element (FE) models were used to predict the natural frequencies and mode shapes of the composite beam in both longitudinal and flexural motion. The models were also used to find the deflections caused by static voltages applied to the PZT actuators: equal magnitude and polarity for longitudinal deflection and equal magnitude but opposite polarity for flexural deflection. These results were then compared with output from the RR model. Dimensions and material properties of the beam are given in table 1.

A mesh of 40 × 4, eight noded, isoparametric membrane elements was used to model the cantilever beam. Layers one element thick were used to model the viscoelastic material, constraining layers and PZT actuators. In the case of longitudinal motion, in order to replicate simple extensional behaviour, all nodes were constrained to move in the longitudinal direction only and Poisson's ratio was set to zero.

The characteristic strain induced in a structure, when a voltage is applied across the activating piezoelectric material, was considered analogous to a thermal strain. The piezoelectric effect was therefore simulated on the FE model via thermal loading. This approach is acceptable if the piezoelectric patch is assumed to be linear.

3.1.1. Static Behaviour. Figure 6 shows the extension induced along the length of the beam and constraining layer when a static 1 volt potential was applied to the PZTs. This was represented in the FE model by setting the thermal coefficient of expansion of the PZT equal to d_{31}/t_p (the other coefficients being set to zero) and then subjecting the structure to a 1°C temperature rise. The results obtained using the RR method match the FE prediction closely. It was found that as the PZT patch size was reduced the number of assumed shapes used to represent the constraining layer extension had to be increased to retain accuracy. Nine shapes were used in the example presented.

The flexural deflection of the beam and the longitudinal deflection of the constraining layer induced by applying a static 1 volt potential to the PZTs (with an opposite polarity for each PZT) is shown in Fig. 7. Once again the close agreement between RR and FE results indicate the validity of the RR approach.

3.1.2. Dynamic behaviour. Comparisons of the first four natural frequencies and mode shapes for both longitudinal and flexural motion, found using FE and RR are shown in Figs. 8 and 9, respectively. These figures show that both methods give very similar results, thus validating the RR approach for obtaining natural frequencies and mode shapes. The constraining layer motion in this case also shows good agreement.

A full dynamic frequency response analysis was not possible as the finite element package used did not allow harmonic thermal loading.

3.2 Experimental Comparison. The experimental verification of the Rayleigh Ritz models developed involved exciting the beams by applying a band limited random voltage signal

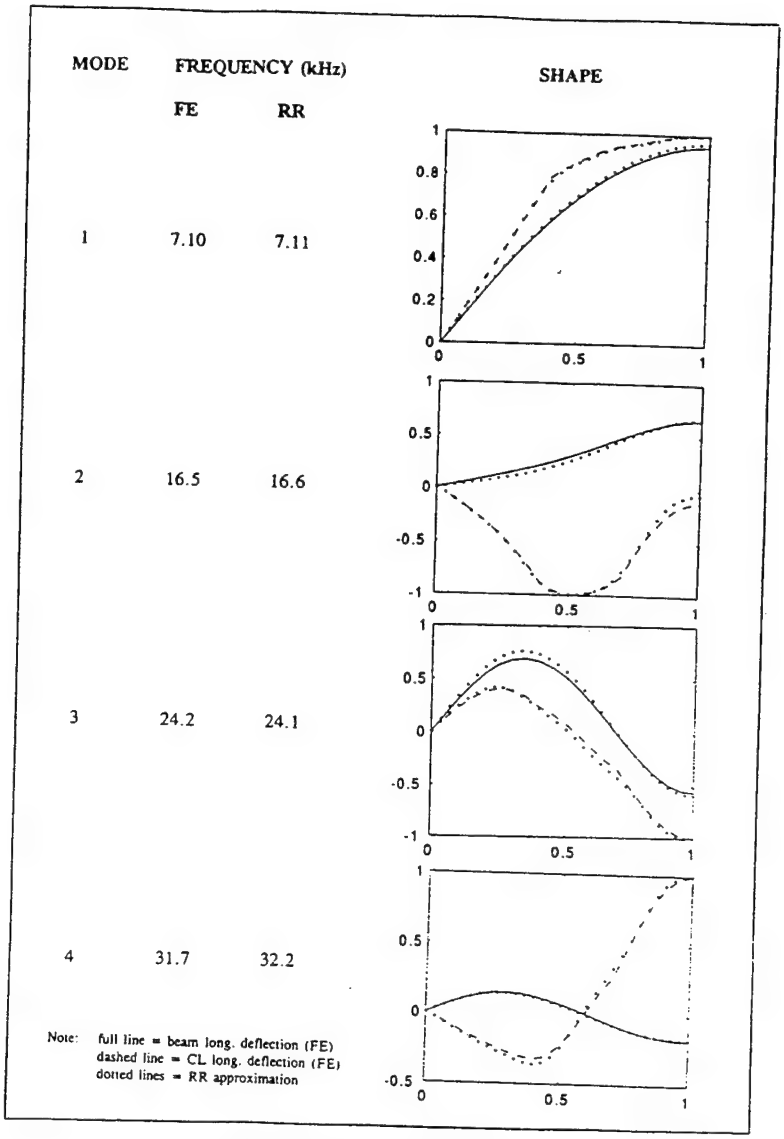

Fig. 8 Longitudinal natural frequencies and mode shapes

to the actuators to give the open loop frequency response. Values predicted by the theoretical model were compared with those obtained experimentally.

Two aluminium beams suspended in the vertical plane from fixed supports were tested. A length of constrained layer damping was applied to both faces of one of the beams, and PZT patches then attached to the constraining layer. For the other beam, the PZT patches were attached directly to the beam surface. The experimental layout is shown in Fig. 10.

The dimensions and physical properties of the beam with the damping treatment applied are shown in Table 2. The other beam was identical excluding the constrained layer damping treatment.

The PZT actuators were excited using a 0–100 kHz random voltage signal of approximately 100V peak-to-peak; the actuators were driven in phase to excite the longitudinal modes, then out of phase to excite the flexural modes. A d.c. bias voltage of approximately 120 volts was applied to the actuators to avoid any danger of depolarisation. A second amplifier was included to ensure that actuation levels at either side of the beam were equal in magnitude: gains were selected to give minimum flexural motion when the actuators were driven in phase, and minimum longitudinal motion when the actuators were driven out of phase. A small accelerometer, connected to a Bruel and Kjaer charge amplifier, was attached to the tip of each beam in an appropriate orientation to measure either the flexural or longitudinal motion.

The output of the high voltage amplifier was reduced to one fiftieth for measurement purposes using a resistor bridge network. The velocity/voltage frequency response function was measured at 4096 equally spaced frequency points over the bandwidth using a DIFA Scadas data acquisition system linked to a HP340 computer running LMS software. A range of 0–10 kHz for axial excitation and 0–100 Hz for the flexural case encompassed the first four modes of each.

Experimental results and theoretical predictions are presented in Figs. 11, 12, 13 and 14. Comparison of the results show that the RR model predicted the resonant frequencies accurately. A good prediction of peak heights was also achieved.

Slight variations in peak heights can be attributed to the lightly damped nature of the structures and the presence of factors that were not modelled such as friction at the clamped

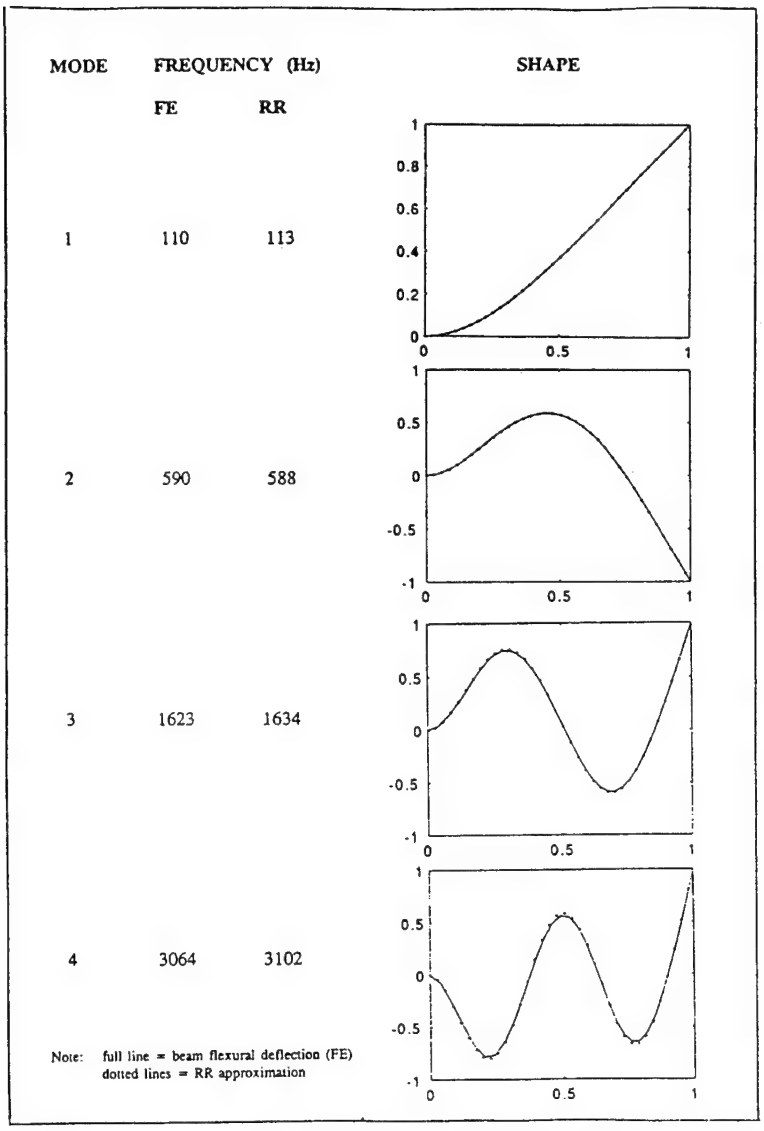

Fig. 9 Flexural natural frequencies and mode shapes

base. The 'noise' on the experimental results may be as a result of interaction with the support frame on which the beams were hung and also in the case of the longitudinal results, from flexural modes not completely cancelled. The effect of the accelerometer mounted on the beam tip was investigated for the longitudinal case by adding a two gram lumped mass in the theoretical model. The frequency response function is shown in Fig. 15. This shows that the differences in frequency for the higher modes (in the 5–10 kHz range) can be attributed, in part, to the effect of the added mass.

4 Investigation of Performance in Relation to Active Damping

The model has been developed to enable "active damping," as defined in this paper, to be investigated. Part of the investigation includes a comparison with conventional active control. The reduction in vibration levels achieved for a cantilever beam subject to a base excitation is investigated using the Rayleigh Ritz mode, modified to include base motion. Although many configurations and control strategies are possible, a full, optimised parametric study would require a paper on its own and is therefore not attempted here.

The study presented here considered two beam configurations:

(i) with actuators bonded directly to the beam (case A) and
(ii) with actuators bonded to a constraining layer (case B).

The dimensions and materials used in the simulation are shown in Table 3.

The tip velocity was the feedback signal used throughout the investigation. This signal, derived from an accelerometer, was used following earlier investigations [7] which showed that velocity feedback provided the most effective control over a large number of modes. The location of the actuator has also been investigated previously [7] where it was shown that the points of maximum curvature at each mode yield the most effective control action. Clearly there must be a compromise between the positions required for the different modes to be attenuated, but in the case of a simple beam such a point can be identified. Earlier work has also shown that co-located actua-

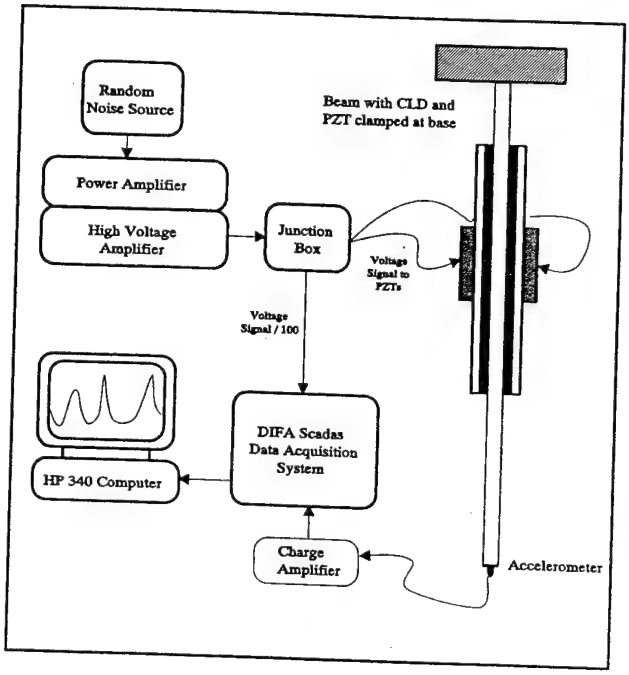

Fig. 10 Experimental lay-out for longitudinal and flexural beam tests

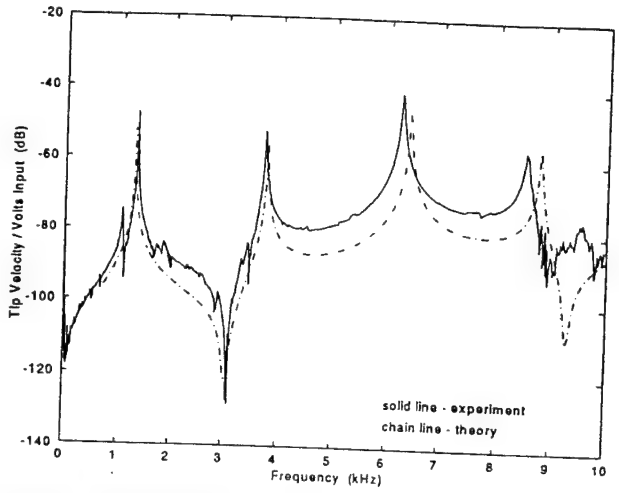

Fig. 12 Frequency response for beam with PZTs bonded to the beam directly-longitudinal motion

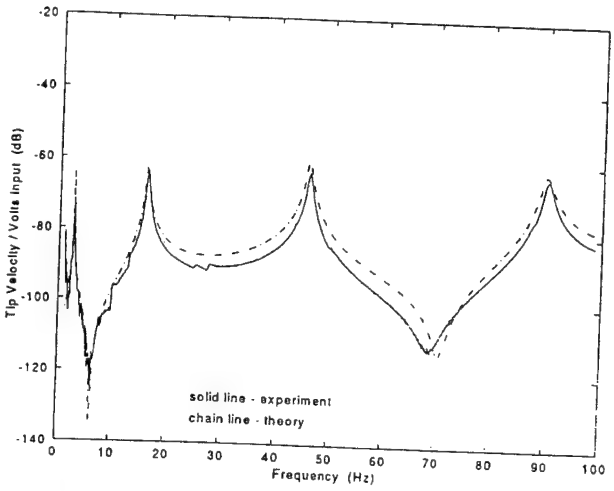

Fig. 13 Frequency response for beam with PZTs bonded to the constraining layer–flexural motion

tors and sensors reduce the spillover effect. However, in this work non-collocation has been used to further demonstrate the benefits of the current approach to the active damping problem.

Figures 16 and 17 show the variation in the base-to-tip transmissibility (i.e., the ratio of the magnitude of the motion at the tip to the magnitude of the prescribed base motion) of the beams as the feedback gain was increased. It can be seen that for the beam with no constraining layer (A), large values of transmissibility were obtained at the resonant frequencies and the third mode became unstable at a relatively low gain of around 50. The added damping gained from applying a constraining layer reduced resonance peaks for beam B considerably. In particular the fourth mode, which was almost unaffected by conventional active control, owing to the positioning of the actuators, was virtually cancelled. The unstable nature of the third mode, due to non-collocation of sensor and actuator, is barely evident: even at maximum gain the peak height is only a little higher.

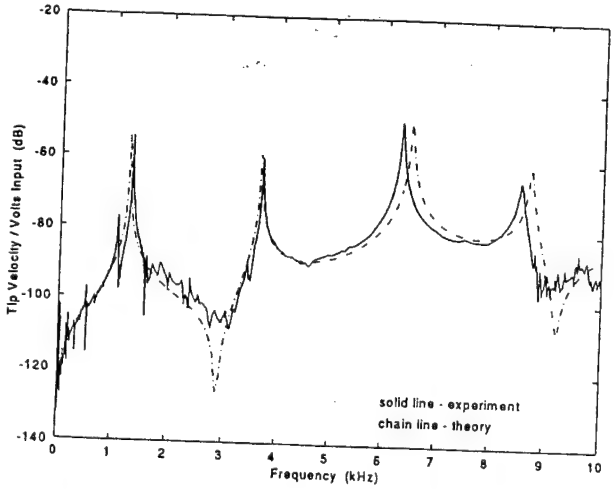

Fig. 11 Frequency response for beam with PZTs bonded to the constraining layer–longitudinal motion

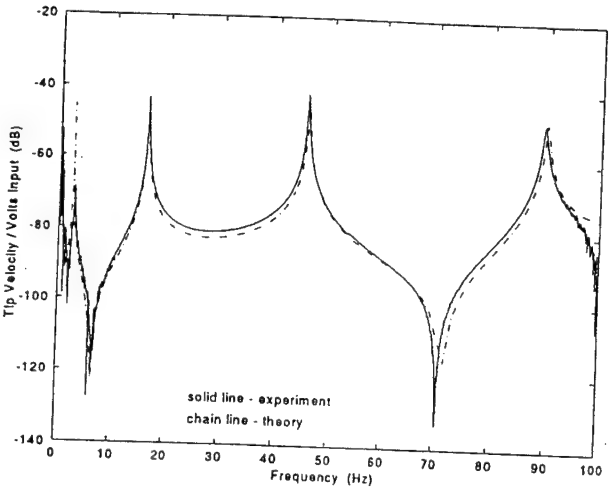

Fig. 14 Frequency response for beam with PZTs bonded to the beam directly–flexural motion

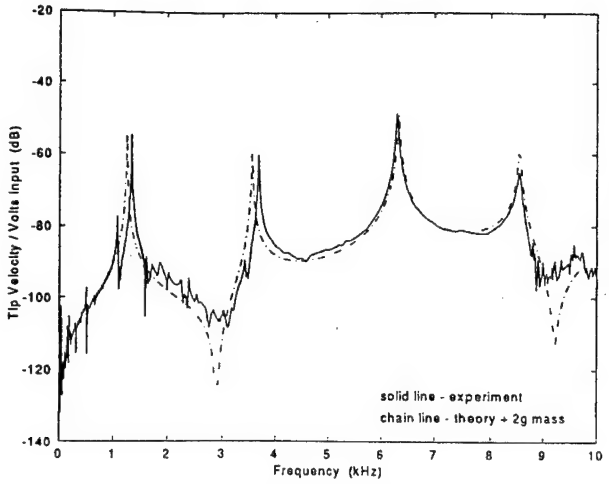

Fig. 15 Frequency response for beam with PZTs bonded to the constraining layer allowing for accelerometer mass–flexural motion

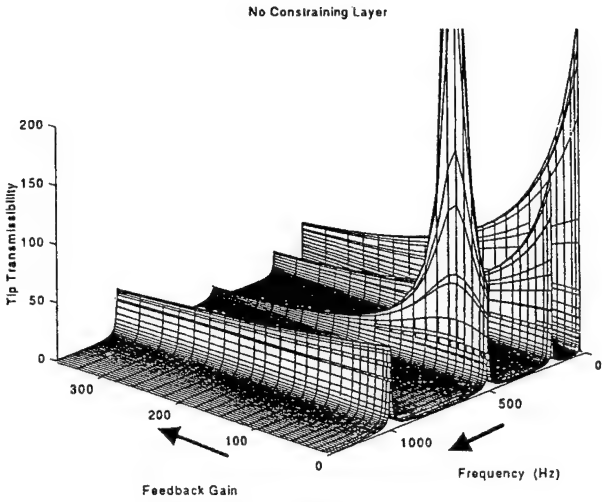

Fig. 16 Beam *A*–tip/base transmissibility

Experimental work [2] has shown that the maximum feedback gain that can be used is limited not only by instability of resonant modes but also by PZT material non-linearity at high voltage and the maximum available voltage itself. Figure 18 shows the variation of actuator voltage required to achieve a desired feedback gain when the base excitation has a peak acceleration of $0.5g$ over the bandwidth. Beam A required much higher voltages to reach the same gain levels than beam B. For example, if the maximum voltage was limited to 200V (400V peak-to-peak) the maximum feedback gains possible would be 50 for beam A and 270 for beam B. This shows that placing actuators on a constraining layer (beam B) not only gives improved reduction in resonant peaks for the same feedback *gain* but also gives the higher gains (and hence further reduction of resonance peaks) for the same *voltage*.

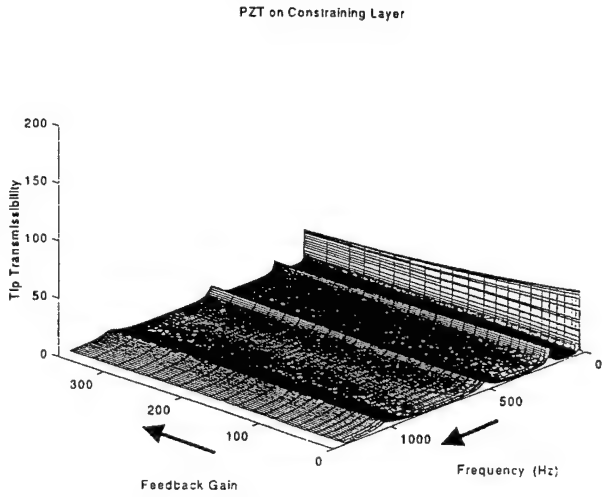

Fig. 17 Beam *B*–tip/base transmissibility

5 Conclusions

In this paper mathematical models have been developed to describe the longitudinal and flexural steady state vibration of

Table 2

Component	Material	Coverage (m)	Cross Section (mm × mm)	Density (kg/m³)	Mod. of Elasticity* (GPa)	Loss Factor
Beam	Aluminium	0 - 1	38 × 3.175	2700	70	0.004
Viscoelastic	ISD 112 **	0.275-0.525	38 × 0.127	1600	0.0001-0.01	0.5 - 1.1
Constr. Layer	Aluminium	0.275-0.525	38 × 0.254	2700	70	0.004
Piezo- Actuator	PZT *** Sonox P5	0.385-0.415	30 × 0.4	7700	62.5 (E_{11})	0.011

* The values quoted correspond to the shear modulus for ISD 112 and Young's modulus for the other materials.
** ISD 112 is a commercial viscoelastic manufactured by the 3M company. Purchased as a CLD preparation including the aluminium constraining layer.
*** Sonox P5 is manufactured by Hoechst CeramTec.

Table 3

Component	Material	Coverage (mm)	Cross Section (mm × mm)	Density (kg/m³)	Mod. of Elasticity (GPa)	Loss Factor
Beam	Aluminium	0 - 300	38 × 3.175	2700	70	0.004
Viscoelastic*	ISD 112	0 - 300	38 × 0.127	1600	0.0001-0.01	0.5 - 1.1
Constr. Layer*	Aluminium	0 - 300	38 × 0.254	2700	70	0.004
Piezo- Actuator	PZT Sonox P5	90 - 120	30 × 0.4	7700	62.5 (E_{11})	0.011

* Applied on beam B only.

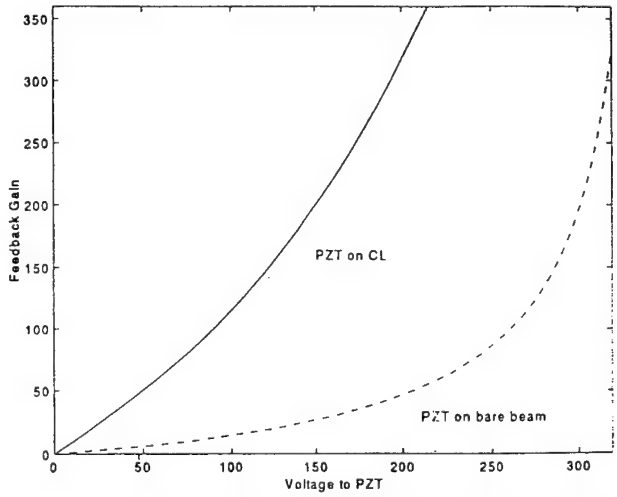

Fig. 18 Relationship between feedback gain and voltage with sinusoidal base motion of 0.5 g peak

beams with actuators bonded to a constrained layer damping treatment. The validity of these models has been verified statically and dynamically through finite element analysis and experimental work.

The derived models provide a convenient tool for the evaluation of the benefits of the "active damping" concept. The models allow the basic improvement in stability to be evaluated. The advantages have been shown to be;

(i) the improved attenuation over a wider range of frequency,
(ii) the reduction in control voltage to achieve the required attenuation,
(iii) the reduced sensitivity of the system stability yields a more robust control system,
(iv) the use of the passive constraining layer provides redundancy in the case of actuator failure or other control loop malfunctions.

The active control of a beam is relatively straightforward. The next stage in the work will be to extend the models to plates so that more realistic vibration control problems can be evaluated.

6 Acknowledgment

The work presented in this paper was financially supported by the U.S. Air Force through the European Office of Aerospace Research and Development (EOARD).

7 References

1. Balas, M. J., "Trends in Large Space Structure Control Theory: Fondest Hopes, Wildest Dreams," *IEEE Transactions on Automatic Control*, Vol. AC-27, pp. 522–535, June 1982.
2. Plump, J. M., & Hubbard, J. E., "Modelling of Active Constrained Layer Damper," 12th International Congress on Acoustics, Paper no. D41, Toronto, July 1986.
3. Baz, A., "Active Constrained Layer Damping," Damping '93 Conference, San Francisco, Feb. 1993.
4. Shen, I. Y., "Bending-Vibration Control of Composite and Isotropic Plates Through Intelligent Constrained Layer Treatments," *Journal of Smart Materials and Structures*, Vol. 3, pp. 59–70, 1994.
5. Van Nostrand, W. C., Knowles, G. J., Inman, D. J., "Active Constrained Layer Damping for Micro-satellites," *Dynamics and Control of Structures in Space*, Vol. 2, pp. 667–681, edited by: Kirk, C. L. & Hughes, P. C.
6. Azvine, B., Tomlinson, G. R., and Wynne, R. J., "Initial Studies in the Use of Active Constrained Layer Damping for Controlling Resonant Vibration," submitted to the *Journal of Smart Materials and Structures*, 1994.
7. Azvine, B., Tomlinson, G. R., Wynne, R. J., and Sensburg, O., "Vibration Suppression of Flexible Structures Using Active Damping," 4th International Conference on Adaptive Structures, Cologne, Nov. 1994.
8. Leibowitz, M. M., & Vinson, J. R., "Active (Piezoelectric) Constrained Layer Damping in Composite Sandwich Structures," 4th International Conference on Adaptive Structures, Cologne, Nov. 1994.
9. Mead, D. J., & Markus, S., "The Forced Vibration of a Three Layer Damped Sandwich Beam with Arbitrary Boundary," *Journal of Sound and Vibration*, Vol. 10, pp. 163–175, 1969.
10. Baz, A., & Ro, J., "Performance Characteristics of Active Constrained Layer Damping," submitted to the *Journal of Smart Materials and Structures*, 1994.
11. Van Nostrand, W. C., Knowles, G. J., Inman, D. J., "Finite Element Methods for Active Constrained Layer Damping," Passive Damping—North American Conference on Smart Structures and Materials, pp. 126–137, Orlando, 1994.
12. Eisele, U., *Introduction to Polymer Physics*, Springer-Verlag, USA, 1990.
13. Blevins, R. D., *Formulas for Natural Frequency and Mode Shape*, Van Nostrand Reinhold, New York, 1979.

Smart Mater. Struct. 4 (1995) 1–6. Printed in the UK

Use of active constrained-layer damping for controlling resonant vibration

B Azvine†, G R Tomlinson‡ and R J Wynne‡

† Dynamics & Control Research Group, University of Manchester, Manchester, UK
and
‡ Staffordshire University, Stafford, UK

Received 30 June 1994, accepted for publication 26 September 1994

Abstract. The work described in this paper is concerned with controlling the strain of the constraining layer of a composite structure in such a way as to enhance the shear generated in the viscoelastic material and hence improve the overall damping of the composite structure.

The results have indicated that this concept of active damping produces very effective levels of vibration suppression. In the case of cantilever beams the vibration levels in the first two modes can be almost eliminated when velocity feedback of the beam tip is used. The results show that the addition of active control and passive damping in a single structure combines the advantages of passive damping in the higher modes and active control in the lower modes. In addition active damping as defined in this paper produces a fail-safe mechanism in case of instability occurring in the feedback loop since a considerable level of passive damping is always present.

Notation

A	area
E	Young's modulus
e	actuator force per unit voltage
b	width of beam
d_{31}	voltage constant
G	shear modulus
h'	distance, neutral axis of beam to actuator
i, j	mode number
K	amplifier gain
L	beam length
m	mass per unit length
M	total applied moment
p	thickness of piezoceramic pads
q_i	generalized coordinate
r, s	constants
t	time
$V(t)$	voltage driving the piezoceramic
x	coordinate
y	displacement in the plane of bending
α	actuator moment per unit voltage
γ	shear angle
ρ	density
ϵ	strain
η	loss factor
Δ	displacement
ω_i	ith natural frequency
ζ_i	ith damping ratio of the composite beam
δ_i	added damping due to velocity feedback
$\phi_i(x)$	ith mode shape function
Ω	displacement function
Ψ	objective function.

1. Introduction

Many advances have been made in the use of piezoelectric ceramics and piezoelectric polymers in vibration and control problems. Theoretical models have been developed [1, 2] to predict the behaviour of an actively controlled structure consisting of alternate layers of piezoelectric sensors and actuators connected to the structure. These types of structure are often referred to as smart structures.

In the area of smart structures the concept of active damping has received considerable attention in the past few years. Active damping can be achieved by using piezoelectric materials to induce extra damping in a structure, hence reducing the vibration levels at resonance in various modes of vibration. Extra damping can be created in a structure in a number of ways. The most common method is to apply forces to the structure which are 90 degrees out of phase to the motion of the structure.

The technique used in this study is to enhance the damping of a passive element in the structure by active means. This can be done effectively when constrained-layer damping (CLD) is used. The constraining layer is bonded to the structure using a viscoelastic material which

0964-1726/95/010001+06$19.50

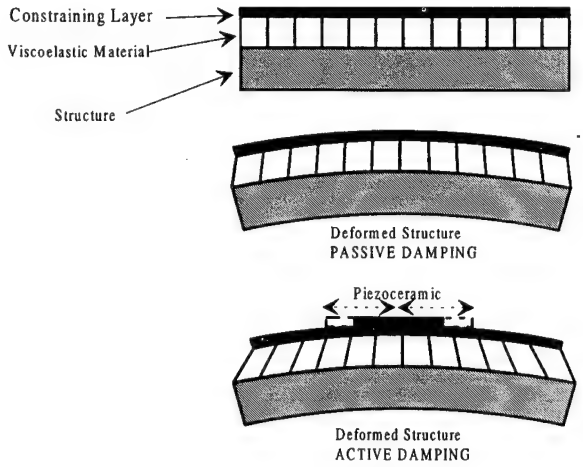

Figure 1. Basic mechanism of active damping.

acts as a passive damping element. By actively controlling the motion of the constraining layer, increased damping via shear energy dissipation is obtained. There are two ways of achieving this. One is to use a piezoelectric polymer as the constraining layer and control its motion by applying the appropriate voltage across it [3, 13, 14]. The second technique is to use piezoelectric materials bonded to a metallic constraining layer and is the approach used in the present study.

2. Active damping

Consider a piezoceramic element bonded to the constraining layer of a beam. The viscoelastic material between the beam and the constraining layer is subject to shear as a result of the constraining layer. The piezoceramic can be used to control the strain of the constraining layer and hence the amount of shear in the viscoelastic material as shown in figure 1.

If we consider the forced vibration of the beam, the force applied by the piezoceramic (PZT) element on the beam produces a bending moment M which is a function of the applied voltage $V(t)$ [4]

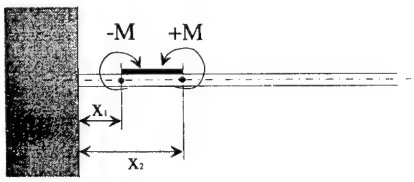

$$M = \alpha\{\phi_i'(x_2) - \phi_i'(x_1)\}V(t) = \alpha_i V(t) \tag{1}$$

where $\alpha = eh'$, h' is the distance between the neutral axis of the composite beam and the piezoactuator and e is the actuator force per unit applied voltage. If the normal modes of the structure ϕ_i are known, the flexural vibration at any point x can be represented by

$$y(x, t) = \sum_{i=1}^{\infty} q_i(t)\phi_i(x) \tag{2}$$

where q_i is the generalized coordinate [5, 6]. The choice of the feedback signal, $V(t)$, determines the damping and stiffness properties of the composite structure. If the feedback voltage is proportional to the velocity of the tip of the beam i.e.

$$V(t) = -K\dot{y}(L, t) = -K\sum_{i=1}^{\infty}\dot{q}_1(t)\phi_i(L) \tag{3}$$

the equation of motion can then be written as

$$\ddot{q}_i(t)+(2\zeta_i\omega_i+\delta_i)\dot{q}_i(t)+\omega_i^2 q_i(t) = \frac{-\alpha_i K\sum_{j\neq 1}^{\infty}\dot{q}_j(t)\phi_j(L)}{\int_0^L m\phi_i^2(x)\,dx} \tag{4}$$

where

$$\delta_i = \frac{-\alpha_i K\phi_i(L)}{\int_0^L m\phi_i^2(x)\,dx}.$$

It can be seen from equation (4) that the overall effect of velocity feedback is an extra term added to the damping coefficient (δ_i) [9–11].

Several experiments were carried out on aluminium beams (150 mm × 38 mm × 3 mm) in order to investigate the active damping concept. The emphasis was on developing a good practical understanding of the way an actively damped beam behaved with various feedback signals and beam actuator/sensor configurations.

The piezoelectric element was a SONOX P5 single-layer plate (30 mm × 30 mm × 0.4 mm) bonded to the constraining layer using X60 strain gauge glue at a location $x = 0.25L$ from the root of the beam, where the curvature of the beam in the first two modes is appreciable. The constraining layer used in the experiment was SOUNDFOIL (manufactured by SOUNDCOAT Co) which consisted of aluminium foil of thickness 0.254 mm coated with modified copolymer of thickness 0.05 mm which was applied directly to the beam.

Typical results are shown in figure 2. Three cases are shown: a beam with no feedback and no added damping (simple beam), a beam with CLD but no feedback (passive damping), and finally a beam with CLD and feedback control (active damping). Considering the beam with CLD only it can be seen that the second mode is attenuated significantly more than the first mode. This is not surprising because the particular passive damping element used performed better at higher frequencies. The normalized damping ratio i.e. the damping ratio in each mode to that of the simple beam (i.e. the beam with no added passive or active damping) is 3.9 in the first mode and 7.7 in the second mode. With active damping the normalized damping ratios in the first and second mode are 26 and 22 respectively. Table 1 summarizes these results. It can be seen that active damping significantly reduces the vibration levels in the first two modes.

3. Assessing the performance of active damping

The active damping mechanism is provided by a combination of extra induced shear strain in the constrained

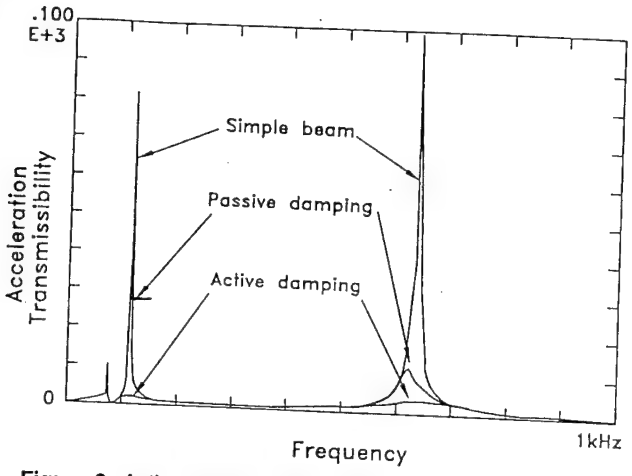

Figure 2. Active damping with single actuator.

Table 1. Comparison of the damping ratios in the first two modes of vibration using active damping.

	Normalized damping ratio	
Beam type	First mode	Second mode
Simple beam	1	1
Beam with CLD	3.9	7.7
Active damping	25.8	22.4

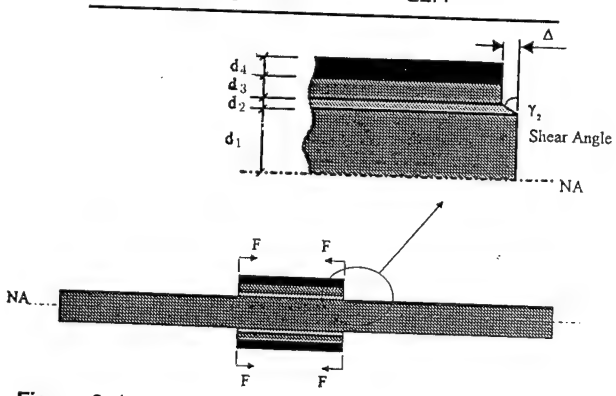

Figure 3. Local active damping with symmetrical actuators.

layer arising from a combination of the bending-induced shear and the additional shear from the active deformation of the PZT element. In order to determine the effect of the induced shear in isolation from the induced-bending effects a symmetrical arrangement can be used as shown in figure 3 where the actuation moments cancel leaving only the axial forces to produce the axial deformation of the constraining layer.

For small strains the axial deformation is

$$\Delta = d_2\gamma_2. \tag{5}$$

The shear forces acting on the constraining layer are

$$F_s = G_2\gamma_2 A_2 \tag{6}$$

where

$$G_2 = G_{2R}(1 + j\eta_1). \tag{7}$$

These produce an axial strain

$$\epsilon_x = \frac{\partial \Delta}{\partial x}. \tag{8}$$

The shear forces produce a change in the stress in the constraining layer such that

$$A\frac{\partial \sigma_x}{\partial x} = G_2\gamma_2 b_3. \tag{9}$$

The resulting axial stress is

$$\sigma_x = E_3\epsilon_x = E_3\frac{\partial \Delta}{\partial x}. \tag{10}$$

Combining equations (9) and (10) results in

$$\frac{\partial^2 \Delta}{\partial x^2} = \frac{G_2\gamma_2}{d_3 E_3}. \tag{11}$$

Now if we assume harmonic excitation of the piezoceramic pads

$$\Delta = Ce^{-jkx} \qquad \text{with } k = \frac{\omega}{\sqrt{E_3/\rho_2}} \tag{12}$$

then

$$\Delta = \frac{G_2\gamma_2}{k^2 d_3 E_3} = \frac{G_2\gamma_2}{\omega^2\rho_3 d_3}. \tag{13}$$

Using the standard equations for a PZT plate

$$\epsilon_{\max} = -d_{31}\frac{V_{\max}}{d_4} \tag{14}$$

therefore

$$\Delta = \epsilon_{\max} L = -d_{31}\frac{VL}{d_4}. \tag{15}$$

Combining equations (13) and (15) results in

$$\gamma_2 = \frac{\omega^2\rho_3 d_3 V_{\max} L d_{31}}{G_2 d_4}. \tag{16}$$

The energy dissipated per cycle in the viscoelastic layer due to the axial motion can be expressed as [12]

$$W_A = \pi\eta_2 G_{2R} d_2 |\gamma_2|^2 = \pi\eta_2 G_{2R} d_2 \left|\frac{\omega^2\rho_3 d_3 V_{\max} L d_{31}}{G_2 d_4}\right|. \tag{17}$$

The shear angle associated with the bending of the beam is

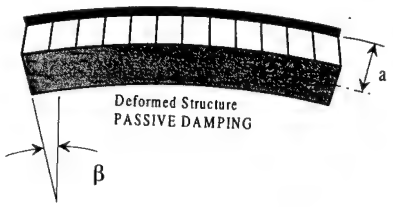

$$\gamma_2' = \frac{\beta a E_3 d_3 k^2}{(E_3 d_3 d_2 k^2 + G_2)}. \tag{18}$$

The energy dissipated per cycle due to the bending is

$$W_B = \pi\eta_2 G_{2R} d_2 |\gamma_2'|^2. \tag{19}$$

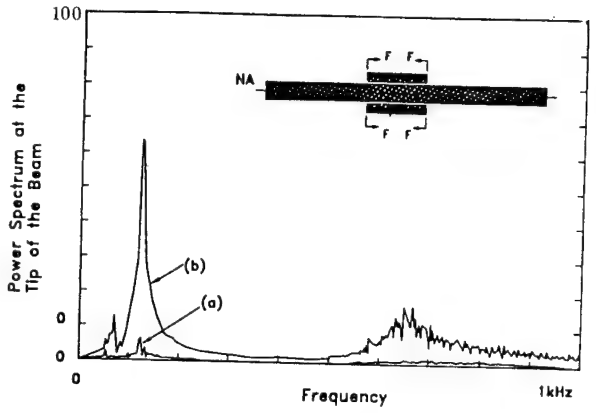

Figure 4. Assessing the efficiency of single or dual PZT element excitation: (a) dual element excitation; (b) single element excitation.

The condition for dissipating extra energy in the constrained-layer material is

$$\frac{W_A}{W_B} = \left|\frac{\gamma_2}{\gamma_2'}\right|^2 > 1$$
$$= \left|\frac{\omega^2 \rho_3 V_{max} L d_{31}}{\beta a G_2 d_4 E_3 k^2}\left(E_3 d_2 d_3 k^2 + G_2\right)\right|^2 \qquad (20)$$

3.1. Experimental tests

In order to test the efficiency of cancelling the induced bending moments, the configuration shown in figure 4 was used whereby a random excitation signal was applied to both elements simultaneously and then to the top PZT element only (the beam being stationary). The results of the experiment showed that when the same signal was applied to both elements the resulting spectrum was almost flat as indicated by figure 4(a), proving that the dynamic bending moments had been effectively cancelled. When the signal was applied to only the top element the dynamics of the beam were excited and the flexural modes were excited as shown in figure 4(b).

To assess the effectiveness of the induced shear damping an experiment was carried out in which active damping with symmetrical actuators was compared to active damping with a single actuator and passive damping. The test configuration was the cantilever beam which was excited at its base and the acceleration transmissibility between the tip of the beam and the base excitation was recorded. A band-limited random signal 0–1 kHz was used. The results are shown in figure 5 and summarized in table 2. It can be seen that a significant percentage of the reduction in the amplitude of vibration in the first mode is due to the induced shear. The effect is less significant in the second mode. It is possible to improve the damping in the second mode by choosing a more suitable location for the piezoceramic element.

An added benefit of the constraining layers arises from the fact that it is possible to increase the feedback gain without inducing instability. Figure 6 shows the results of an experiment in which two identical beams were used, one with no constraining layer and the other with a global (full coverage) constraining layer in which the beam tip velocity was obtained. It can be seen that with the constraining-layer material the feedback voltage could be increased by a factor of almost 2.5, with a corresponding reduction in the tip velocity, before saturation of the PZT element occurred.

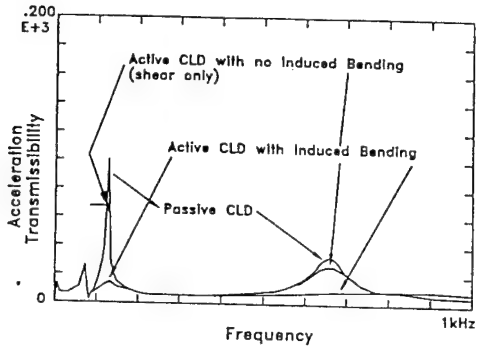

Figure 5. Active damping with and without bending moments.

Table 2. Reduction in the amplitude in the first two modes of vibration using active damping with and without bending moments.

	Reduction in amplitude (%)	
Beam type	First mode	Second mode
Beam with passive damping	0	0
Active damping with pure shear	48	15
Active damping with shear and bending	84	82

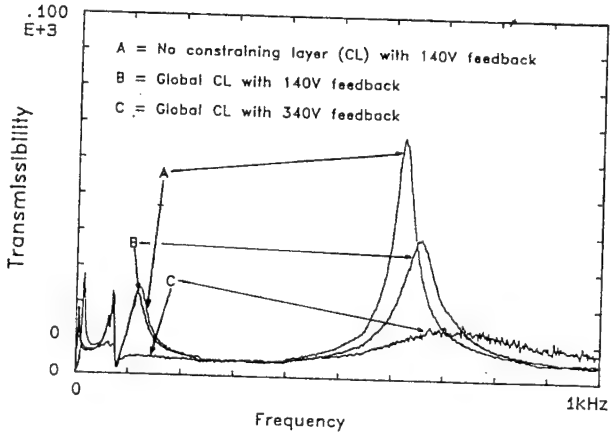

Figure 6. Maximum reduction in the tip velocity with and without constrained-layer damping.

4. Effect of actuator location

Because the strain in the constraining layer is modified by the piezoceramic element attached to it, the maximum differential strain across the viscoelastic layer can be generated at a location on the beam where the maximum surface strain occurs. Consider the area of the beam

covered by the piezoceramic pad. The optimum location for the pad is where the difference between the displacement at every cross section along the length of the piezoceramic pad and on the beam surface is a maximum. The beam surface strain is proportional to the curvature and hence the displacement at any point on the beam surface of an element of length dx is

$$\Delta_B = \phi''(x)\,dx. \tag{21}$$

Assuming a linear distribution of strain in the piezoceramic pad, the extension of an element length δx at any point on the ceramic is

$$\Delta_p = (rx + s)\delta x \tag{22}$$

where r and s are constants. The relative displacement of the piezoceramic element and the beam surface at any point can be written as

$$\Delta_R = \Delta_B - \Delta_p = [\phi''(x) = (rx + s)]\,dx. \tag{23}$$

The total relative displacement which is a measure of the induced shear in the viscoelastic material is

$$\Omega = \int_{x_1}^{x_2} [\phi''(x) - (rx + b)]\,dx = \phi'(x_2) - \phi'(x_1) - \left[r\left(\frac{x_2^2}{2} - \frac{x_1^2}{2}\right) + s(x_2 - x_2)\right] \tag{24}$$

where x_1 and x_2 represent the coordinates of the ends of the piezoceramic element on the beam and a and b are constants depending on the piezoceramic element properties and dimensions. The objective is to maximize the above expression over the length of the beam in every mode. If a single element is to be used to control more than one mode then the effectiveness of active damping can be formulated as an objective function with a separate term for each mode, where the term corresponding to each mode has a weighting factor. The weighting factors determine the relative reduction of amplitude required in each mode. If a single mode is selected then the weighting factors for all the other modes are set to zero and the optimization problem reduces to finding the position where the curvature is a maximum in that particular mode. The objective function can be written as

$$\Psi = \sum \lambda_n \Omega_n^2. \tag{25}$$

A numerical search technique can be used to solve this problem. The objective function can be plotted against the location of the actuator to find the maximum or minimum points where the gradient is equal to zero. Figure 7 shows the objective function plotted for the first two modes with $\lambda_1 = 1$ and $\lambda_2 = 0.2$. It can be seen that the objective function has a maximum value at $x_1 = 0$. The next local maximum is at $x_1 = 0.4$.

To demonstrate the validity of the above discussion an experiment was carried out in which two beams of length L, covered with constrained-layer damping material and with a piezoceramic element attached to the constraining layer were used. The piezoceramic element on one beam was placed at $0.25L$ from the clamped end and on the second beam at $0.4L$. A periodic random signal was applied to an excitor driving the clamped end of each beam and

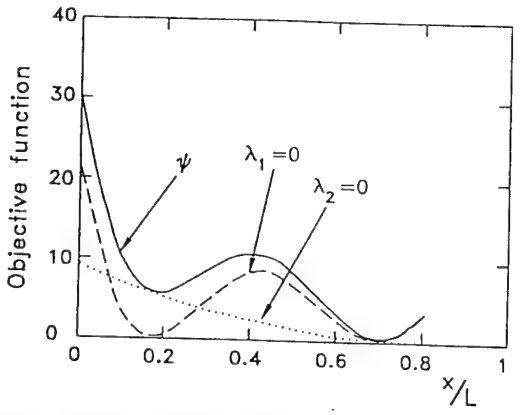

Figure 7. Objective function based on the location of a single actuator.

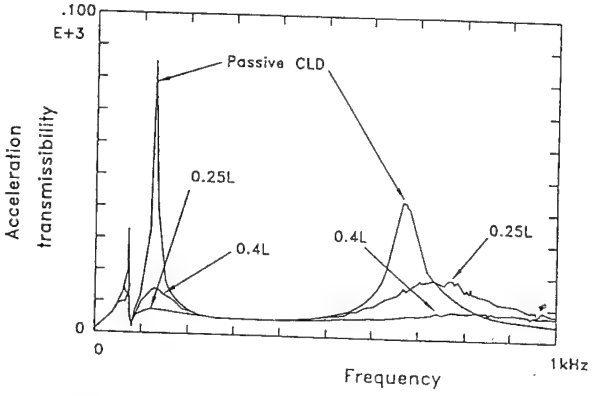

Figure 8. Effect of actuator location on active damping with a single actuator.

the tip velocity was used as the feedback signal to the PZT elements. The acceleration transmissibility transfer function between the beam tip and the base was measured for each beam and was compared to the transfer function of an identical beam without an active element. The results are shown in figure 8. It can be seen that the vibration levels have been reduced considerably in both beams compared to the beam with passive damping. A closer examination of the results reveal that the beam with the piezoceramic element located at $0.25L$ produces a lower resonance peak in the first mode of vibration and a higher peak in the second mode compared to the beam with the piezoceramic element located at $0.4L$.

5. Conclusions

The use of active piezoceramic elements combined with passive constrained-layer damping materials has been shown to produce very effective levels of damping in a cantilever beam.

Vibration levels in the first and second bending modes of forced vibration of the beams have been reduced significantly. These reductions in the vibration levels can only be achieved when the hybrid system of piezoceramic

materials is used with the constrained-layer damping material.

Combining an active element with a passive damping mechanism has the ultimate advantage of providing a failsafe mechanism and allows greater feedback gains to be used, resulting in improved vibration reduction capabilities.

Acknowledgments

The work described in this paper was supported by the US Air Force through the European Office of Aerospace Research and Development (EOARD). The authors are grateful for the financial support to carry out this work. The authors would also like to acknowledge the help of J A Rongong during the experimental studies.

References

[1] Pan J, Hanse C H and Snyder S D 1992 A study of the response of a simply supported beam to excitation by piezoelectric actuator *J Intell. Mater. Syst. Struct.* **3**

[2] Anderson E H and Crawley E F 1989 Piezo-ceramic actuation of one and two dimensional structures *NASA and NSF Report SSL#5-89*

[3] Bailey T, Gruzen A and Madden P 1988 RCS/Piezoelectric distributed actuator study *Technical Report for a Force Astronautics Laboratory produced at the Charles Stark Draper Lab. Inc., Report No AFAL-TR-88-038*

[4] Burdess J S and Fawcett J N 1992 Experimental evaluation of a piezoelectric actuator for the control of vibration in cantilever beams *Proc. Inst. Mech. Eng.* vol 206

[5] Warburton G B 1976 *The Dynamical Behaviour of Structures* 2nd edn (Oxford: Pergamon)

[6] Thomas W T 1988 *Theory of Vibration with Applications* 3rd edn (Englewood Cliffs, NJ: Prentice Hall)

[7] Freymann I R and Stumper E 1992 Active damping augmentation of elastomechanical systems using piezoelectric sensors and actuators paper presented at *75th AGARD-SMP Meeting on Smart Structures for Aircraft and Spacecraft (Germany, 1992)*

[8] Nashif A D, Jones D I and Henderson J P 1985 *Vibration Damping* (New York: Wiley)

[9] Azvine B 1993 Vibration control *via* active damping *Internal Report* Dynamics & Control Research Group, Department of Engineering, University of Manchester

[10] Azvine B, Tomlinson G R, Wynne R J and Sensburg O 1993 Vibration reduction *via* active damping Paper presented at *Int. Conf. on Active Damping in Mechanical Engineering (Lyon, 1993)*

[11] Azvine B, Tomlinson G R, Wynne R J and Sensburg O 1993 Vibration suppression of flexible structures using active damping Paper presented at *4th Int. Conf. on Adaptive Structures (Cologne, 1993)*

[12] Cremer L, Heckel M and Ungar E E 1973 *Structure Borne Sound* (Berlin: Springer)

[13] Baz A and Ro J 1994 Actively-controlled constrained layer damping *Sound & Vibration Magazine* March

[14] Baz A 1993 Active constrained layer damping *Damping 93 Conf. (San Francisco, 1993)*

APPENDIX II

Technical Paper Number 3:

Initial Studies into the use of Active Constrained Layer Damping

for Controlling Resonant Vibration.

Initial Studies into the Use of Active Constrained Layer Damping for Controlling Resonant Vibration

B. Azvine*, G.R. Tomlinson+, R.J. Wynne+
Dynamics & Control Research Group,
+*University of Manchester, Manchester, U.K.* * *Staffordshire University, Stafford, U.K.*

ABSTRACT

The work described in this paper is concerned with controlling the strain of the constraining layer of a composite structure in such a way as to enhance the shear generated in the viscoelastic material and hence improve the overall damping of the composite structure.

The results have indicated that this concept of active damping produces very effective levels of vibration suppression. In the case of cantilever beams the first two modes can be almost eliminated when velocity feedback of the beam tip is used. The results show that the addition of active control and passive damping in a single structure combines the advantages of passive damping in the higher modes and active control in the lower modes. In addition active damping as defined in this paper produces a fail safe mechanism in case of instability occurring in the feedback loop since passive damping is always present.

ACKNOWLEDGEMENT

The work described in this report was supported by U.S. Air Force through the European Office of Aerospace Research and Development (EOARD). The authors are grateful for the financial support to carry out the work. The authors would also like to acknowledge the help of Mr. J.A. Rongong.

NOTATION

A	Area
E	Young's modulus
b	Width
d	Thickness
G	Shear modulus
i,j	Mode number
K	Amplifier gain with acceleration and velocity feedback respectively
L	Beam length
m	Mass per unit length
M	Total applied moment
q_i	Generalised coordinate
t	Time
V(t)	Voltage driving the piezoceramic
x	Coordinate
y	Displacement in the plane of bending
α	Constant depending on the geometry of the beam
γ	Shear angle
ρ	Density
ε	Strain
Λ	Displacement
ω_i	i^{th} natural frequency
ζ_i	i^{th} damping ratio of the composite beam
$\phi_i(x)$	i^{th} mode shape function
λ, Ψ	Displacement function, Objective function

0-8194-1488-3/94/$6.00

1. INTRODUCTION

Many advances have been made in the use of piezoelectric ceramics and piezoelectric polymers in vibration and control problems. Theoretical models have been developed[1] to predict the behaviour of an actively controlled structure consisting of alternate layers of piezoelectric sensors and actuators connected to the structure. These types of structure are often referred to as smart structures.

In the area of smart structures the concept of active damping has received considerable attention in the past few years. Active damping can be achieved by using piezoelectric materials to induce extra damping in a structure, hence reducing the vibration levels at resonance in various modes of vibration. Extra damping can be created in a structure in a number of ways. The most common method is to apply forces to the structure which are 90 degrees out of phase to the motion of the structure.

The technique used in this study is to enhance the damping of a passive element in the structure by active means. This can be done effectively when constrained layer damping is used. The constraining layer is bonded to the structure using a viscoelastic material which acts as a passive damping element. By actively controlling the motion of the constraining layer, increased damping via shear energy dissipation is obtained. There are two ways of achieving this. One is to use a piezoelectric polymer as the constraining layer and control its motion by applying the appropriate voltage across it[2]. The second technique is to use piezoelectric materials in addition to a constraining layer. The latter approach is used in the present study.

2. ACTIVE DAMPING

Consider a piezoceramic pad bonded to the constraining layer of a beam. The viscoelastic material between the beam and the constraining layer is subject to extra shear as a result of the constraining layer. The piezoceramic can be used to control the strain of the constraining layer and hence the amount of shear in the viscoelastic material as shown in Fig.1.

If we consider the forced vibration of the beam, the force applied by the piezoceramic (PZT) on the beam produces a bending moment M which is a function of the applied voltage, V(t)[3],

$$M = \alpha\{\phi_i'(x_2) - \phi_i'(x_1)\}V(t)$$

$$= \alpha_i V(t) \qquad (1)$$

where α is a constant depending upon the dimensions of the beam and the constraining layer.

If the normal modes of the structure ϕ_i are known, the flexural vibration at any point x can be represented by

$$y(x,t) = \sum_i q_i(t)\,\phi_i(x) \qquad (2)$$

where the generalised coordinate q_i must satisfy equation 3[4,5]. The choice of the feedback signal, V(t), determines the damping and stiffness properties of the composite structure. If the feedback voltage is proportional to the velocity of the tip of the beam i.e.

$$V(t) = -K\dot{y}(L,t)$$

$$= -K \sum_{i=1}^{\infty} \dot{q}_i(t)\phi_i(L) \tag{3}$$

The equation of motion can then be written as;

$$\ddot{q}_i(t) + (2\zeta_i\omega_i + \eta_i)\dot{q}_i(t) + \omega_i^2 q_i(t) = \frac{-\alpha_i K_2 \sum_{j\neq i}^{\infty} \dot{q}_i(t)\phi_j(L)}{\int_0^L m\phi_i^2 dx} \tag{4}$$

It can be seen from Equation 4 that the overall effect of velocity feedback is an extra term added to the damping coefficient[9].

Several experiments were carried out on aluminium beams (150 mm x 38 mm x 3 mm) in order to investigate the active damping concept. The emphasis was on developing a good practical understanding of the way an actively damped beam behaves with various feedback signals and beam actuator/sensor configurations.

The piezoelectric actuator was a sonox P5 single layer plate (30 mm x 30 mm x 0.4 mm) bonded to the constraining layer using X60 strain gauge glue at a location of x = 0.25L; where the curvature of the beam in the first two modes is appreciable. The constraining layers used in this experiments was SOUNDFOIL (manufactured by SOUNDCOAT Co) which consisted of aluminium foil of thickness 0.010" coated with modified copolymer of thickness 0.002" which was applied directly to the beam.

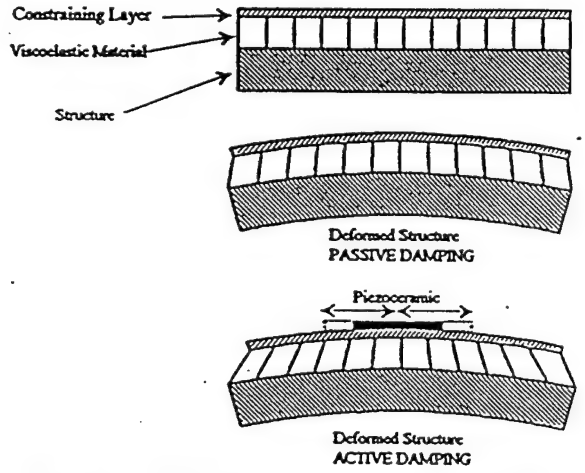

Figure 1 - Basic Mechanism of Active Damping

Typical results are shown in Fig.2. Three cases are shown, a beam with no feedback and no added damping (simple beam), a beam with CLD but no feedback (passive damping), and finally a beam with CLD and feedback control (active damping). Considering the beam with CLD only it can be seen that the second mode is attenuated significantly more than the first mode. This is not surprising because passive damping elements tend to perform better at higher frequencies. The normalised damping ratio i.e. the damping ratio in each mode to that of the simple beam (i.e. the beam with no added passive or active damping) is 3.9 in the first mode and 7.7 in the second mode. With active damping the normalised damping ratios in the first and second mode are 26 and 22 respectively. Table 1 summarises these results.

It can be seen that active damping can reduce the vibration levels in the first two modes effectively.

3. ASSESSING THE PERFORMANCE OF ACTIVE DAMPING

The active damping mechanism is provided by a combination of extra induced shear strain in the constrained layer arising from a combination of the bending induced shear and the additional shear from the active deformation of the PZT element. In order to assess the effect of the induced shear in isolation from the induced bending moments a symmetrical arrangement can be used as shown in Fig.3.

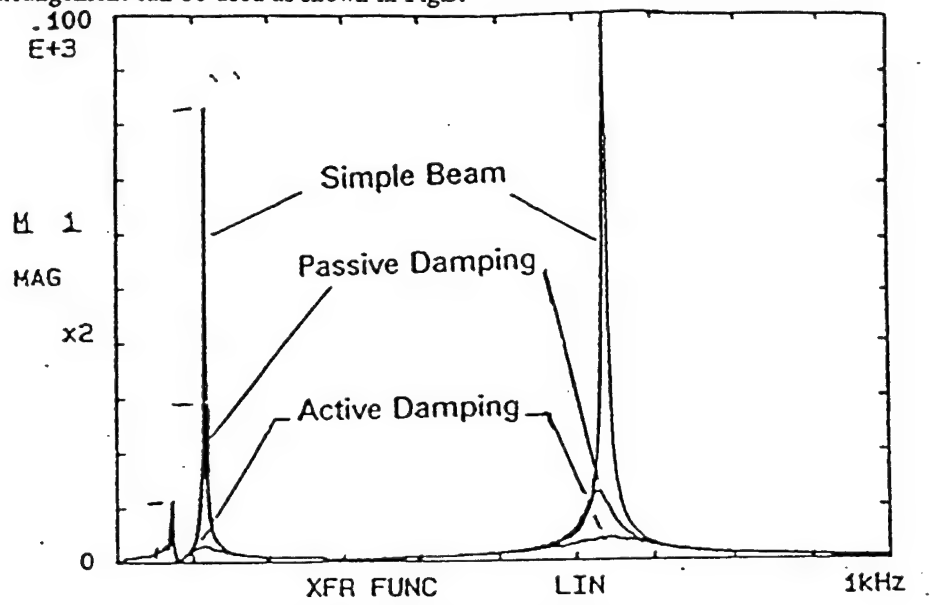

Figure 2 - Active Damping with Single Actuator

Table I - Comparison of the Damping Ratios in the First Two Modes of Vibration Using Active Damping

Beam Type	Normalised Damping Ratio	
	First Mode	Second Mode
Simple Beam	1	1
Beam with CLD	3.9	7.7
Active Damping	25.8	22.4

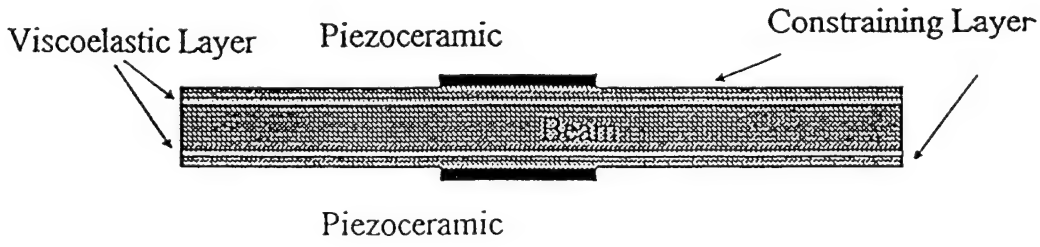

Figure 3 - Beam with Symmetrical Actuators to Cancel Induced Bending Moments

Consider a system where the piezoceramic is active over the constraining layer (CL) section on both sides of the beams. The actuation moments cancel leaving only the axial forces to produce the axial deformation of the combined piezoceramic and

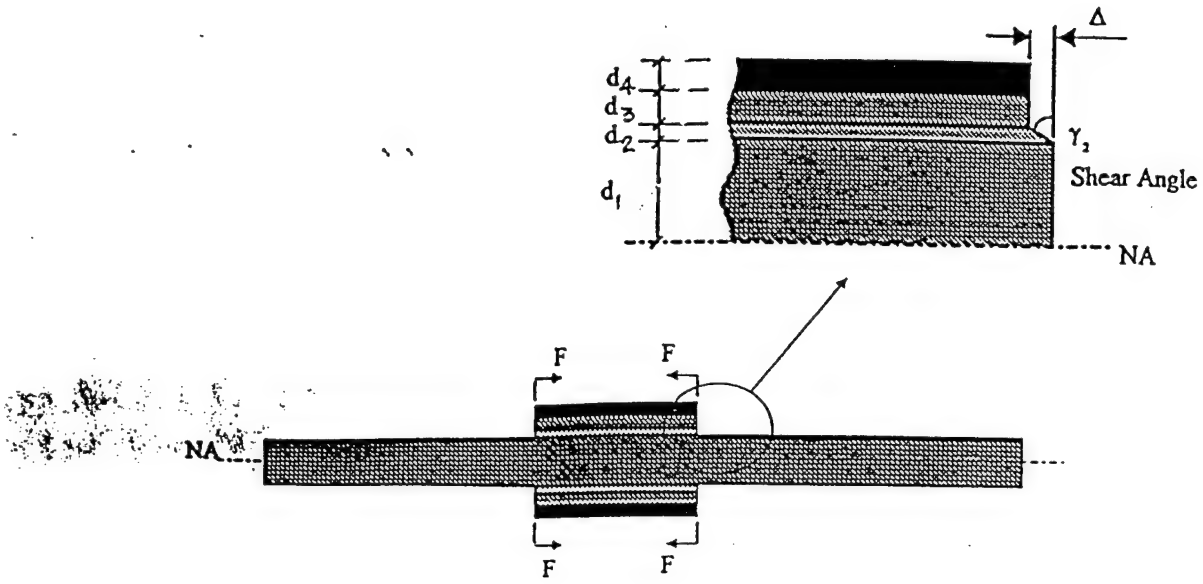

Figure 4 - Local Active Damping with Symmetrical Actuators

constraining layer, Δ. For small strains the deformation is,

$$\Delta = d_2\gamma_2 \tag{5}$$

The shear forces acting on the CL are;

$$F_s = G_2\gamma_2 A_2 \tag{6}$$

where,

$$G_2 = G_{2R}(1 + j\eta_2) \tag{7}$$

These produce an axial strain,

$$e_x = \frac{\partial \Delta}{\partial x} \tag{8}$$

The shear forces produce a change in the stress in the CL such that

$$A\,\frac{\partial \sigma_x}{\partial x} = G_2\gamma_2 b_3 \tag{9}$$

Now

$$\sigma_x = E_3 e_x = E_3 \frac{\partial \Delta}{\partial x} \tag{10}$$

Combining eqns 9 and 10 results in

$$\frac{\partial^2 \Delta}{\partial x^2} = \frac{g_2 \gamma_2}{d_3 E_3} \tag{11}$$

Now if we assume harmonic excitation of the piezoceramic pads,

$$\Delta = C e^{-jkx}; \quad \text{with } k = \frac{\omega}{\sqrt{\frac{E_3}{\rho_3}}}$$

Then,

$$\Delta = \frac{G_2 \gamma_2}{k^2 d_3 E_3} = \frac{G_2 \gamma_2}{\omega^2 \rho_3 d_3} \tag{13}$$

Using the standard eqns for a PZT plate

$$\epsilon_{max} = -d_{31} \frac{V_{max}}{d_4} \tag{14}$$

Therefore

$$\Delta = \epsilon_{max} L = -d_{31} \frac{V.L}{d_4} \tag{15}$$

Combining eqns 13 and 15 results in

$$\gamma_2 = \frac{\omega_2 \rho_3 d_3 \, V_{max} L \, d_{31}}{G_2 d_4} \tag{16}$$

The energy dissipated per cycle in the viscoelastic layer due to the axial motion can be expressed as [11]

$$W_A = \pi \, \eta_2 \, G_{2R} \, d_2 \, |\gamma_2|^2$$

$$= \pi \, \eta_2 \, G_{2R} \, d_2 \left| \frac{\omega^2 \rho_3 d_3 \, V_{max} \, L d_{31}}{G_2 d_4} \right|^2 \tag{17}$$

The shear angle associated with the bending of the beam is

$$\gamma_2' = \frac{aE_3d_3d_2k^2\beta}{d_2(E_3d_3d_2k^2+G_2)} \tag{18}$$

The energy dissipated per cycle due to bending is,

$$W_B = \pi\eta_2 \, G_{2R}d_2|\gamma_2'|^2 \tag{19}$$

The condition for dissipating extra energy in the constrained layer material is

$$\frac{W_A}{W_B} = \left|\frac{\gamma_2}{\gamma_2'}\right|^2 > 1$$

$$= \left|\frac{\omega^2\rho_3d_3V_{max}Ld_{31}}{\beta aG_2d_4E_3k^2}\,(E_3d_2d_3k^2+G_2)\right|^2 \tag{20}$$

3.1 Experimental Tests

In order to test the efficiency of cancelling the induced moments, the configuration shown in Fig. 3 was used whereby a random excitation signal was applied to the top PZT element and then to both elements simultaneously. The results of the experiment showed that when the same signal was applied to both elements the resulting spectrum was almost flat proving that the dynamic bending moments had been effectively cancelled.

To assess the effectiveness of the induced shear damping an experiment was carried out in which active damping with symmetrical actuators was compared to active damping with single actuator and passive damping. The results are shown in Fig. 5. It can be seen that a significant percentage of the reduction in the amplitude of vibration at the first mode is due to the induced shear alone. The effect is less significant in the second mode. It is possible to improve the damping in the second mode by choosing a more suitable location for the piezoceramic pad. However this may have detrimental effects on the damping in the first mode (see section 4).

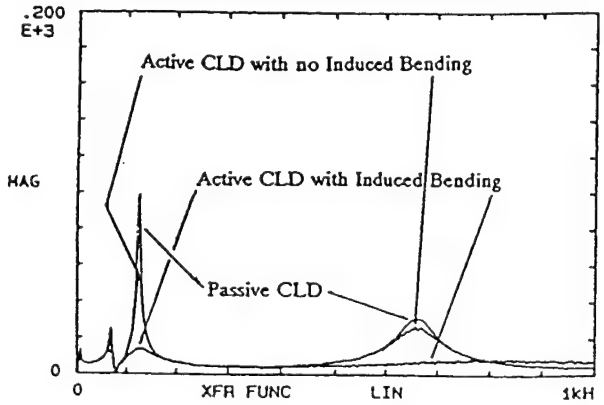

Figure 5 - Active Damping with and without Bending Moments

Table II - Reduction in the Amplitude in the first two Modes of Vibration Using Active Damping with and without Bending Moments

Beam Type	Reduction in Amplitude/Percentage First Mode	Second Mode
Beam with Passive Damping	0	0
Active Damping with Pure Shear	48	15
Active Damping with Shear and Bending	84	82

Comparison of active damping and active control reveals a very important practical limitation of active control. Active control is defined as attaching the piezoceramic pad directly to the structure without any constrained layer damping material between the pad and the structure. A test was carried out to investigate the limitation on the actuator voltage levels for each mechanism. The objective of the test was to increase the amplifier gain up to the point where the feedback loop saturated and to note the applied voltage. The tests showed that for the actively controlled beam the saturation voltage was 140 Volts peak to peak while the saturation voltage for the actively damped beam was 340 Volts peak to peak. This resulted in a further reduction of 50% in the amplitude of vibration at the tip of the beam compared to the actively controlled beam.

4. EFFECT OF ACTUATOR LOCATION

Because the strain in the constraining layer is modified by the piezoceramic pad attached to it, the maximum differential strain across the viscoelastic layer can be generated at a location on the beam where the maximum surface strain occurs. Consider the area of the beam covered by the piezoceramic pad. The optimum location for the pad is where the difference between the displacement at every cross section along the length of the piezoceramic pad and on the beam surface is a maximum. The beam surface strain is proportional to the curvature and hence the displacement at any point on the beam surface of an element of length dx is,

$$\Delta_B = \phi'' (x)dx \tag{21}$$

Assuming a linear distribution of strain in the piezoceramic pad, the extension of an element of length δx at any point on the ceramic is,

$$\Delta_p = (ax+b)\delta x \tag{22}$$

The relative displacement of the piezoceramic and the beam surface at any point can be written as,

$$\begin{aligned} \Delta_R &= \Delta_B - \Delta_p \\ &= [\phi'' (x) - (ax+b)]dx \end{aligned} \tag{23}$$

the total relative displacement which is a measure of induced shear in the viscoelastic material is,

$$\Omega = \int_{x_1}^{x_2} \left[\phi''(x) - (ax+b)\right]dx = \phi'(x_2) - \phi'(x_1) - \left[a\left[\frac{x_2^2}{2} - \frac{x_1^2}{2}\right] + b(x_2 - x_2)\right] \tag{24}$$

where x_1 and x_2 represent the coordinates of the ends of the piezoceramic pad on the beam and a and b are constants depending on the piezoceramic pad properties and dimensions. The objective is to maximise the above expression over the length of the beam in every mode. If a single pad is to be used to control more than one mode then the effectiveness of active damping can be formulated as an objective function with a separate term for each mode, where the term corresponding to each mode has a weighting factor. The weighting factors determine the relative reduction of amplitude required in each mode. If a single mode is selected then the weighting factors for all the other modes are set to zero and the optimisation problem reduces to finding the position where the curvature is a maximum in that particular mode. The objective function is formulated in eqn 25.

$$\Psi = \sum \lambda_n \Omega_n^2 \tag{25}$$

For example, for the first two modes the objective function is,

$$\Psi = \lambda_1 \Omega_1^2 + \lambda_2 \Omega_2^2 \tag{26}$$

A numerical search technique can be used to solve this problem. The objective function can be plotted against the location of the actuator to find the maximum or minimum points where the gradient is equal to zero. The selection of weighting factors λ_n us very important, the range is between 0 and 1. Fig. 6 shows the objective function plotted for the first two modes with $\lambda_1 = 1$ and $\lambda_2 = 0.2$. It can be seen that the objective function has a maximum value at $x_1 = 0$. The next local maximum is at $x_1 = 0.4$.

To demonstrate the validity of the above discussion an experiment was carried out in which two beams of length L, covered with constrained layer damping material and with a piezoceramic pad attached to the constraining layer, were used. The piezoceramic pad on one beam was placed at 0.25L from the clamped end and on the second beam 0.4L. A periodic random signal was applied to an exciter driving the clamped end of each beam and the tip velocity was used as the feedback signal to the ceramic pads. The transmissibility transfer function between the beam tip and the base was measured for each beam and was compared to the transfer function of an identical beam without an active element. The results are shown in Fig. 7. It can be seen that the vibration levels have been reduced considerably in both beams compared to the beam with passive damping. A closer examination of the results reveal that the beam with the piezoceramic pad located at 0.25L produces a lower resonance peak in the first mode of vibration and a higher peak in the second mode compared to the beam with the piezoceramic pad located at 0.4L.

The active damping methodology is applied to an aircraft instrument panel. The structure can be modelled as a plate clamped along the two short sides and free at the others. The mode shapes and curvature were obtained using finite element analysis. The objective was to control the first bending and torsion modes of the plate.

In order to compare the simple uncontrolled plate to the plate with active damping, Fig. 8 is presented from which it can be seen that there are real benefits to be gained by combining active control and passive constrained layer damping.

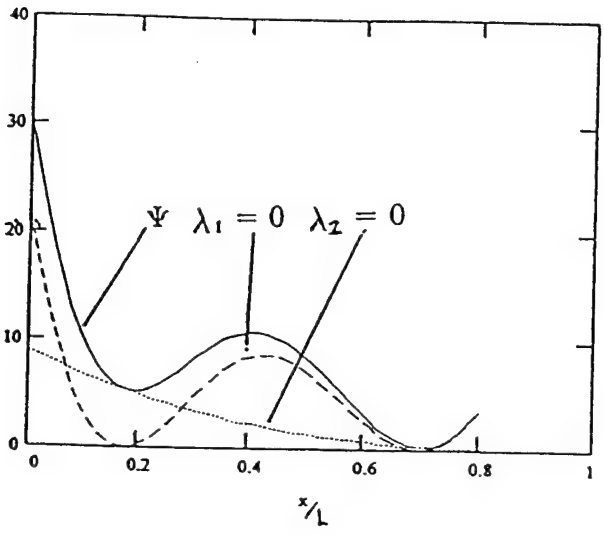

Figure 6 - Objective Function Based on the Location of A Single Actuator

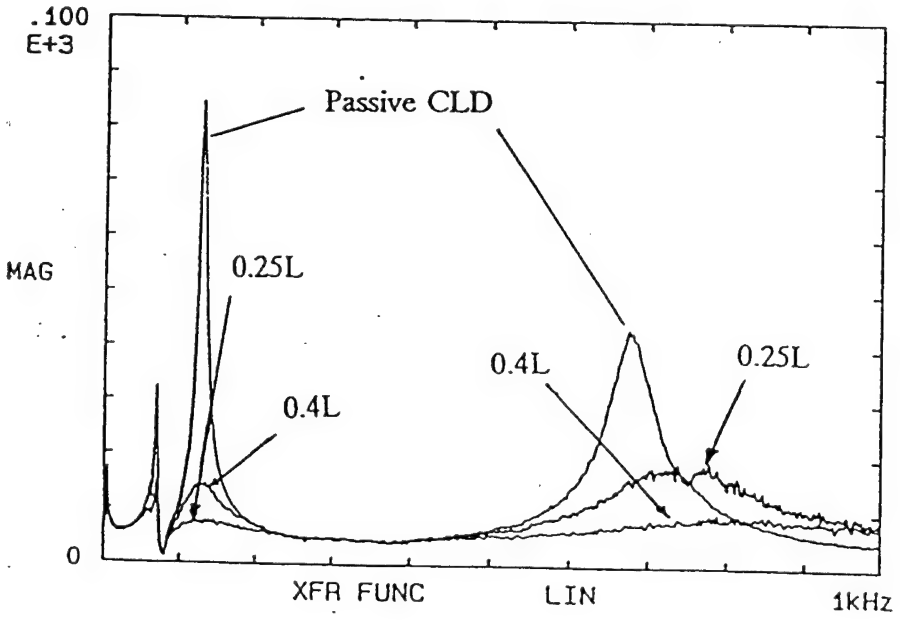

Figure 7 - Effect of Actuator Location on Active Damping with Single Actuator

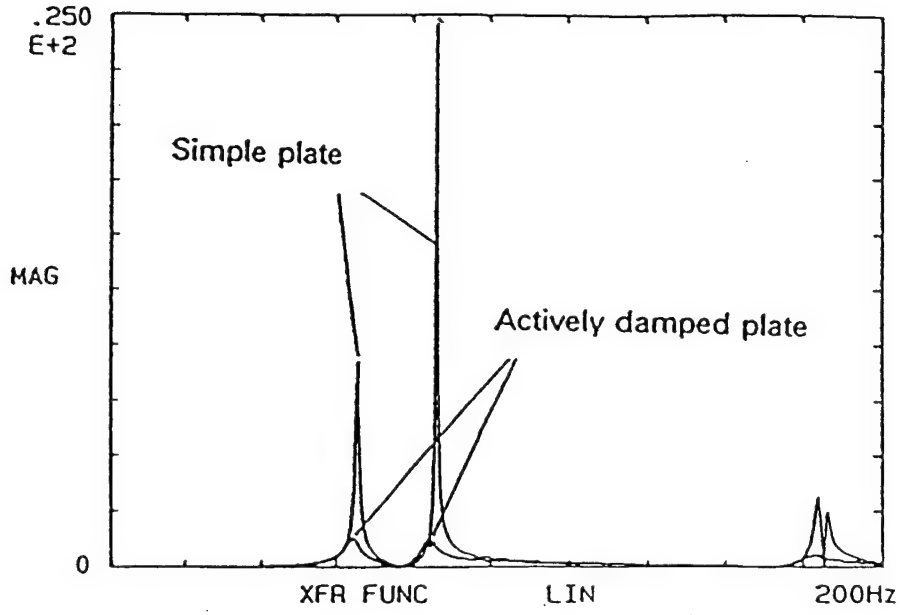

Figure 8 - Active Damping Applied to a plate structure

5. CONCLUSIONS

The use of piezoceramic pads combined with passive constrained layer damping materials and an appropriate feedback circuit has been shown to produce very effective levels of damping in cantilever beams.

Vibration levels in the first and second bending modes of forced vibration of beams/plates have been reduced significantly. These significant reductions in the vibration levels of the two modes can only be achieved when the hybrid system of piezoceramic materials is used with the constrained layer damping material.

Combining an active element with a passive damping mechanism has the ultimate advantage of providing a failsafe mechanism and allows greater feedback gains to be used, resulting in improved vibration reduction capabilities.

6. REFERENCES

1. J. Pan, C.H. Hanse & S.D. Snyder, "A study of the response of a simply supported beam to excitation by piezoelectric actuator", *J. of Intell. Mater. Syst. and Struct.*, Vol. 3 - Jan 1992.

2. T Baily, A Gruzen & P. Madden, "RCS/Piezoelectric distributed actuator study", *Technical Report for a Force Astronautics Lab., produced at the Charles Stark Draper Lab. Inc.*, Rep. No. AFAL-TR-88-038, 1988.

3. J.S. Burdess & J.N. Fawcett, "Experimental evaluation of a piezoelectric actuator for the control of vibration in cantilever beams", *Proc. of Inst. of Mech Engrs.*, Vol. 206, 1992.

4. G.B. Warburton, *The Dynamical Behaviour of Structures*, 2nd Ed., Pergamon Press Ltd, 1976.

5. W.T. Thomson, *Theory of Vibration with Applications*, 3rd Ed. Prentice Hall, 1988.

I.R. Freymann & E. Stumper, "Active damping augmentation of elastomechanical systems using piezoelectric sensors and actuators", Paper presented at the 75th AGARD-SMP Meeting on *Smart Structures for Aircraft and Spacecraft*, Germany 5-7 Oct, 1992.

A.D. Nashif, D.I. Jones & J.P. Henderson, *Vibration Damping*, John Wiley & Sons, 1985.

B. Azvine, "Vibration control *via* active damping", Internal Report, Dynamics & Control Research Group, Dept of Engrg, University of Manchester, 1993.

B. Azvine, G.R. Tomlinson, R.J. Wynne & O. Sensburg, "Vibration reduction *via* active damping", paper presented at Int. Conf. on Active Damping in Mech. Eng., Lyon, France, 15-17 June, 1993.

B. Azvine, G.R. Tomlinson, R.J. Wynne & O. Sensburg, "Vibration suppression of flexible structures using active damping", paper presented at 4th Int. Conf. on Adaptive Struct., Cologne, Germany, Nov. 1993.

L. Cremer, M. Heckel and E.E. Ungar, *Structure Borne Sound*, Springer-Verlag, 1973.

APPENDIX III

Technical Papers 4 and 5:

Passive and Active Constrained Layer Damping

of Ring Type Structures.

Suppression of Ring Vibration Modes of High Modal

Diameter Using Constrained Layer Damping Methods.

4th
Presented at the 1 Smart Structures & Maths Conf, San Diego, March '97 (Proceedings not yet published)

Passive and active constrained layer damping of ring type structures

Jem A. Rongong and Geoffrey R. Tomlinson

Department of Mechanical Engineering, University of Sheffield, Sheffield S1 3JD, UK.

ABSTRACT

The performance of constrained layer damping treatments can be enhanced by optimising the segment length or through active control by inducing strains in the constraining layer. This paper investigates the effect of these methods on the flexural and extensional modes of a ring over a wide frequency range. Finite element models are first verified experimentally and then used in parametric studies. It is shown that segmentation of the constraining layer does not increase the maximum damping obtainable for a particular configuration but alters the mode number at which the maximum occurs. It is also shown that the optimum viscoelastic layer stiffness for active constrained layer damping is higher than that for the passive case.

Keywords: constrained layer damping, active constrained layer damping, viscoelastic materials, sandwich rings, finite element, vibration damping

1 INTRODUCTION

Surface treatments involving materials that display viscoelastic characteristics can be used to attenuate vibrations in many structures such as aircraft panels, car bodies and space vehicles. A constrained layer damping (CLD) treatment is formed by sandwiching a thin, compliant layer of viscoelastic material between a stiff constraining layer and the vibrating structure. Relative motion between the constraining layer and the structure deforms the viscoelastic material thereby dissipating energy.

The performance of CLD when used to suppress flexural vibrations in beams and plates has been extensively studied over the last forty years. Early work[1,2] identified shear deformation in the viscoelastic layer as being the principal mechanism for energy dissipation. The loss factor of a structure treated with CLD was shown to depend not only on the loss factor of the viscoelastic material but also on the thickness and elastic moduli of the viscoelastic and constraining layers. Subsequent work has found that when the viscoelastic layer is soft and thick, significant levels of damping can be obtained through transverse extensional deformations in the viscoelastic layer.[3,4]

Studies considering partially covered beams have shown that the total coverage does not always result in the highest loss factors.[5] Efforts have been made to identify the optimum length of a CLD treatment applied to a beam. The first analyses assumed a uniform strain distribution in the base structure to derive an expression for the optimum length.[6] It has recently been shown that if the strain in the base structure is non-uniform, this optimum length is significantly increased.[7]

In the last decade active constrained layer damping (ACLD) methods have received considerable attention.[8–13] An ACLD approach enhances the shear deformation in the viscoelastic layer by inducing appropriate strains in the constraining layer. This is usually achieved either by using a piezoelectric material to form the constraining layer or by bonding a piezoelectric actuator to an existing passive constraining layer.[10] The strain in the piezoelectric actuator

and hence the deformation of the constraining layer can then be controlled by varying the electric potential across the piezoelectric material. Polyvinylidine fluoride (PVDF) film[8,9] and lead zirconate titanate (PZT) patches[11,12] have been used successfully as actuators to control vibrations in beams and plates. Significant improvements in performance over passive CLD have been demonstrated.

The passive damping supplied by the viscoelastic layer gives significant advantages over a purely active control approach, in which the actuators are bonded directly to the structure. In particular the effect of spillover,[14] where uncontrolled modes become unstable, is significantly reduced using ACLD. Theoretical and experimental comparisons have also been made between ACLD and active control of a structure with passive CLD.[11,13] These studies have shown that the stiffness of the viscoelastic layer is critical to the transfer of control effort from the actuator to the base structure.

Ring type structures are often found as components in rotating machinery. Vibrations developed can excite flexural modes of high nodal diameter. Recent studies[15] have shown that for a particular CLD treatment a graph of loss factor against damping shows two maxima as in figure 1. The first peak occurs when shear damping of the viscoelastic

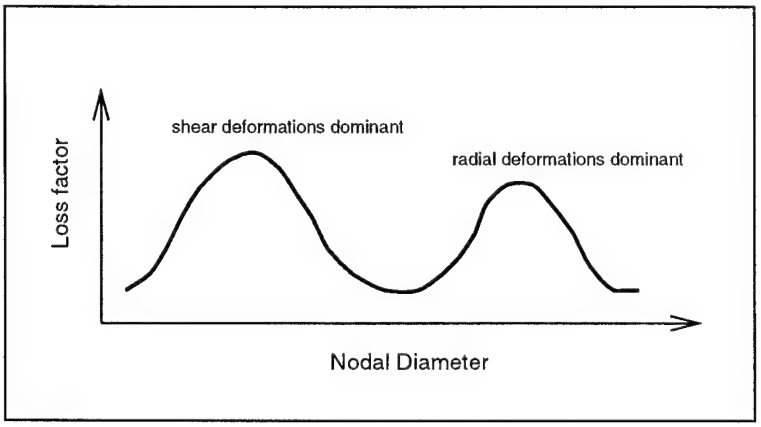

Figure 1: Typical plot of loss factor against nodal diameter for a ring with CLD

layer is optimised and the second when radial deformations become significant. The height of the peaks are affected mainly by the loss factor of the viscoelastic material and the flexural stiffness of the constraining layer. The modes at which these peaks occur depend mainly on the stiffness (in shear or extensional deformation) of the viscoelastic layer.

This paper examines the effect of methods used to enhance the performance of CLD, namely segmentation and ACLD, on the flexural (and extensional) modes of a ring. Frequency domain experimental and theoretical results are used to investigate the damping achieved over a large number of vibration modes. Numerical studies using finite element (FE) analysis are carried out to identify generic behaviour. The validity of the FE analysis methods used are then verified experimentally.

2 MODELLING VISCOELASTIC BEHAVIOUR

The mechanical properties of viscoelastic materials vary with both frequency and temperature. This behaviour can be modelled accurately in the frequency domain using the complex modulus obtained from the material master curve. Figure 2 shows the master curve or *international plot* for the shear modulus of 3M ISD112 - a popular damping material. The complex shear modulus $G^*(\omega)$ is defined as,

$$G^*(\omega) = G'(1 + j\eta) \qquad j = \sqrt{-1} \tag{1}$$

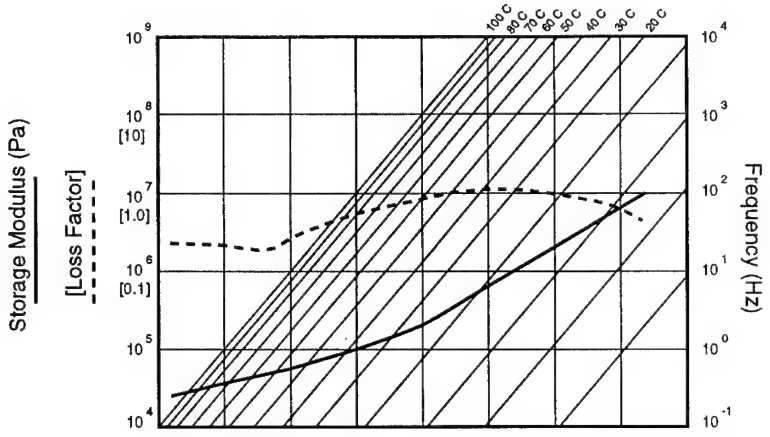

Figure 2: Shear modulus master curve for ISD 112

where G' and η are the storage modulus and loss factor respectively. These values can be used directly to carry out harmonic forced response calculations for viscoelastic structures.

Modal strain energy (MSE) analysis is an approximate method for obtaining loss factor and natural frequency data from a FE model.[16] It is based on an elastic analysis involving free eigenmodes and is therefore computationally inexpensive. Assuming low levels of damping in the base structure and constraining layer the loss factor of a ring with a CLD treatment can be estimated using,

$$\eta_{total} = \frac{\eta_r U_r + \eta_c U_c + \eta_v U_v}{U_{total}} \approx \eta_v \frac{U_v}{U_{total}} \tag{2}$$

where η is the loss factor, U is the modal strain energy and the subscripts r, c and v refer to the ring, constraining layer and viscoelastic layer respectively. It can be shown that the MSE method assumes proportional damping[17] and that it is the first order approximation to a full asymptotic solution.[18] It also does not allow for the frequency dependence of the viscoelastic material: to get correct values the eigenvalue calculation must be carried out for each mode using the material properties at that particular frequency. MSE analysis has been used successfully to predict the damping in the first thirty modes of steel-polyurethane-steel sandwich rings.[15]

3 SEGMENTED CLD

MSE analysis was used to estimate the loss factors of rings covered with CLD made up of 2, 4, 8 and 16 segments. The basic dimensions are presented in table 1. Two dimensional, eight noded biquadratic finite elements were used

Part	radius (mm)	thickness (mm)	width (mm)	density (kg/m^3)	Young's modulus (GPa)	Poisson's ratio
Ring	182.5	2.5	25	7860	205	0.3
Viscoelastic layer		0.127	25	1000	variable	0.499
Constraining layer		0.254	25	2700	70	0.33

Table 1: Dimensions and material properties

to model the CLD treated rings. Convergence studies found that the first thirty vibration modes could be calculated accurately using 240 elements around the circumference of the composite ring. The viscoelastic and constraining

layer were each one element Through the thickness, single elements were sufficient to model the viscoelastic and constraining layers and two were required for the ring.

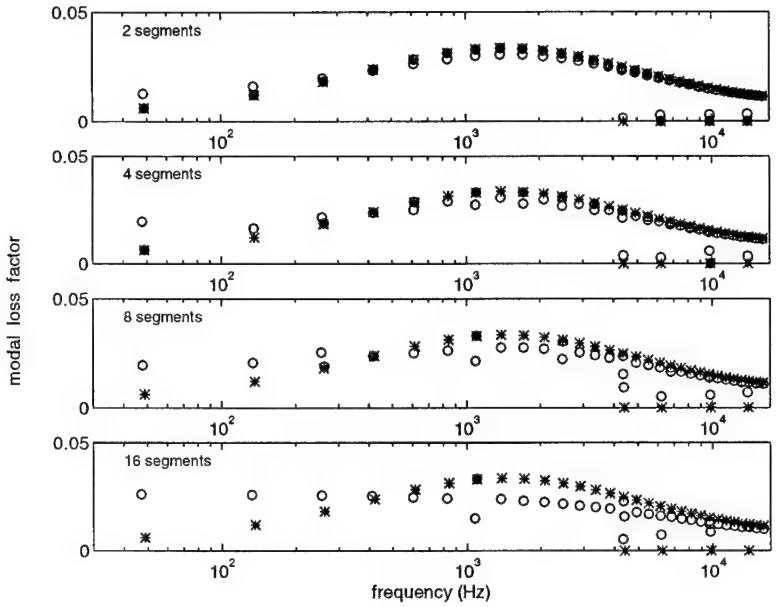

Figure 3: Loss factors of ring with segmented constraining layer $E_v = 15$ MPa (*** unsegmented, ooo segmented)

Figures 3, 4 and 5 show the modal loss factor against frequency of these rings for different values of viscoelastic layer Young's modulus (E_v). Results for segmented CLDs are marked with an 'o' and are compared with the unsegmented case marked with an asterisk.

The values of Young's modulus for the viscoelastic layer were chosen to illustrate the effect of segmentation on the double humped damping curve of figure 1. Figure 3 shows the first (shear) peak, figure 4 shows the start of the second (radial deformation) peak and figure 5 focuses on the area to the left of the first peak where the stiffness of the viscoelastic layer is higher than the optimum value. Note that the modes with very low loss factors near 4, 6, 10 and 15 kHz are extension modes.

In general, for flexural modes coinciding with the shear peak as in figure 3, segmentation offers no advantages as the configuration is optimised: in fact shorter segments lead to a lower peak. Figure 4 shows that in the trough between the peaks and on the second peak the segment length has very little effect. For modes to the left of the shear peak, where the loss factors achieved are suboptimal because the viscoelastic layer is either too thin or the shear modulus is too high, reducing the segment length improves the damping. This effect is most noticeable in figure 5. It is interesting to note that this improvement in damping achieved with segmentation never exceeds the height of the shear peak. This indicates that optimum performance can be achieved without segmenting the constraining layer, but by selecting the suitable values for the thickness and modulus of the viscoelastic layer. However in practice it is not always possible to do this - a designer is limited to real materials - and when this occurs segmentation can be used to shift the optimum peak to the required modes.

For extension modes, figures 3 and 5 show that increasing the number of segments, or alternatively reducing the segment length significantly improves the loss factor achieved.

From these graphs it can be seen that a pair of modes close in frequency but with significantly different damping levels often occur when a segmented CLD is used: for example, in figure 3 the ring with the 16 segment CLD has two modes near 1 kHz that have loss factors of 0.015 and 0.035 respectively.

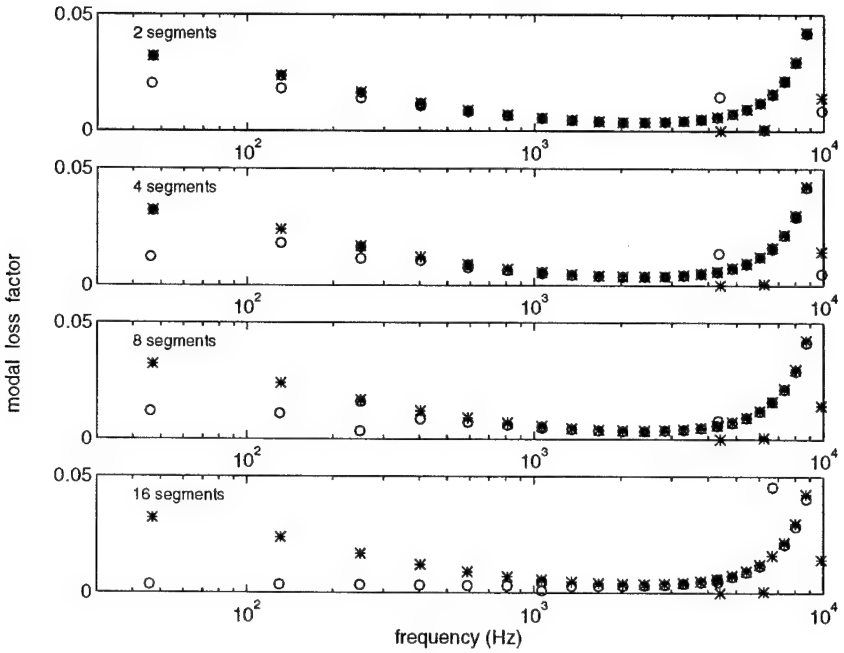

Figure 4: Loss factors of ring with segmented constraining layer $E_v = 0.5$ MPa (*** unsegmented, ooo segmented)

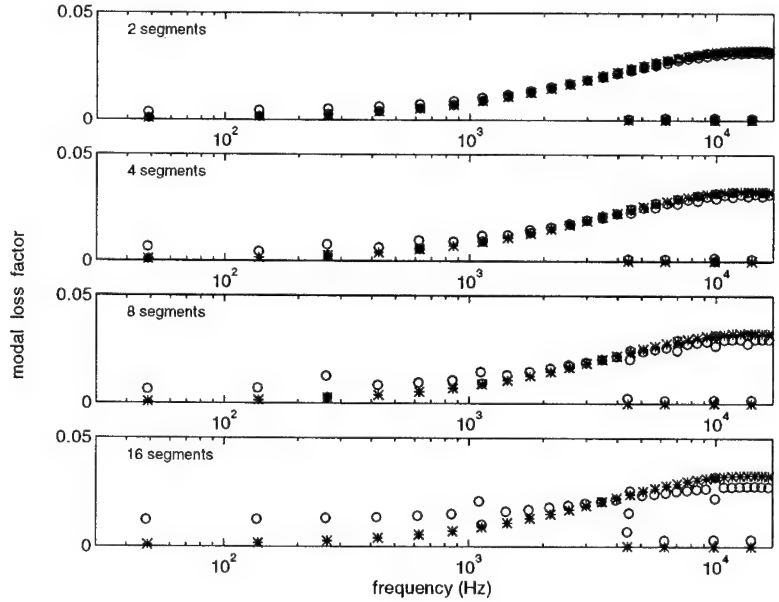

Figure 5: Loss factors of ring with segmented constraining layer $E_v = 150$ MPa (*** unsegmented, ooo segmented)

These are in fact modes with the *same* nodal diameter (8) but the positioning of the nodes with respect to the segments differs. The higher loss factor corresponds to the mode in which the nodes are aligned with the gaps between the CLD segments. Figure 6 shows the difference between these modes: mode 16 gives a significantly lower level of damping than mode 17. This behaviour only occurs when the nodal diameter of the vibration mode is a multiple of half the number of segments.

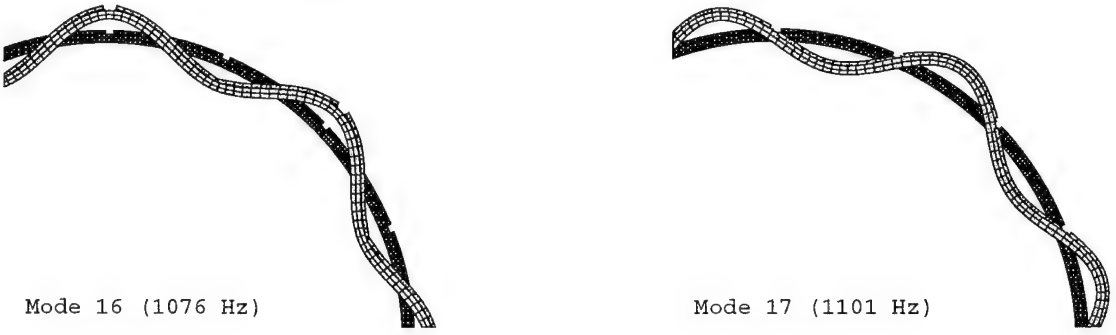

Figure 6: 8 nodal diameter mode shapes for ring with 16 segment CLD

4 VERIFICATION OF MSE METHOD FOR THE SEGMENTED CLD TREATMENT

To validate the numerical methods used in the previous section a comparison was made between the natural frequencies and loss factors obtained using MSE analysis to those obtained from direct forced response calculations and experimental results.

Four 250 mm length strips of aluminium backed ISD 112 damping tape were applied evenly to a steel ring. Dimensions and material properties are given in table 1 and figure 2. The ring was then suspended on soft elastic (free-free) supports and excited with an electrodynamic shaker using a 0-2 kHz band limited random noise source. The experimental layout is shown in figure 7. The response was measured using a minature accelerometer and frequency

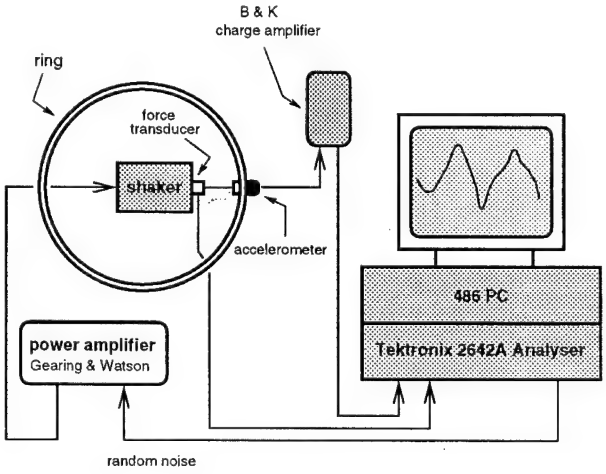

Figure 7: Schematic diagram of experimental set-up

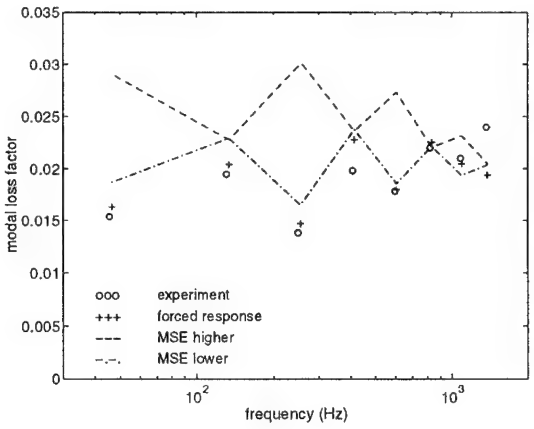

Figure 8: Modal loss factors with a 4 segment constraining layer: driving point opposite a gap between segments

response data was obtained using a PC based Fourier transform analyser. Estimates of natural frequency and modal loss factor for the first eight modes were made by fitting a single degree of freedom curve to the mobility plot. This

method gave good results as the resonances were well separated. Interactions with torsion modes and the support structure made measurements unreliable for higher modes (above 1.5 kHz). Three successive tests were made with the stinger rod of the shaker attached at different points on the ring. This was to investigate the pairs of modes of the same nodal diameter but different loss factors discussed in the previous section. With reference to figure 6 an excitation point opposite a gap between the segments was selected to drive modes with the lower loss factor. The second driving point was placed opposite a point half way along a segment (to excite the modes with higher damping) and a final point was fixed exactly between the first two points.

Theoretical predictions were made using both a direct forced response calculation (modal values obtained by curve fitting) and also using MSE analysis. Values for frequency dependent shear modulus of ISD 112 at 19° C were obtained from the international plot (figure 2). With the MSE method, the frequency dependent behaviour was included by following an iterative process calculating each eigenvalue in turn using the correct value for the elastic modulus of the viscoelastic material.

Comparisons of the results from the three different methods are presented in figures 8, 9 and 10. These figures show

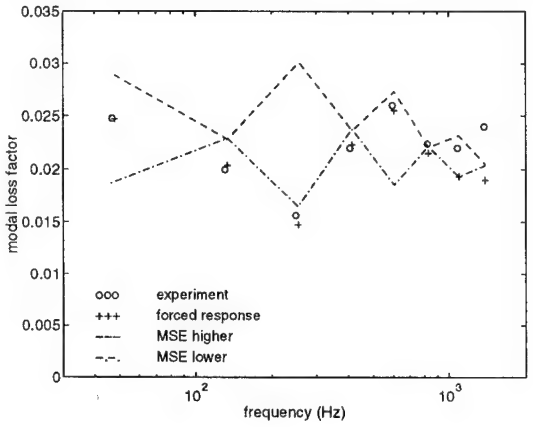

Figure 9: Modal loss factors with a 4 segment constraining layer: driving point opposite the centre of a segment

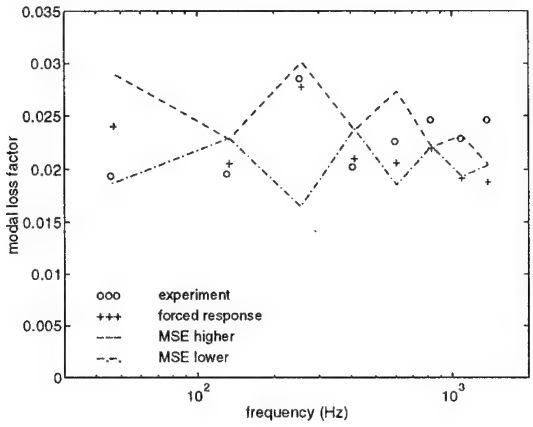

Figure 10: Modal loss factors with a 4 segment constraining layer: half way between previous points

good agreement between the experimental and theoretical forced response results. Figure 8 shows that when the excitation is at a gap between segments the behaviour follows the modes with lower damping obtained using MSE analysis. In figure 9 it can be seen that when the driving point is at the midpoint of a segment, the modes (apart from 4 nodal diameters at 250 Hz) excited correspond to the ones with higher damping. Finally figure 10 shows that for a driving point in a different position the loss factors obtained are between the limits indicated from an MSE analysis. In general it can be concluded that the results obtained using MSE analysis are valid and that for modes where the nodal diameter is a multiple of half the number of segments, the damping depends on the positioning of the exciting force.

5 ACTIVE CONSTRAINED LAYER DAMPING (ACLD) FOR A RING

The linear relationship linking stress, strain and electric field for piezoelectric materials can be written in tensor form as,

$$\epsilon = s^E \sigma + dE \tag{3}$$

where ϵ is the strain, s^E the compliance at constant electric field, σ the strain, d piezoelectric strain constants and E the applied electric field. For ACLD applications it is common to use a thin plate-like piezoelectric actuator poled in the thickness direction. Under these conditions the relationship can be simplified considerably. A voltage applied across the thickness of such an actuator bonded to a structure induces strains in the structure proportional to the d_{31} strain constant.

Various different control strategies have been employed in studies on ACLD. The work presented here is an initial study on the effect of activating the constraining layer on a wide range of modes of a ring. A voltage proportional to the radial velocity on the ring is used to control the strain deformation of a small piezoceramic (PZT) patch bonded to the constraining layer as shown in figure 11. A similar system has been used with considerable success to control first two modes of a cantilever beam.[10] Figure 12 shows a schematic diagram of the velocity feedback

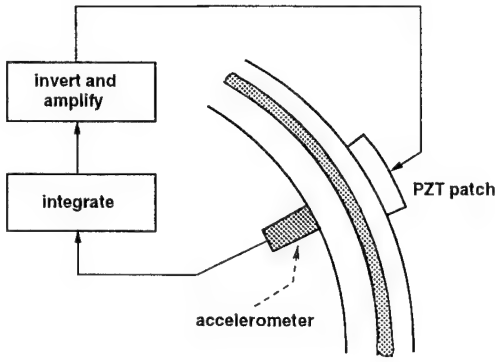

Figure 11: Velocity feedback control system

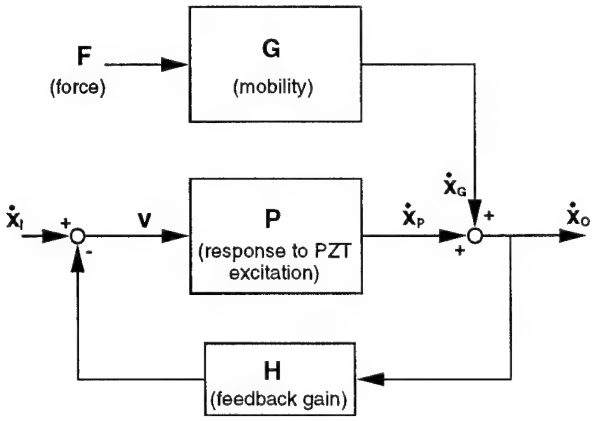

Figure 12: Schematic diagram of velocity feedback strategy

strategy employed. The object is to minimise the output velocity $\dot{x}_o$ with respect to the force F. As the set input $\dot{x}_i$ is zero, the model can be expressed mathematically as,

$$\frac{\dot{x}_o}{F} = \frac{G}{1+HP} \tag{4}$$

Note that this model assumes linear behaviour and ignores the effect of voltages generated *by* the actuator when it is deformed. Equation 4 indicates that it is possible to calculate the controlled response by measuring the mobility $G(=\frac{\dot{x}_G}{F})$ and the response to piezoelectric excitation $P(=\frac{\dot{x}_P}{v})$ separately.

To verify this model G and P were calculated numerically for the ring used in the previous section with a 5 mm PZT actuator bonded to the centre of one of the constraining layer segments. Measurements of these functions were made experimentally using a band limited 0-5 kHz random noise signal. As before, the velocity was obtained by using an accelerometer and integrating the signal, and the force F was measured using a force transducer. The piezoelectric drive voltage was amplified to approximately 100 V peak-to-peak. Dimensions and material properties of the PZT actuator are shown in table 2. The magnitude and phase of these responses predicted numerically are compared with

length (mm)	thickness (mm)	density (kg/m^3)	d_{31} (10^{-12} C/N)	Young's modulus (GPa)	Poisson's ratio
5	0.4	7700	-180	62.5	0.3

Table 2: Dimensions and material properties for Sonox P5 PZT actuator

the experimental values in figures 13 and 14. The figures show good agreement verifying the models used.

The methods developed were used to study the effect of viscoelastic layer stiffness on the performance of ACLD. Over the frequency range considered (10-5000 Hz) the elastic modului of a viscoelastic material can vary significantly: for example, the modulus of ISD112 increases by a factor of almost twenty. This can result in significantly different strain transfer behaviour between low and high modes. To investigate this effect the performance obtained using three different values of Young's modulus for the viscoelastic layer were compared.

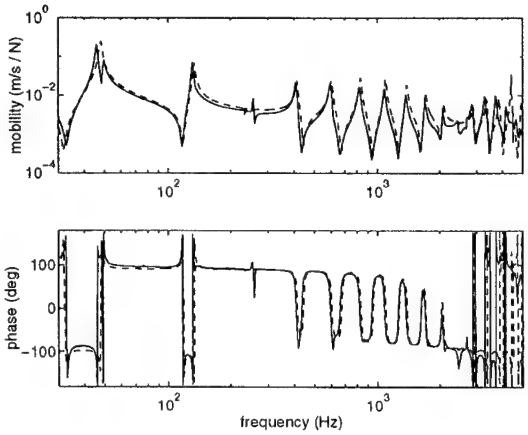

Figure 13: Mobility (G): full line for experimental and dashed line for simulated data

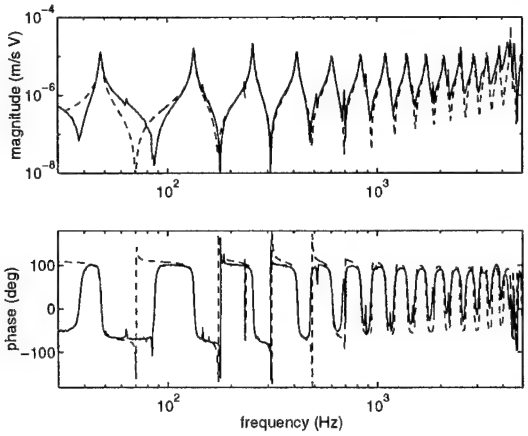

Figure 14: Response to PZT excitation (P): full line for experimental and dashed line for numerical data

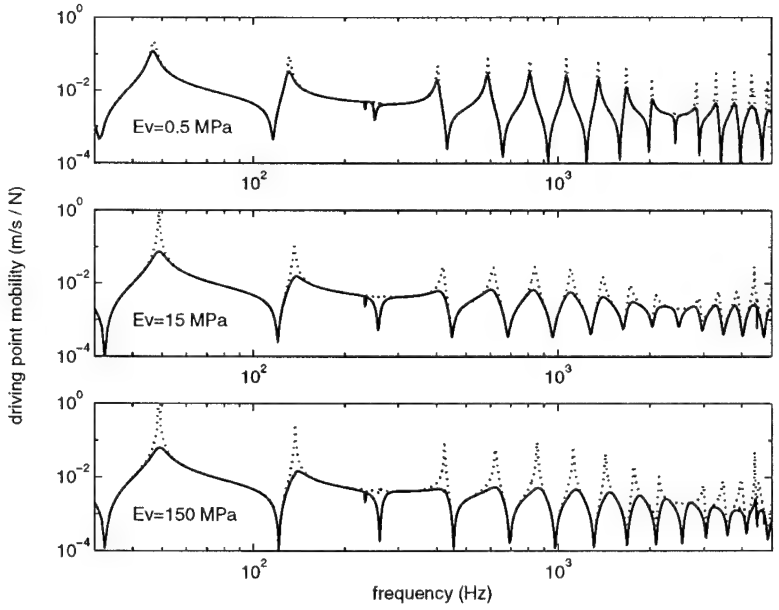

Figure 15: Simulated ACLD on a ring with different values of Young's modulus (dashed line for passive case)

Figure 15 shows the simulated results of ACLD applied to a ring with a full constraining layer. It can be seen that although the passive damping is optimised using a Young's modulus of 15 MPa, the 150 MPa case gives better performance when the constraining layer is activated. This result indicates that an ACLD treatment using a real viscoelastic material would show improved control performance in the high frequency modes.

6 CONCLUSIONS

In this paper the effect of segmenting the constraining layer on the overall value of damping for a CLD treated ring was studied. For flexural modes it was found that segmenting improved the damping only if the viscoelastic layer is stiffer than the optimum case. For extension modes however segmentation always improves the damping.

Active constrained layer damping was also considered. It has been shown that it is possible to enhance the damping of a large number of modes using a simple velocity feedback approach. It has also been shown that the optimal stiffness of the viscoelastic layer is higher for ACLD than for the passive case.

7 ACKNOWLEDGEMENTS

The authors are grateful to Rolls Royce plc for financial support provided for the work presented here.

8 REFERENCES

[1] Kerwin E M , 'Damping of flexural waves by a constrained viscoelastic layer', *J. Acoust. Soc. Am.*, **31**, pp 952-962, 1959.

[2] Mead D J and Markus S, 'Loss factors and resonant frequencies of encastre damped sandwich beams', *J. Sound Vibr.* **12**, pp 99-112, 1970.

[3] Douglas B E and Yang J C S, 'Transverse compressional damping in the vibratory response of elastic-viscoelastic-elastic beams', *AIAA J.*, **16**, pp 925-930, 1978.

[4] Miles N N and Reinhall P G, 'An analytical model for the vibration of laminated beams including the effects of both shear and thickness deformation in the adhesive layer', ASME J. Vibr. Acoust., **108**, pp 56-64, 1986.

[5] Nokes D S and Nelson F C, 'Constrained layer damping with partial coverage', *Shock Vibr. Bull.*, **38**, pp 5-12, 1968.

[6] Plunkett R and Lee C T, 'Length optimisation for constrained layer damping', *J. Acoust. Soc. Am.*, **48**, pp 150-161, 1970.

[7] Demoret K B and Torvik P J, 'Optimal length of constrained layers on a substrate with linearly varying strain', *ASME Design Eng. Tech. Conf.*, **84-3**(C), pp 719-726, 1995.

[8] Baz A and Ro J, 'Vibration of plates with active constrained layer damping', *Smart Mater. Struct.*, **5**, pp 272-280, 1996.

[9] Yellin J M and Shen I Y, 'A self-sensing active constrained layer damping treatment for an Euler-Bernoulli beam', *Smart Mater. Struct.*, **5**, pp 628-637, 1996.

[10] Azvine B, Tomlinson G R and Wynne R J, 'Use of active constrained layer damping for controlling resonant vibration', *Smart Mater. Struct.*, **4**, pp 1-6, 1995.

[11] Van Nostrand W C, Knowles G J and Inman D J, 'Active constrained layer damping for micro-satellites', *Dynamics and Control of Structures in Space II*, pp 667-681, 1993.

[12] Liao W H and Wang K W, 'Analysis and design of viscoelastic materials for active constrained layer damping treatments', *SPIE Proc. Conf. on Smart Struct. and Mater.*, **2720**, pp 212-223, 1996.

[13] Huang S C, Inman D J and Austin E M, 'Some design considerations for active and passive constrained layer damping treatments', *Smart Mater. Struct.*, **5**, pp 301-313, 1996.

[14] Balas M J, 'Trends in large space structure control theory: fondest hopes, wildest dreams', *IEEE Transact. Autom. Control*, **AC-27**, pp 522-535, 1982.

[15] Rongong J A and Tomlinson G R, 'Suppression of ring vibration modes of high nodal diameter using constrained layer damping methods', *Smart Mater. Struct.*, **5**, pp 672-684, 1996.

[16] Johnson C D and Kenholz D A, 'Finite element prediction of damping in structures with constrained viscoelastic layers', *AIAA J.*, 20, pp 1284-1290, 1982.

[17] Slater J C, Belvin W K and Inman D J, 'A survey of modern methods for modelling frequency dependent damping in finite element models', *Proc. 11^{t}h Modal Analysis Conf.*, pp 1508-1512, 1993.

[18] Ma B A and He J F, 'A Finite Element Analysis of Viscoelastically Damped Sandwich Plates', *J. Sound Vibr.*, **152**, pp 107-123, 1992.

Smart Mater. Struct. 5 (1996) 672–684. Printed in the UK

Suppression of ring vibration modes of high nodal diameter using constrained layer damping methods

J A Rongong and G R Tomlinson

Department of Mechanical Engineering, University of Sheffield, Sheffield, UK

Received 10 July 1996, accepted for publication 16 September 1996

Abstract. Constrained layer damping treatments utilize the energy dissipative properties of viscoelastic materials to increase the passive damping in structures. This paper investigates the performance of constrained layer damping treatments applied to a ring. An analytical model is developed to predict the behaviour of such a ring over a large number of modes. Relative motion between the ring and constraining layer in both the circumferential and radial directions are considered. Predictions of steady state dynamic behaviour obtained using the model are validated by comparison with results from experiments and finite element analysis. The model is then used to evaluate the effect of various parameters on the damping achieved. It is shown that for any particular configuration a plot of damping against mode number has two maxima. These peaks occur when optimum values for the deformation of the viscoelastic layer are achieved firstly for shear and secondly for radial extension and compression.

Nomenclature

English

CL	constraining layer
CLD	constrained layer damping
E	Young's modulus
F	force
G	shear modulus
$[K]$	stiffness matrix
$[M]$	mass matrix
MSE	modal strain energy
Q	generalized force
R	radius of centroid
T	kinetic energy
U	strain energy
VL	viscoelastic layer
b	width
g	time varying coefficient
h	time varying coefficient
i	$\sqrt{-1}$
m	mass per unit length
q	generalized coordinate
t	thickness
t	time
u	circumferential displacement
w	radial displacement
z	radial distance from centreline

Greek

ϵ	direct strain
γ	shear strain
η	loss factor
φ	radial deformation shape function
ν	Poisson's ratio
θ	angle round ring
ρ	mass density
ω	frequency
ψ	tangential deformation shape function

Subscripts

P	point P
Q	point Q
R	radial
θ	circumferential
c	constraining layer
r	ring
v	viscoelastic layer

Superscripts

T	transpose
$\cdot$	time derivative
$'$	space derivative

1. Introduction

Constrained layer damping (CLD) is widely used in the aerospace and automotive industries as a surface treatment to attenuate resonant structural vibrations. Energy is dissipated through the deformations of a compliant

0964-1726/96/050672+13$19.50

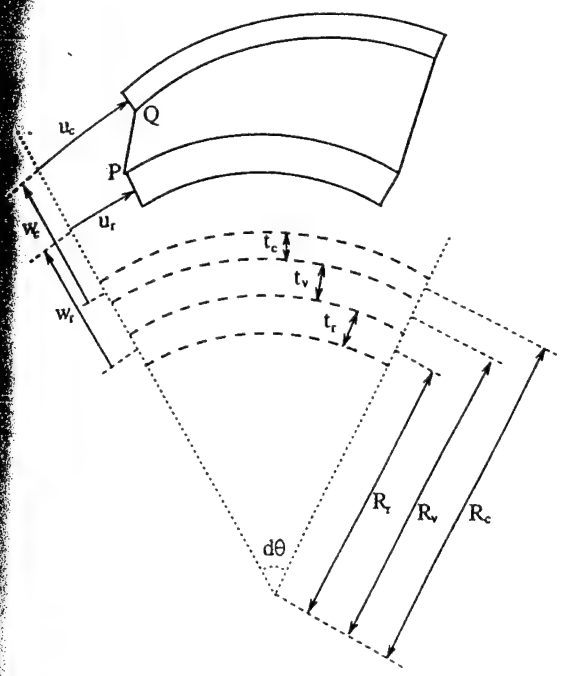

Figure 1. Deformation of a sandwich ring.

layer of viscoelastic material, sandwiched between the base structure and a stiff constraining layer (CL). The performances of such treatments have been studied by many researchers. The overall damping achieved has been shown not only to be dependent on the inherent damping in the viscoelastic material but also on the thickness and elastic modulus of each layer.

Sandwich beams and plates have received much attention since the work of Kerwin [1] in the late 1950s. Subsequent work has often been based on the sixth order partial difference equations of Mead and Markus [2]. These equations assume that all layers move the same amount in the transverse direction, that the viscoelastic layer carries shear stress only. It has been shown that the shear deformation and rotary inertia of the structure and CL are significant if the flexural wavelength is less than four times the thickness [3, 4]. More recently, studies allowing transverse extensional deformation of the viscoelastic layer have shown that damping values can be higher than those indicated by the sixth order theory when the viscoelastic layer is soft or thick [5, 6].

Ring type structures including CLD have also received some attention. System loss factors and resonance frequencies for curved beams [7, 8] and sandwich rings [9] have been obtained. These analyses however, studied only the first three or four modes and to the authors' knowledge there have been no studies encompassing high order modes (in the region of 20–40 nodal diameters) that could be excited by rotating machinery.

This paper presents a study on the performance of constrained layer damping applied to a solid ring over a wide range of modes. Analytical and finite element models are verified experimentally and the effect of various parameters on the damping achieved are investigated.

2. Modelling viscoelastic elements in structures

The mechanical properties of viscoelastic materials vary with both frequency and temperature. Several theoretical and empirical methods have been developed to simulate and analyse this behaviour [10, 11]. The approach used in this paper involves the use of the complex modulus which is defined by the material master curve and gives an accurate frequency domain model. (A time domain model can also be derived from this by either the use of the Fourier transform [12] or by curve fitting to a Prony series [11].) The frequency dependent complex shear modulus $G^*(\omega)$ is defined by:

$$G^*(\omega) = G'(1 + \eta) \tag{1}$$

where G' and η are the frequency dependent storage modulus and loss factor respectively.

The modal strain energy (MSE) method is based on an elastic analysis involving free eigenmodes. It is particularly popular for finite element studies as it is computationally inexpensive. The loss factor of a viscoelastic sandwich ring is estimated using,

$$\eta_{structure} = \frac{\eta_r U_r + \eta_c U_c + \eta_v U_v}{U_{structure}} \tag{2}$$

where U is the modal strain energy and the subscripts r, c and v refer to the ring, constraining layer and viscoelastic layer respectively. The added effect of the constrained layer damping treatment on the system loss factor can therefore be approximated by,

$$\eta_{added} = \frac{\eta_c U_c + \eta_v U_v}{U_{structure}} \cong \eta_v \frac{U_v}{U_{structure}} \qquad \text{as } \eta_v \gg \eta_c. \tag{3}$$

Thus, the ratio of the strain energy in the viscoelastic layer to the total strain energy (referred to in this paper as the MSE ratio) determines the damping introduced by a particular configuration and allows comparisons to be made between different designs.

It can be shown that the MSE method assumed proportional damping [13] and is limited to the analysis of lightly damped structures. It also does not allow for the frequency dependence of the elastic modulus: to get the correct values the eigenvalue calculation must be carried out for each mode using the material properties at that particular frequency [9]. More accurate predictions can be obtained by using a direct forced response calculation as this method includes the frequency dependent properties. However, as it is very time consuming it is only used in this paper to verify results obtained from MSE calculations.

3. Analytical model of sandwiching ring

This section describes an analytical model of a two-dimensional solid ring with a constrained layer damping treatment applied to it. Lagrange's equation coupled with the assumed modes summation method is used to obtain the equations of motion in generalized coordinates. The analysis is similar to that of He and Rao [8] for a curved sandwich beam but models the inertia and strain in the viscoelastic layer differently. Figure 1

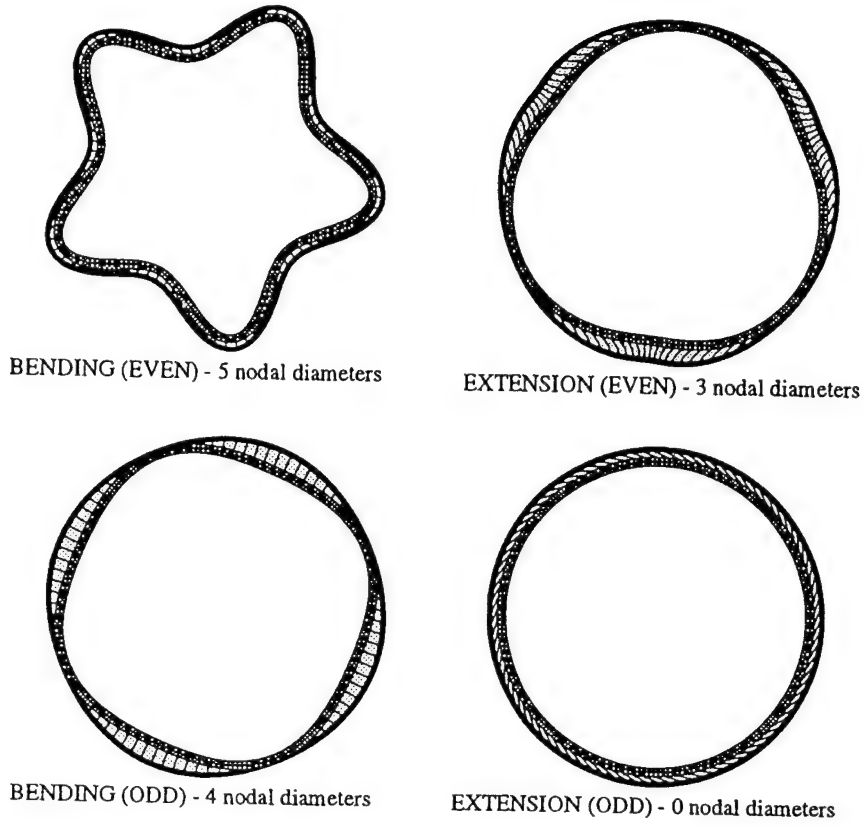

Figure 2. Constrained layer damped ring mode types.

shows the deformations considered in the analysis and the nomenclature used.

The main assumptions in setting up the equations are as follows:

(i) linear elastic behaviour in all the layers (viscoelastic behaviour, represented by the complex modulus, is included at a later stage using the correspondence principle [14])

(ii) extensional and shear deformations are linear through the thickness of the viscoelastic layer

(iii) shear deformation of the ring and constraining layer is insignificant

(iv) perfect bonding occurs between the layers.

The variation in the displacement of the ring centreline in the radial and tangential directions respectively are given by

$$w_r = \varphi_r(\theta) g_r(t) \tag{4}$$

and

$$u_r = \psi_r(\theta) h_r(t) \tag{5}$$

where φ_r and ψ_r describe the deformation shape (dependent on the angle θ) and g_r and h_r are time varying coefficients. For the constraining layer the displacements are given by,

$$w_c = \varphi_c(\theta) g_c(t) \tag{6}$$

and

$$u_c = \psi_c(\theta) h_c(t). \tag{7}$$

For the viscoelastic layer, from assumption (ii), the deformations in the circumferential and radial directions are,

$$u_v = \frac{u_P + u_Q}{2} + \frac{z_v}{t_v}(u_Q - u_P) \tag{8}$$

and

$$w_v = \frac{w_P + w_Q}{2} + \frac{z_v}{t_v}(w_Q - w_P) \tag{9}$$

where

$$u_P = \left(1 + \frac{t_r}{2R_t}\right) u_r - \frac{t_r}{2R_r} w_r'$$

$$u_Q = \left(1 - \frac{t_c}{2R_c}\right) u_c + \frac{t_c}{2R_c} w_c'$$

$$w_P = w_r$$

$$w_Q = w_c.$$

Note that the symbol $'$ is used to denote $\partial/\partial\theta$ and $\dot{}$ to denote the time derivative $\partial/\partial t$. The kinetic energy of the ring is obtained from,

$$T_r = \tfrac{1}{2} \int_0^{2\pi} \int_{-t_r/2}^{t_r/2} \rho_r b_r \left[\dot{w}_r^2 + \left(\frac{R_r + z_r}{R_r} \dot{u}_r + \frac{z_r}{R_r} \dot{w}_r' \right)^2 \right] \times (R_r + z_r)\, dz_r\, d\theta \tag{10}$$

where the symbols are as defined in the nomenclature. Similarly for the constraining layer,

$$T_c = \tfrac{1}{2} \int_0^{2\pi} \int_{-t_r/2}^{t_r/2} \rho_c b_c \left[\dot{w}_c^2 + \left(\frac{R_c + z_c}{R_c} \dot{u}_c + \frac{z_c}{R_c} \dot{w}_c' \right)^2 \right]$$

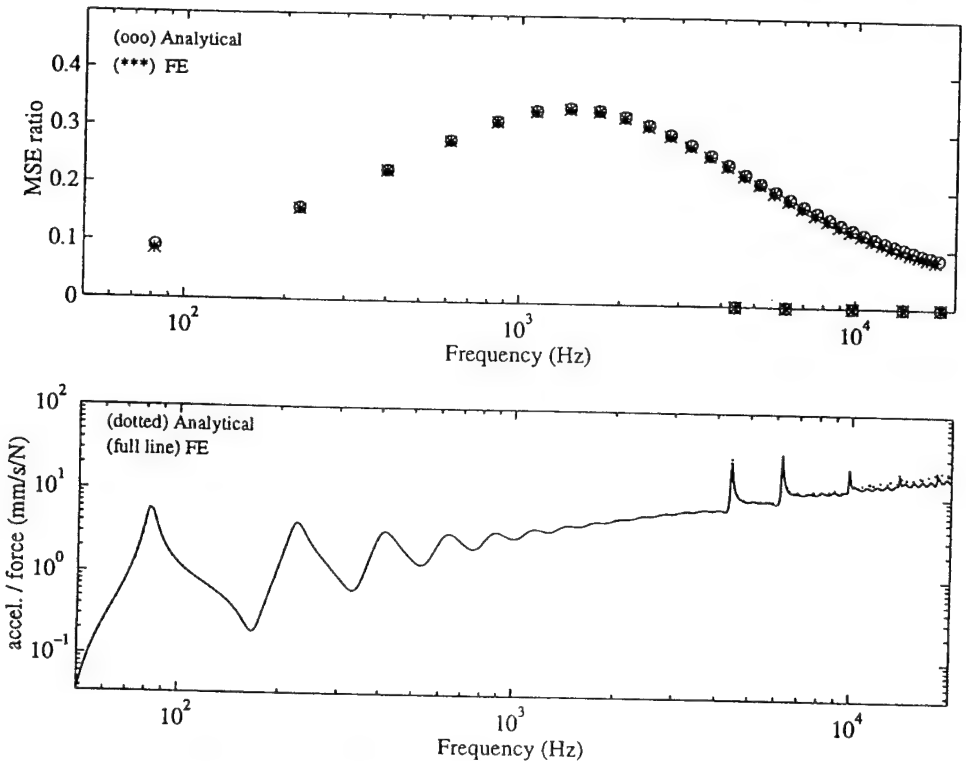

Figure 3. Comparison of analytical and FE results for ring A.

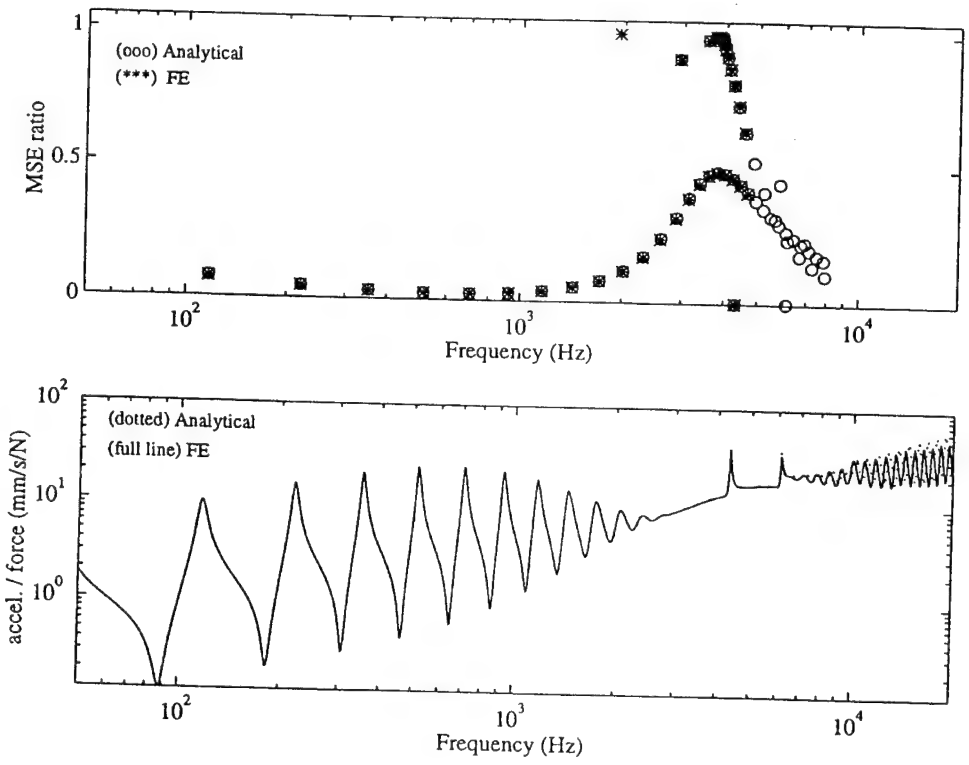

Figure 4. Comparison of analytical and FE results for ring B.

$$\times(R_c + z_c)\,dz_c\,d\theta. \tag{11}$$

The kinetic energy for the viscoelastic layer is obtained by substituting equations (8) and (9) into,

$$T_v = \tfrac{1}{2}\int_0^{2\pi}\int_{-t_v/2}^{t_v/2} \rho_v b_v\left[\dot{u}_v^2 + \dot{w}_v^2\right](R_v + z_v)\,dz_v\,d\theta. \tag{12}$$

As shear and radial strains in the ring are ignored and the circumferential strain at any point on the ring is given by [15],

$$\epsilon_{\theta_r} = \frac{u_r'}{R_r} + \frac{w_r}{R_r + z_r} - \frac{z_r w_r''}{R_r(R_r + z_r)} \tag{13}$$

the strain energy expression for the ring is,

$$U_r = \tfrac{1}{2}\int_0^{2\pi}\int_{-t_r/2}^{t_r/2} E_r b_r\left[\frac{u_r'}{R_r} + \frac{w_r}{R_r + z_r} - \frac{z_r w_r''}{R_r(R_r + z_r)}\right]^2 \times(R_r + z_r)\,dz_r\,d\theta \tag{14}$$

and for the constraining layer,

$$U_c = \tfrac{1}{2}\int_0^{2\pi}\int_{-t_c/2}^{t_c/2} E_c b_c\left[\frac{u_c'}{R_c} + \frac{w_c}{R_c + z_c} - \frac{z_c w_c''}{R_c(R_c + z_c)}\right]^2 \times(R_c + z_c)\,dz_c\,d\theta. \tag{15}$$

For the viscoelastic layer, substituting equations (7) and (8) into the expressions for strain in cylindrical coordinates [16] give,

$$\epsilon_{\theta_v} = \frac{1}{R_v + z_v}\left[\tfrac{1}{2}\left(u_P' + u_Q' + w_P + w_Q\right) + \frac{z_v}{t_v}\left(u_Q' - u_P' + w_Q - w_P\right)\right] \tag{16}$$

$$\epsilon_{r_v} = \frac{w_Q - w_P}{t_v} \tag{17}$$

and

$$\gamma_v = \frac{u_Q - u_P}{t_v} + \frac{1}{R_v + z_v}\left[\tfrac{1}{2}\left(w_P' + w_Q' - u_P - u_Q\right) + \frac{z_v}{t_v}\left(w_Q' - w_P' + u_Q + u_P\right)\right]. \tag{18}$$

The strain energy is defined by,

$$U_v = \tfrac{1}{2}\int_0^{2\pi}\int_{-t_v/2}^{t_v/2} b_v\left[\frac{E_v}{1-\nu^2}\left(\epsilon_{R_v}^2 + 2\nu\epsilon_{R_v}\epsilon_{\theta_v} + \epsilon_{\theta_v}^2\right) + G_v\gamma_v^2\right](R_v + z_v)\,dz_v\,d\theta. \tag{19}$$

Lagrange's equation states that,

$$\frac{d}{dt}\left(\frac{\partial(T-U)}{\partial\dot{q}_k}\right) - \frac{\partial(T-U)}{\partial q_k} = Q_k \tag{20}$$

where q_k are generalized coordinates, Q_k the generalized force, T and U the kinetic and potential energy respectively. Examination of the energy expressions show that for this model, Lagrange's equations can be reduced to,

$$\frac{d}{dt}\left(\frac{\partial(T_r + T_c + T_v)}{\partial\dot{q}_k}\right) - \frac{\partial(U_r + U_c + U_v)}{\partial q_k} = Q_k. \tag{21}$$

Substituting the energy terms into equation (21) and taking the derivatives with respect to each of the time dependent variables in equations (4) to (7) gives four coupled equations of motion. These can be represented in matrix form as

$$[M]\ddot{q} + [K]q = \underline{F} \qquad q = [\,g_r \quad g_c \quad h_r \quad h_c\,]^T \tag{22}$$

where M and K are the mass and stiffness matrices and F the forcing terms. For reasons of space the full expressions for these terms are not presented here but can be easily derived as shown. The correspondence principle is used to include the viscoelastic material behaviour. Each elastic modulus value that appears in the stiffness matrix is substituted by its corresponding complex modulus value (as in equation (1)) to give the full viscoelastic model for the sandwich ring giving,

$$[M]\ddot{q} + \left[K_{STORAGE} + iK_{LOSS}\right]q = \underline{F}. \tag{23}$$

The assumed modes summation method approximates the deformed shape using a series of comparison functions which must satisfy the physical boundary conditions. One set of suitable shape functions are the mode shapes of a freely vibrating ring. Applying this method to the displacements in equations (4) to (7) gives,

$$\begin{aligned} w_r &= \sum_{j=1}^{n} \varphi_{jr}\cdot g_{jr} \\ u_r &= \sum_{j=1}^{n} \psi_{jr}\cdot h_{jr} \\ w_c &= \sum_{j=1}^{n} \varphi_{jc}\cdot g_{jc} \\ u_c &= \sum_{j=1}^{n} \psi_{jc}\cdot h_{jc} \end{aligned} \tag{24}$$

where,

$$\varphi_{jr} = \varphi_{jc} = \cos((j-1)\theta) \text{ and } \psi_{jr} = \psi_{jc} = \sin((j-1)\theta) \tag{25}$$

where the mass and stiffness matrices have size $4n \times 4n$, n being the number of terms in the series expansion. However, due to the orthogonality of the comparison functions used, the mass and stiffness matrices become banded diagonal matrices and are therefore computationally inexpensive.

4. Theoretical and experimental validation

The model derived in the previous section includes assumptions regarding the nature of the stresses and strains developed in the sandwich ring. This section presents the work carried out to validate the model both experimentally and using finite element analysis. The accuracy of the model is evaluated by considering the loss factors and resonance frequencies obtained over a large number of modes. In addition to this the trends indicated by the MSE analysis are compared with the frequency response.

Excluding rigid body modes, two basic types of mode shape are encountered in a two-dimensional analysis of free rings: these are bending and extensional. Bending

Table 1. Base ring dimensions.

Variables	Symbol	Value
Nominal radius (mm)	R_r	183.75
Thickness (mm)	t_r	2.5
Depth (mm)	b_r	25
Young's modulus (GPa)	E_r	205
Density (kg m^{-3})	ρ_r	7860
Poisson's ratio	ν_r	0.3
Loss factor (%)	η_r	0.5

modes involve sinusoidal deflections mainly in the radial direction whereas in extensional modes the circumferential deformations dominate. Where CLD is applied to a ring, odd and even modes are found for each nodal diameter. The base ring and the constraining layer move in the same direction in even modes and in opposite directions in odd modes. Typical examples of these modes are shown in figure 2.

Table 1 contains the basic dimensions of the rings used for model verification. The data for the various CLD treatments applied to them is presented in table 2. (The material properties of the constraining layer are identical to those of the base ring.) The use of several different configurations ensured the validity of the model over a wide range.

4.1. Comparison of analytical and finite element analysis

The finite element analysis results presented here were obtained from a two-dimensional model built using eight noded quadratic elements. Convergence studies using various mesh densities showed that a model consisting of two elements through the thickness of each layer and 240 elements around the circumference was sufficient for MSE analysis and forced response calculations.

Figures 3 and 4 show the comparison of results from the analytic and finite element models for rings A and B. It can be seen that there is good agreement between the two models both for MSE analysis and for direct forced response calculations. (The MSE ratio results for ring B for the finite element analysis stop at around 5 kHz due to insufficient memory on the computer used.) It can also be seen that the MSE ratio and the frequency response show similar trends: when the MSE ratio is low (as seen with the extension modes) the frequency response shows distinct modes as sharp spikes but when the MSE ratio is high the peaks in the frequency response disappear.

4.2. Experimental verification

Theoretical and experimental tests were carried out for rings C and D. The rings and constraining layers were manufactured by turning sections of a cold-forged steel pipe on a lathe. The void between the ring and constraining layer was filled with polyurethane and cured. The thinnest void into which the polyurethane could be introduced successfully was found to be 1 mm thereby setting a minimum thickness for the viscoelastic layer.

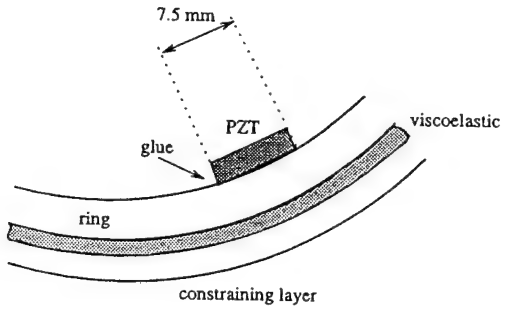

Figure 5. PZT attached to ring.

The rings were suspended in the axial direction using soft elastic supports to simulate free boundary conditions. A thin strip of PZT material was glued on the inner surface of each ring to act as an induced strain actuator as shown in figure 5. The rings were then excited by applying a band limited random signal of 100 volts peak-to-peak across the PZT. This method was used because such PZT devices can deliver significant strains even at high frequencies and also because the shape of the actuator ensured that unwanted three-dimensional modes were not excited. The response was measured using a miniature accelerometer mounted in the radial direction. The input and output signals were controlled and processed using a HP300 computer running LMS software. A schematic diagram of the experimental design is shown in figure 6.

The theoretical values of natural frequency and loss factor were calculated using MSE analysis. The frequency dependence of the material properties of polyurethane at 22 °C are presented in figure 7. An iterative approach was used to find the correct values of Young's modulus and loss factor for each mode. The analytical model was therefore used to save computational time and effort. Experimentally the loss factors for each mode were estimated from the Nyquist circle to minimize the residual effects of close modes.

Predicted and measured values of loss factor are plotted against frequency for rings C and D in figures 8 and 9 respectively. These show fair agreement between theoretical and analytical values for both the bending and extension modes. (Extension modes can be identified as the modes in which the damping is near zero.) Possible causes for discrepancies between the results include interference of the support structures and a wide tolerance band on the viscoelastic material data.

Overall, it can be concluded that the analytical model developed in the previous section can be used to give reasonable predictions of the behaviour of CLD treatments applied to rings.

5. Parametric study

This section presents a theoretical parametric study carried out on a ring with CLD to highlight the effect of each parameter on the damping of the structure. The ratio of modal strain energy between the viscoelastic layer and the

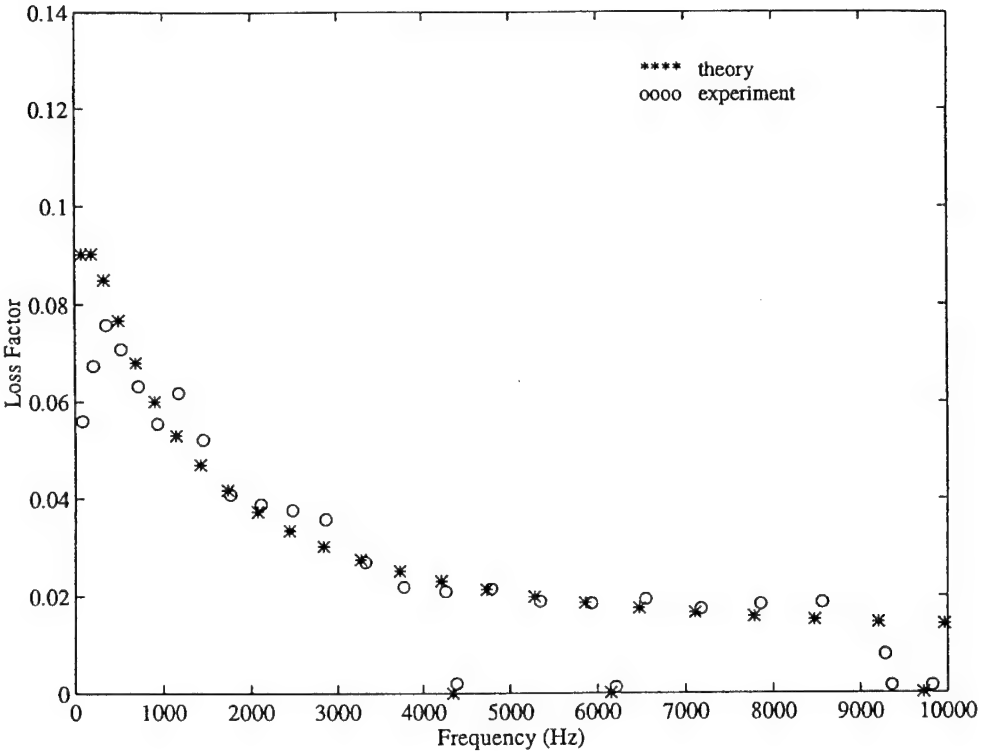

Figure 8. Modal loss factors for ring C.

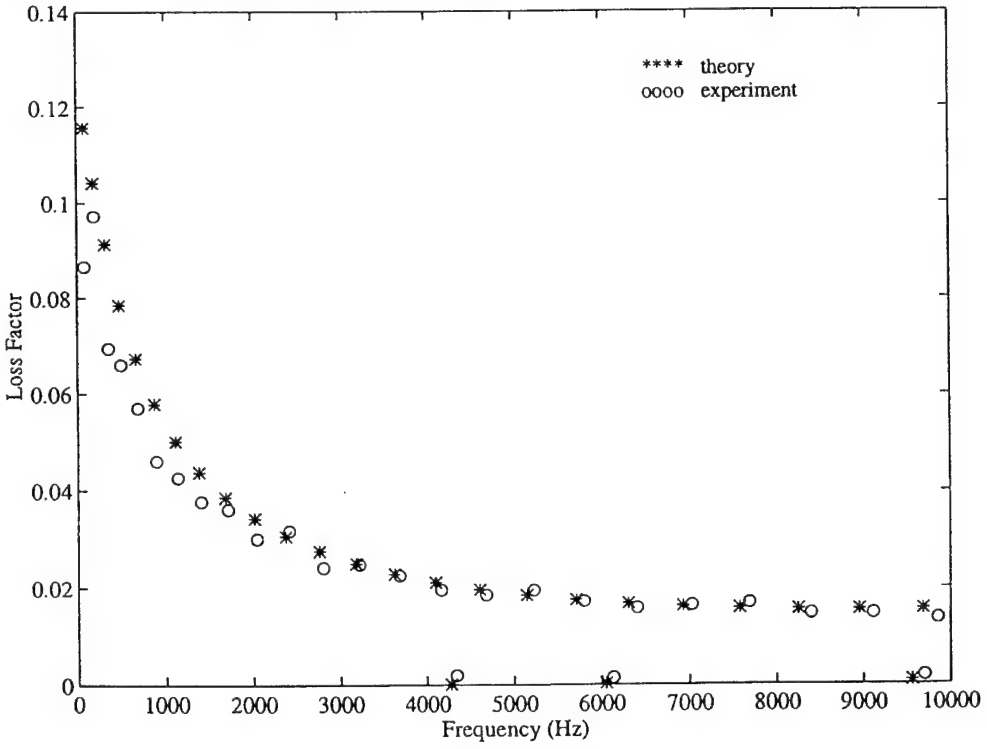

Figure 9. Modal loss factors for ring D.

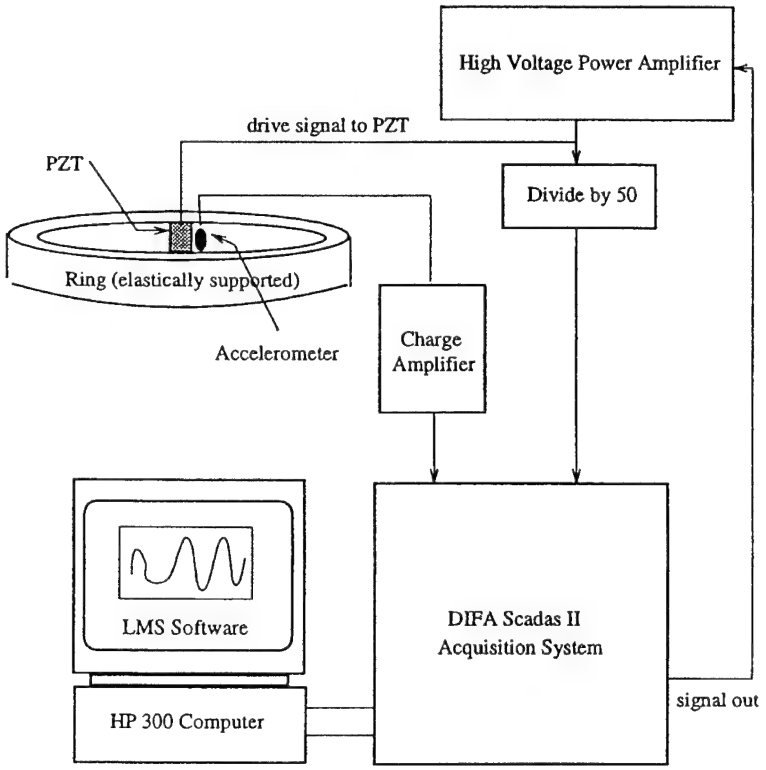

Figure 6. Schematic diagram of experimental set-up.

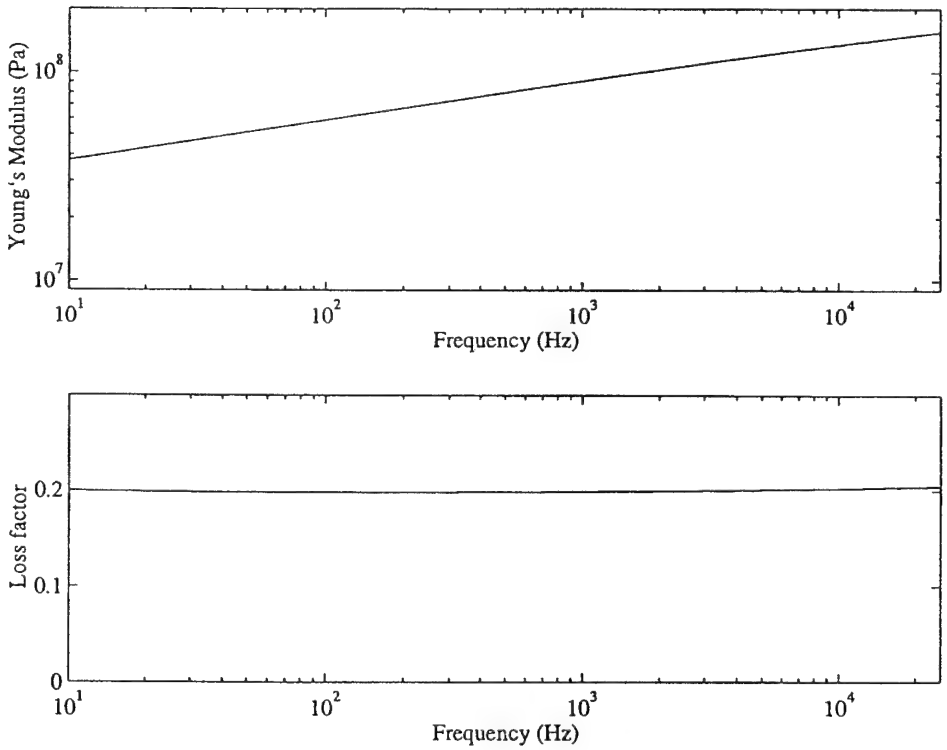

Figure 7. Material properties for polyurethane at 22 °C.

Table 2. Properties of CLD treatments.

Variable	Symbol	Ring A	Ring B	Ring C	Ring D
VL thickness (mm)	t_v	0.2	1	1	1
VL modulus (MPa)	E_v	50	2	50–300*	50–300*
VL density (kg m^{-3})	ρ_v	1000	1000	1000	1000
VL Poisson's ratio	ν_v	0.4999	0.4999	0.4999**	0.4999**
VL loss factor (%)	η_v	0.8	0.8	0.10–0.22*	0.10–0.22*
CL thickness (mm)	t_c	2	1	2	1

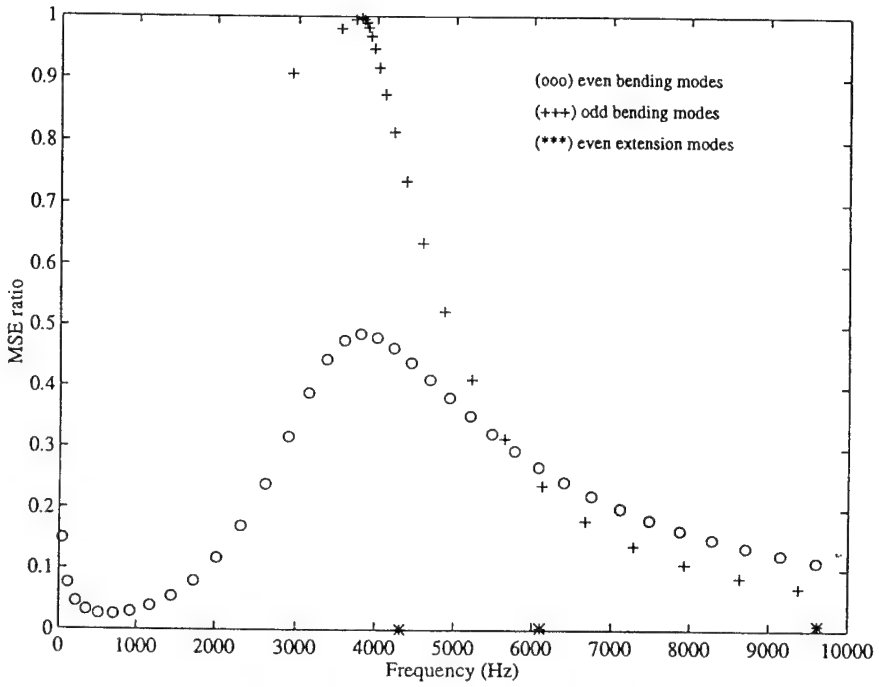

Figure 10. MSE ratios of different mode types of ring B.

full structure (the MSE ratio) is used as a performance indicator. The present study focuses on the bending modes as extension modes tend to occur at much higher frequencies. Even modes typically have lower natural frequencies and loss factors than odd modes for all but a few high nodal diameter cases as can be seen in figure 10. This study uses the lower of the two values of MSE ratio recovered for even and odd modes of the same nodal diameter. For convenience the elastic modulus of the viscoelastic layer is considered to be independent of frequency.

The general trend of the results is shown in figure 11. Two areas of high MSE ratio (and hence damping) can be identified, one in which the viscoelastic layer deforms mainly in hear and the other in which radial motion between the constraining layer and the ring causes significant radial extension and compression of the viscoelastic layer. Dimensions of the ring used for the parametric study are given in table 3.

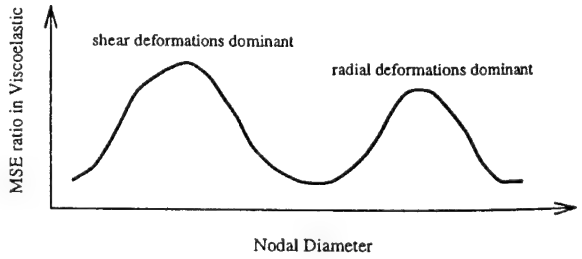

Figure 11. Typical curve for the MSE ratio (damping) for bending modes of a ring with CLD.

5.1. Viscoelastic layer modulus (Ev)

Figure 12 shows the effect of changing the viscoelastic layer modulus on the MSE ratio. When the modulus is high ($10 < E_v < 100$ MPa) shear is the predominant deformation in the viscoelastic layer but when it is low ($E_v < 1$ MPa) radial deformations are significant particularly in the higher modes.

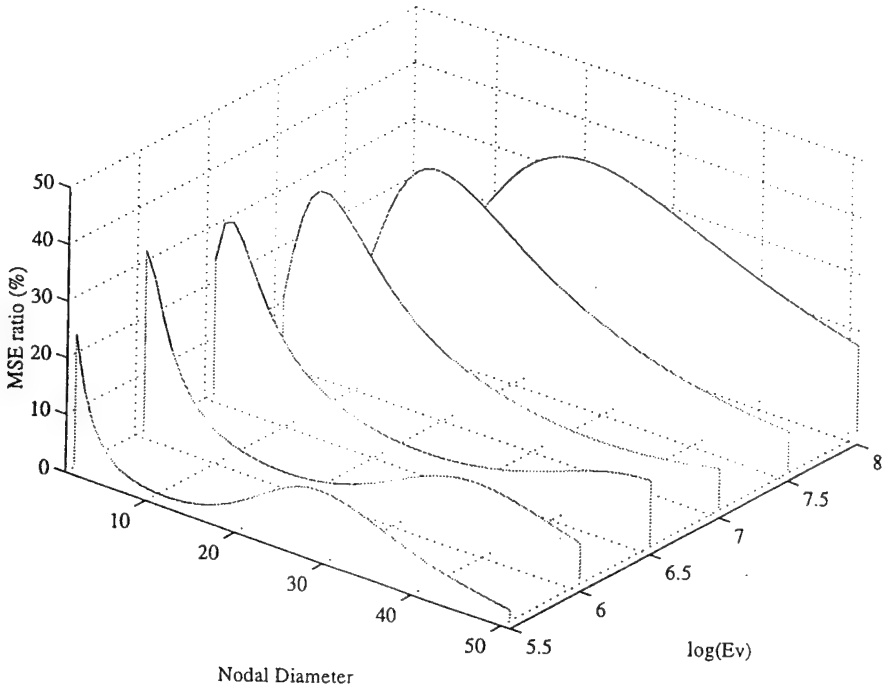

Figure 12. Effect of VL modulus on bending modes (tc = 3 mm, tv = 0.127 mm).

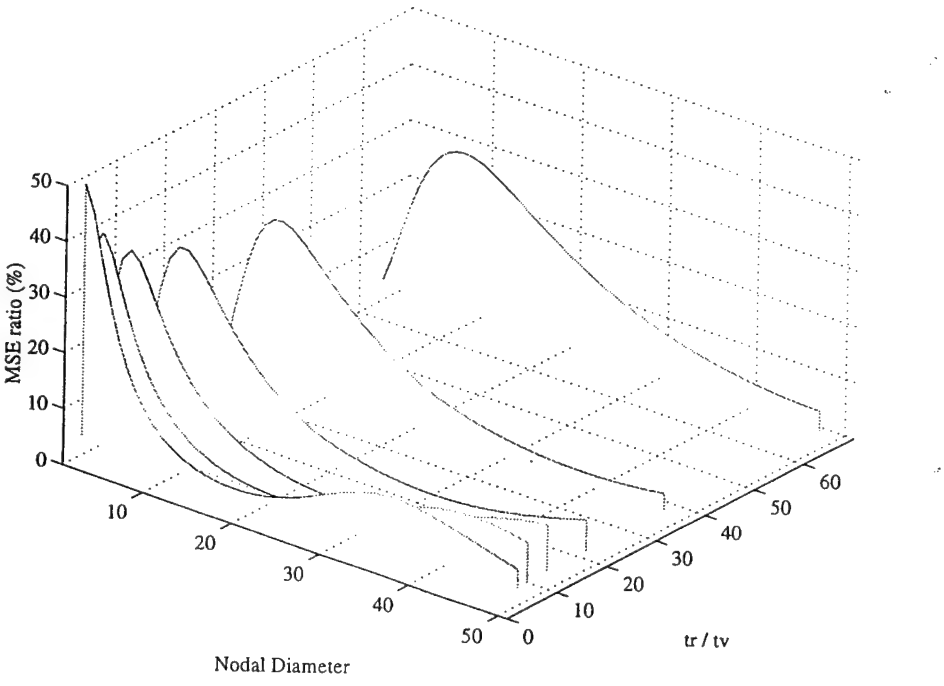

Figure 13. Effect of VL thickness on bending modes (tc = 3 mm, Ev = 14 MPa).

5.2. Viscoelastic layer thickness (t_v)

Figure 13 shows that increasing the thickness of the viscoelastic layer has a similar effect to reducing the modulus. However, the peak MSE ratio value is higher for a thick viscoelastic layer due to the increased amount of damping material available.

5.3. Constraining layer thickness (t_c)

Figure 14 shows that the height of the shear peak increases with constraining layer thickness reaching a maximum when the base ring and constraining layer are of equal thickness. This is clearly not the case for the radial deformation peak. By increasing the number of modes

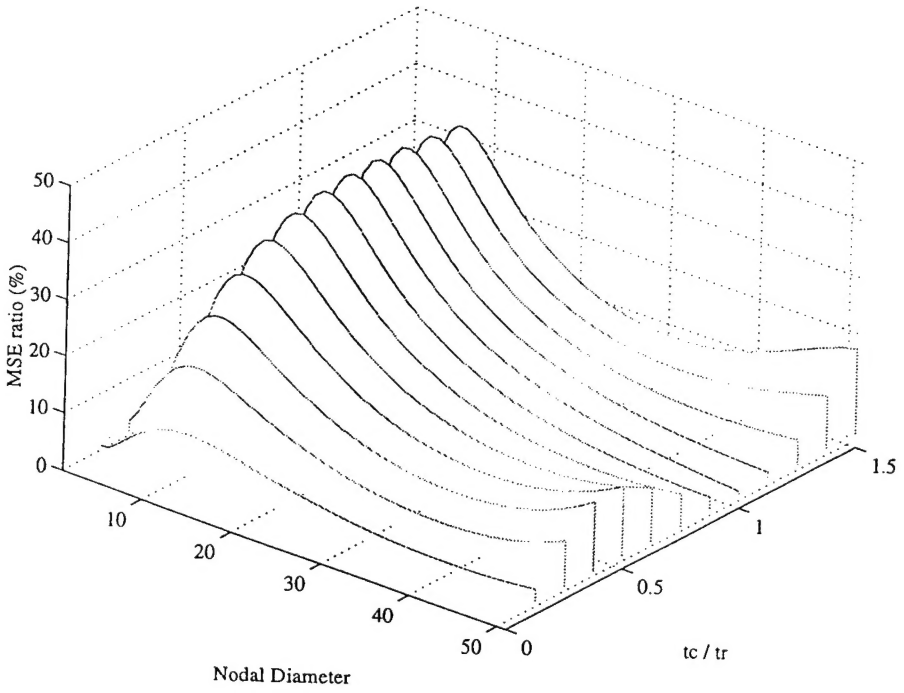

Figure 14. Effect of CL thickness on bending modes (tv = 0.127 mm, Ev = 14 MPa).

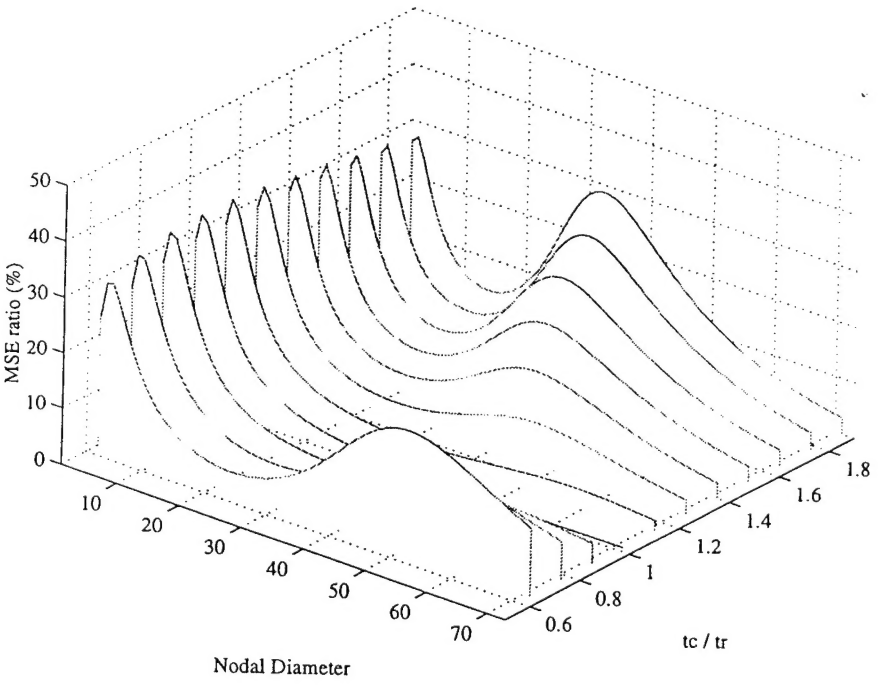

Figure 15. Effect of CL thickness on bending modes (tv = 0.127 mm, Ev = 3 MPa).

considered from 50 to 70 and reducing the viscoelastic layer modulus from 14 to 3 MPa, the effect on radial deformation peak can be seen as shown in figure 15. This figure indicates that a significant difference between the thicknesses of the two outer layers is desirable for radial deformation dependent damping.

5.4. Constraining layer elastic modulus and density (E_c and ρ_c)

From figure 16 it can be seen that increasing the constraining layer modulus improves the MSE ratio of the shear peak slightly but significantly reduces the height of

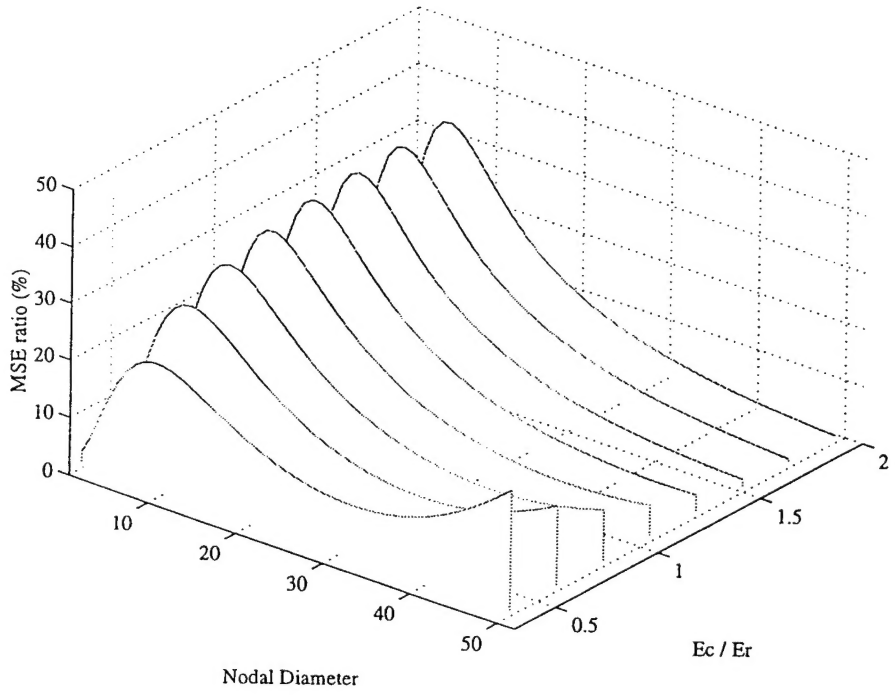

Figure 16. Effect of CL modulus on bending modes (tv = 0.127 mm, Ev = 14 MPa, tc = 3 mm).

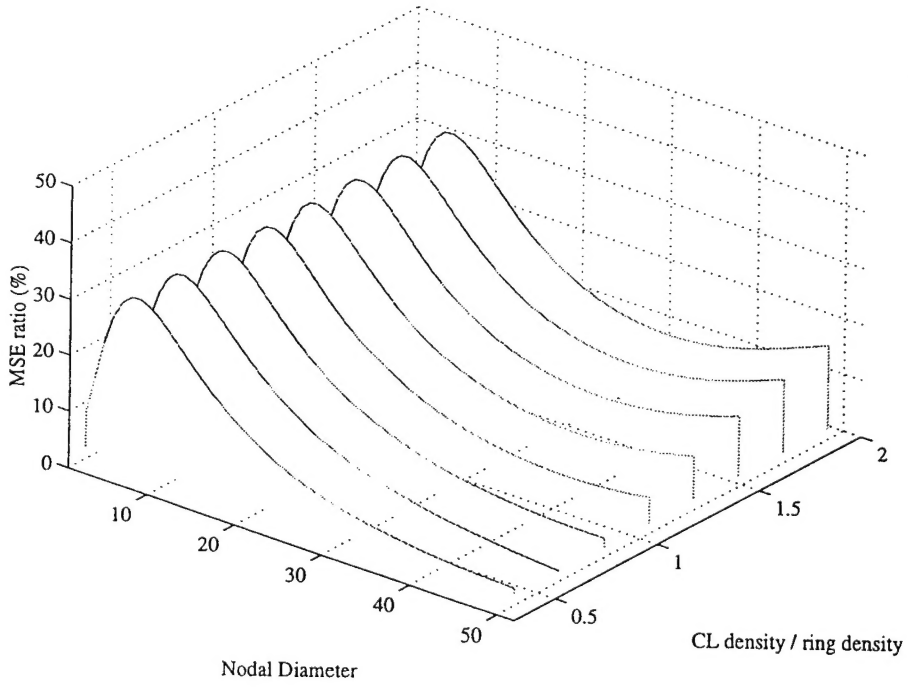

Figure 17. Effect of CL density on bending modes (tv = 0.127 mm, Ev = 14 MPa, tc = 3 mm).

the radial deformation peak. Figure 17 shows that the constraining layer density has little effect on the shear peak but an increase density of the constraining layer increases the radial deformation peak probably as a result of increased relative motion between the outer layers.

5.5. Summary of the parametric study

The parametric study shows that varying the viscoelastic layer elastic modulus or thickness has the primary effect of moving the peak values to higher or lower modes. The peak heights are mainly dependent on the constraining layer thickness, modulus and density. The first (shear)

Table 3. Properties of sandwich ring used for parametric study.

Variable	Symbol	Value
Ring nominal radius (mm)	R_r	375
Ring thickness (mm)	t_r	4
VL thickness (mm)	t_v	0.127
CL thickness (mm)	t_c	3
Ring and CL Young's modulus (GPa)	E_r, E_c	110
VL Young's modulus (MPa)	E_v	14
Ring and CL Poisson's ratio	ν_r, ν_c	0.3
VL Poisson's ratio	ν_v	0.4999
Ring and CL density (kg m^{-3})	ρ_r, ρ_c	4553
VL density (kg m^{-3})	ρ_v	1000

peak is maximized when the flexural rigidity of the ring and constraining layer are equal. The height of the second (radial deformation) peak depends not only on the rigidity but also on relative flexural inertias of the ring and constraining layer and is minimized when they are equal as for that condition there is little relative radial motion.

6. Conclusions and further work

An analytic model has been developed that predicts that natural frequency and loss factors of a three layer sandwich ring. Accurate results for thin rings can be obtained even at high mode numbers by allowing the inner (viscoelastic) layer to deform both radially and circumferentially. Results compare well with those from finite element analysis and experimental work.

Modal strain energy analysis has been used to study the effect of different parameters on the performance of constrained layer damping applied to a ring. This has shown that for the bending modes, a graph plotting the damping against mode number follows a double humped curve. The first peak is the well known viscoelastic layer shear deformation curve. The second peak is caused by radial deformations in the viscoelastic layer. The height and position of each peak depend on several variables and a configuration maximizing the shear peak minimizes the height of the radial deformation peak.

The second peak is particularly interesting for applications where damping is required at high mode numbers or where manufacturing and material constraints do not allow the design to be optimized for shear—optimum shear configurations often require a very thin viscoelastic layer. A complete experimental study considering not only rings but also three-layer beams should be carried out to verify the behaviour of this second peak. Studies considering the performance of segmented and active constrained layer methods at high frequency and modal order would also be valuable.

Acknowledgments

The authors are grateful for the financial support provided by Rolls Royce plc for the work presented in this paper. The authors also wish to thank Professor Jan Wright at Manchester University for his help and advice in developing the analytic ring model.

References

[1] Kerwin E M 1959 Damping of flexural waves by a constrained viscoelastic layer *J. Acoust. Soc. Am.* **31** 952–62

[2] Mead D J and Markus S 1969 The forced vibration of a three-layer damped sandwich bam with arbitrary boundary conditions *J. Sound Vibr.* **10** 163–75

[3] Rao D K 1977 Vibration of short sandwich beams *J. Sound Vibr.* **52** 253–63

[4] Mead D J 1982 Flexural vibration of damped sandwich beams *J. Sound Vibr.* **83** 363–77

[5] Miles N N and Reinhall P G 1986 An analytical model for the vibration of laminated beams including the effects of both shear and thickness deformation in the adhesive layer *ASME J. Vibr. Acoust.* **108** 56–64

[6] Frostig Y and Baruch M 1994 Free vibrations of sandwich beams with a transversely flexible core: a high order approach *J. Sound Vibr.* **176** 195–208

[7] Vaswani J, Asnani N T and Nakra B C 1988 Vibration and damping analysis of curved sandwich beams with a viscoelastic core *Composite Struct.* **10** 231–45

[8] He S and Rao M D 1992 Prediction of loss factors of curved sandwich beams *J. Sound Vibr.* **159** 101–13

[9] Johnson C D and Keinholz D A 1982 Finite element prediction of damping in structures with constrained viscoelastic layers *AIAA J.* **20** 1284–90

[10] Ferry J D 1956 *Viscoelastic Properties of Polymers* (New York: Wiley)

[11] Chan Y W 1995 Characterization and prediction of the dynamic response of viscoelastic elements *PhD Thesis* University of Manchester

[12] Bracewell R N 1978 *The Fourier Transform and Its Applications* 2nd edn (New York: McGraw-Hill)

[13] Slater J C, Belvin W K and Inman D J 1993 A survey of modern methods for modelling frequency dependent damping in finite element models *Proc. 11th Int. Modal Analysis Conf. (1993)*

[14] Christensen R M 1971 *The Theory of Viscoelasticity: An Introduction* (New York: Academic)

[15] Blevins R D 1979 *Formulas for Natural Frequency and Mode Shape* (Van Nostrand Reinhold)

[16] Fenner R T 1986 *Engineering Elasticity: Application of Numerical and Analytical Techniques* (England: Wiley)

REPORT DOCUMENTATION PAGE

Form Approved OMB No. 0704-0188

1. AGENCY USE ONLY (Leave blank)	2. REPORT DATE	3. REPORT TYPE AND DATES COVERED
	April 1997	Final Report

4. TITLE AND SUBTITLE

Constrained Layer Damping and Piezoceramic Active Control

5. FUNDING NUMBERS

F6170894W0133

6. AUTHOR(S)

Geoffrey Tomlinson

7. PERFORMING ORGANIZATION NAME(S) AND ADDRESS(ES)

University of Sheffield
Mappin Street
Sheffield S1 3JD
United Kingdom

8. PERFORMING ORGANIZATION REPORT NUMBER

N/A

9. SPONSORING/MONITORING AGENCY NAME(S) AND ADDRESS(ES)

EOARD
PSC 802 BOX 14
FPO 09499-0200

10. SPONSORING/MONITORING AGENCY REPORT NUMBER

SPC 94-4015

11. SUPPLEMENTARY NOTES

12a. DISTRIBUTION/AVAILABILITY STATEMENT

Approved for public release; distribution is unlimited.

12b. DISTRIBUTION CODE

A

13. ABSTRACT (Maximum 200 words)

The work achieved the following aspects:

1) Mathematical models for both longitudinal and flexural hybrid constrained layer/piezoceramic active damping concepts have been developed using analytical (Rayleigh-Ritz) and FE models and validated experimentally. These are described in Technical Papers 1 and 2 in Appendix 1.
2) The methodology was applied to a plate structure representing an aircraft instrument panel and the first three modes of vibration (two lexure, one torsion) were effectively suppressed using the hybrid method. The results are described in the Technical Paper Number 3 Appendix 2.
3) The technology has been extended to ring structures (i.e., applicable to aero engines) as described in Technical Papers 4 and 5 in Appendix III.

Appendices:
Technical Paper 1. Modelling of a Hybrid Constrained Layer/Piezoceramic Approach to Active Damping. Transactions of the ASME, Vol. 119, Jan 97, p.120-130.
Technical Paper 2. Use of Active Constrained-Layer Damping for Controlling Resonant Vibration. Published in Smart Mater. Struct. 4 (1995), p.1-6.
Technical Paper 3. Initial Studies into the Active Constrained Layer Damping for Control Resonant Vibration. Published in SPIE, Vol. 2193, p.138-149.
Technical Paper 4. Passive and Active Constrained Layer Damping of Ring Type Structures. Presented at the 4th Smart Structures and Materials Conference, San Diego, March 1997.
Technical Paper 5. Suppression of Ring Vibration Modes of High Nodal Diameter Using Constrained Layer Damping Methods. Published in Smart Mater. Struct. 5 (1996), p..672-684.

14. SUBJECT TERMS

EOARD, Constrained layer damping, Active layer damping, Vibration damping, Viscoelastic materials, Piezoceramics (PZT), Aerodynamics

15. NUMBER OF PAGES

16. PRICE CODE

N/A

17. SECURITY CLASSIFICATION OF REPORT	18. SECURITY CLASSIFICATION OF THIS PAGE	19. SECURITY CLASSIFICATION OF ABSTRACT	20. LIMITATION OF ABSTRACT
UNCLASSIFIED	UNCLASSIFIED	UNCLASSIFIED	UL